(4)

Technical Document 1369
October 1988

Effective Use of the Electromagnetic Products of TESS and IREPS

W. L. Patterson

NAVAL OCEAN SYSTEMS CENTER
San Diego, California 92152-5000

E. G. SCHWEIZER, CAPT, USN
Commander

R. M. HILLYER
Technical Director

ADMINISTRATIVE INFORMATION

This study was performed by the Tropospheric Branch, Code 543, Naval Ocean Systems Center (NOSC), on the effective use of electromagnetic propagation products available from the Tactical Environmental Support System (TESS), developed by the Naval Oceanographic Office, and the Integrated Refractive Effects Prediction System (IREPS), developed by NOSC.

Released by
H. V. Hitney, Head
Tropospheric Branch

Under authority of
J. E. Richter, Head
Ocean and Atmospheric
Sciences Division

JG

REPORT DOCUMENTATION PAGE

1a. REPORT SECURITY CLASSIFICATION UNCLASSIFIED	1b. RESTRICTIVE MARKINGS
2a. SECURITY CLASSIFICATION AUTHORITY	3. DISTRIBUTION/AVAILABILITY OF REPORT Approved for public release; distribution is unlimited.
2b. DECLASSIFICATION/DOWNGRADING SCHEDULE	
4. PERFORMING ORGANIZATION REPORT NUMBER(S) NOSC Technical Document 1369	5. MONITORING ORGANIZATION REPORT NUMBER(S)
6a. NAME OF PERFORMING ORGANIZATION Naval Ocean Systems Center 6b. OFFICE SYMBOL (If applicable) Code 543	7a. NAME OF MONITORING ORGANIZATION
6c. ADDRESS (City, State and ZIP Code) San Diego, CA 92152-5000	7b. ADDRESS (City, State and ZIP Code)
8a. NAME OF FUNDING/SPONSORING ORGANIZATION Naval Ocean Systems Center 8b. OFFICE SYMBOL (If applicable) Code 402	9. PROCUREMENT INSTRUMENT IDENTIFICATION NUMBER
8c. ADDRESS (City, State and ZIP Code) San Diego, CA 92152-5000	10. SOURCE OF FUNDING NUMBERS PROGRAM ELEMENT NO. 62435N; PROJECT NO. RM35G80; TASK NO. CDB6; AGENCY ACCESSION NO. DN488760
11. TITLE (Include Security Classification) EFFECTIVE USE OF THE ELECTROMAGNETIC PRODUCTS OF TESS AND IREPS	
12. PERSONAL AUTHOR(S) W. L. Patterson	
13a. TYPE OF REPORT Final 13b. TIME COVERED FROM TO	14. DATE OF REPORT (Year, Month, Day) October 1988 15. PAGE COUNT 151
16. SUPPLEMENTARY NOTATION	

17. COSATI CODES			18. SUBJECT TERMS (Continue on reverse if necessary and identify by block number)
FIELD	GROUP	SUB-GROUP	
			Forward looking infrared (FLIR) Radio detection and ranging (RADAR)

19. ABSTRACT (Continue on reverse if necessary and identify by block number)

This document gives the basic principles of electromagnetic radiation, its use in object detection systems such as RADAR and FLIR, the effects of the atmosphere upon electromagnetic wave propagation, and provides guidelines in the interpretation and effective use of electromagnetic propagation products available from assessment programs such as the Tactical Environmental Support System (TESS) and the Integrated Refractive Effects Prediction Systems (IREPS).

Key words:)

20. DISTRIBUTION/AVAILABILITY OF ABSTRACT ☐ UNCLASSIFIED/UNLIMITED ☒ SAME AS RPT ☐ DTIC USERS	21. ABSTRACT SECURITY CLASSIFICATION UNCLASSIFIED
22a. NAME OF RESPONSIBLE INDIVIDUAL W. L. Patterson	22b. TELEPHONE (Include Area Code) (619) 553-1423 22c. OFFICE SYMBOL Code 543

CONTENTS

CONTENTS (Cont'd)

CONTENTS (Cont'd)

FIGURES

FIGURES (Cont'd)

FIGURES (Cont'd)

FIGURES (Cont'd)

FIGURES (Cont'd)

TABLES

1.0 INTRODUCTION AND PURPOSE

The purpose of this document is to introduce the reader to the basic principles of electromagnetic radiation, its use in object detection systems such as radio detection and ranging (RADAR) and forward looking infrared (FLIR), the effects of the atmosphere on electromagnetic wave propagation, and to provide guidelines in the interpretation and effective use of electromagnetic propagation products available from assessment programs such as the Tactical Environmental Support System (TESS) or the Integrated Refractive Effects Prediction System (IREPS).

An electromagnetic propagation assessment system is very dynamic in nature. With new technology, additional products will become available and old products will be refined or modified. Therefore, the discussion of assessment products will be directed toward a product class such as a display of propagation loss versus range rather than to a specific product within a specific version of TESS or IREPS.

TESS, developed by the Naval Oceanographic Office, provides tailored meteorological, electromagnetic propagation, oceanographic, acoustic, and satellite ephemeris and tracking products in direct support of fleet air, surface, planning, and antisubmarine warfare operations. Specifically, TESS is a rapid-response, on-scene, environmental prediction system used to assess the effects of the environment on fleet sensor, platform, and weapon systems. For a complete description of TESS and its operation, refer to the TESS user's manual published by the Naval Oceanographic Office.

IREPS, developed by the Naval Ocean Systems Center, provides shipboard environmental-data processing and display capability for comprehensive refractive-effects assessment for naval surveillance, communications, electronic warfare, and weapons guidance systems. For a complete description of IREPS and its operation, refer to the IREPS user's manual published by the Naval Ocean Systems Center.

2.0 NATURE OF RADIATION

2.1 DEFINITION OF ELECTROMAGNETIC RADIATION

Electromagnetic radiation is energy which is propagated through a medium in the form of an advancing disturbance in electric and magnetic fields. Often, the term "radiation" is also used to describe the process of propagation.

In classical electromagnetic theory these disturbances are "waves" propagating through the media. The wave's speed of propagation, ν, through a medium of magnetic permeability (the degree to which the rate of energy flow across boundaries is changed), μ, and specific inductive capacity (how well the media may be magnetized), κ, is given by

$$\nu = \frac{c}{(\mu\kappa)^{.5}} \qquad (1)$$

where c is the speed of light equal to 2.997930×10^{10} cm per second. In a vacuum, the wave propagates with the speed of light. In air, however, the wave propagates with speed slightly slower than the speed of light.

Electromagnetic radiation can be characterized both by wavelength, λ, (the mean distance between maxima or minima) and frequency, f, (the rate of recurrence of an event in periodic motion). The relationship between frequency, wavelength and speed is given by

$$\lambda = \frac{\nu}{f} \quad . \qquad (2)$$

In the metric system, the units of wave frequency are cycles per second (Hz). Multiples (or submultiples) of units have an assigned prefix to describe how many multiples. For example, kilohertz means 1000 Hz. Table 1 gives some selected prefixes associated with the multiples of units.

Table 1. Decimal multiples and submultiples.

Multiples or Submultiples	Prefixes	Symbol
10^{12}	tera	T
10^{9}	giga	G
10^{6}	mega	M
10^{3}	kilo	k
10^{2}	hecto	h
10	decca	da
10^{-1}	deci	d
10^{-2}	centi	c
10^{-3}	milli	m
10^{-6}	micro	μ
10^{-9}	nano	η
10^{-12}	pico	p

In discussions of radiation associated with electromagnetic systems such as radars, several additional definitions are required. These, as illustrated in figure 1, are as follows:

a. Wave magnitude—the maximum displacement of a waveform on a plane perpendicular to the direction of propagation.

b. Wave phase—a particular appearance or state in a regularly recurring cycle of changes. For example, waves a and b in figure 1 are *in phase* while waves c and d are out *of phase*.

c. Wave polarization—the direction of the electric field relative to the direction of propagation and a reference plane (usually the earth's surface). For example, waves e and f of figure 1 are horizontally and vertically polarized respectively.

d. Power—the amount of energy transferred past a given point per unit time. The unit is joule/second or a Watt.

e. Intensity—energy transferred across a given area per unit time (power density). The unit is watt/m^2. In radar propagation, it is convenient to speak of relative intensities, for example, a ratio of power density at a receiving antenna, I_r, to the power density at a transmitting antenna, I_t. This ratio, r, is given as

$$r = 10 \log_{10} \left(\frac{I_r}{I_t}\right) \qquad (3)$$

The unit of intensity ratios is the Bel with the decibel (dB) being the most commonly used submultiple. Although the decibel is a measure of relative rather than absolute intensity, it is possible to set up an absolute scale by arbitrarily defining some particular intensity as a reference. For example, the lowest sound intensity detectable by the human ear is called the threshold of audibility (10^{-10} microwatts cm^{-2}). Using this intensity as a reference, other sound intensities may now be compared. Sounds with power densities below this reference will not be detectable by the human ear and sounds with power densities above this reference will. On such a scale, sounds in average conversation have intensities of about 60 dB, a boiler factory noise level might be about 100 dB, and the threshold of pain about 130 dB. In a like manner, a radar receiver's "threshold of audibility," or its sensitivity, often referred to as power density relative to a milliwatt (abbreviated dBm), may be used as the defined standard. Echos with power densities above the sensitivity will be detected, and echos with power densities below the sensitivity will not be detected.

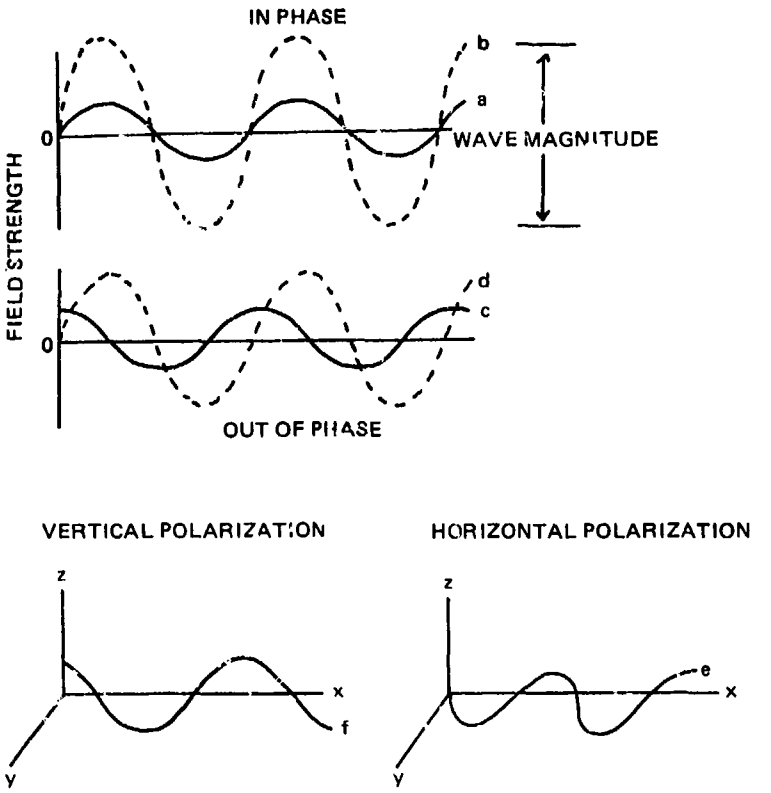

Figure 1. Illustration of wave magnitude, phase, and polarization.

2.2 ELECTROMAGNETIC SPECTRUM

Electromagnetic radiation is produced in a continuous spectrum of different wavelengths. The division of this continuum of wavelengths into a number of named subportions is useful in classifying the types of physical systems capable of emitting radiation of those wavelengths. For example, gamma rays are emitted from the nuclei of atoms as they undergo nuclear rearrangements, visible light is emitted by atoms whose electrons are undergoing changes in energy states, and radio waves are emitted by acceleration of free electrons in metals such as through an antenna wire. An abbreviated portion of the electromagnetic spectrum is illustrated in figure 2 along with commonly used names for the various portions of the spectrum. The electromagnetic propagation programs of TESS and IREPS are restricted to frequencies between 100 and 20,000 megahertz.

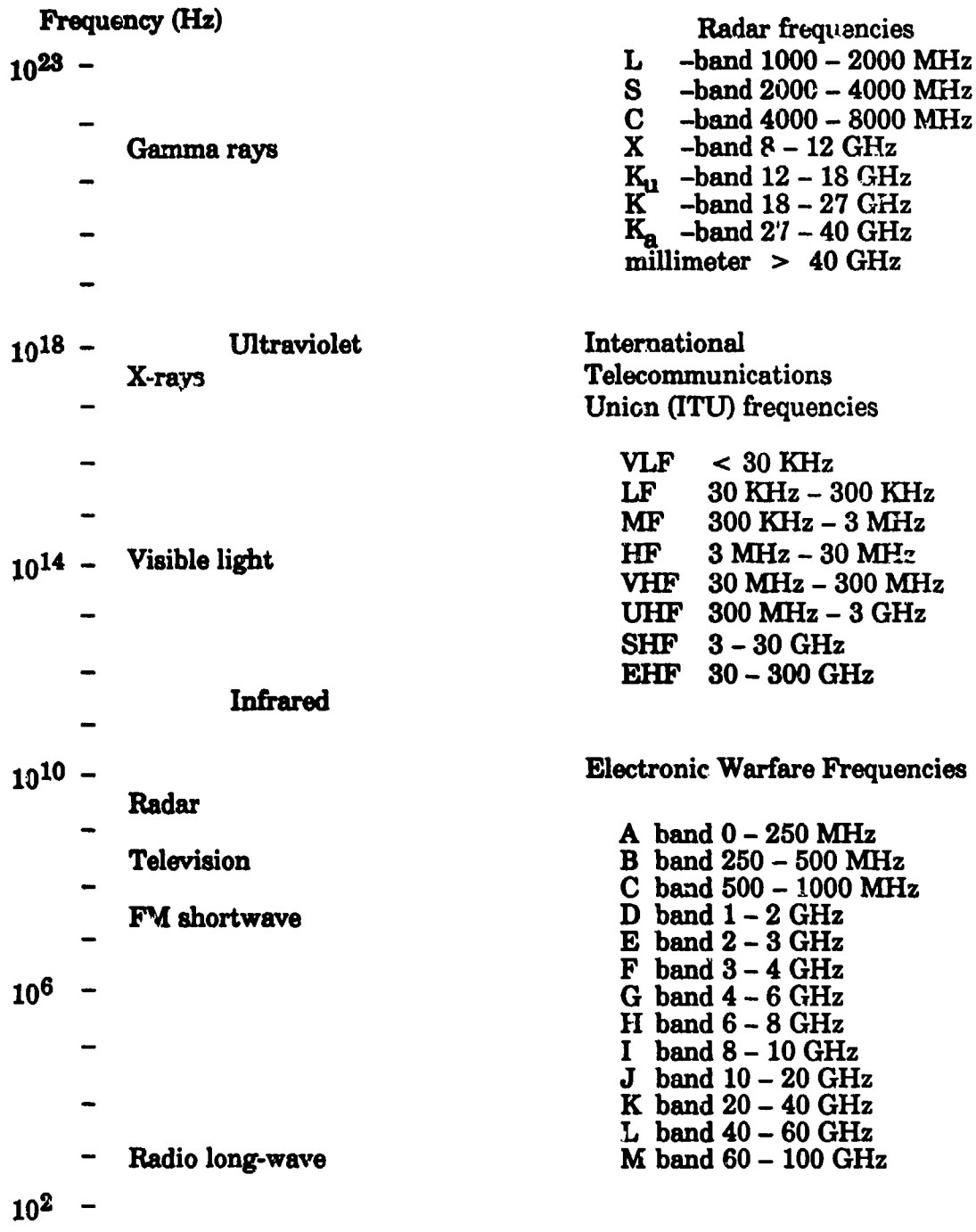

Figure 2. Electromagnetic spectrum and frequency bands.

2.3 INFRARED RADIATION

Since the signal source for a FLIR system is within the infrared (IR) portion of the electromagnetic spectrum, it is proper to describe in more detail the nature of IR radiation.

All physical bodies with temperatures above absolute zero radiate some electromagnetic energy. As the temperature is raised, two characteristics of the IR radiation are affected: (1) the total power radiated increases as the 4th power of the temperature in degrees Kelvin, and (2) the dominant wavelength of the radiant power becomes shorter.

For bodies near the mean temperature of the earth's surface, the peak power comes at wavelengths near 10 μm. At 3 μm, radiated power is reduced to approximately 1 percent of the peak, and no discernible radiation occurs at visual wavelengths (below 1 μm). For temperatures of a few thousand degrees Kelvin (e.g., the sun's surface) the peak power lies in the visual region, with only a few percent above 2-μm wavelength, and virtually none above 8 μm.

Not all bodies of the same temperature radiate equal amounts of energy. A theoretical "black body" is one that absorbs and reradiates all energy at all wavelengths. No energy is reflected from the black body. The ratio of a body's total radiated energy to the black body's total radiated energy is called the body's emissivity. The greatest emissivity a body may have is unity and the least is zero. Emissivity varies inversely with reflectivity. Hence polished metals, which may be highly visible in the visual wavelengths, may have emissivities as low as 0.05 at IR wavelengths and may, therefore, be undetectable by a particular FLIR system.

Thus, radiated power is a function of (1) absolute temperature of the target, (2) its emissivity, and (3) the wavelength of radiation.

2.4 ELECTROMAGNETIC RADIATION ABSORPTION

The earth's atmosphere is filled with absorbing agents, components of the atmosphere which extract energy from the supply of radiation. This extracted energy raises the agent molecule to a higher level of vibration (heats it up). Some radiation is absorbed by aerosols such as fine dust swept up by the wind or soot from volcanoes or industrial plants. These aerosols tend to be broadband absorbers. That is, they absorb radiation over a wide range of frequency bands. However, some atmospheric molecules (notably water vapor, carbon dioxide, and ozone) have many strong absorption bands which will have a large influence upon FLIR operation and radar performance above K_u band.

The loss of energy to the absorbing agent reduces the electromagnetic radiation power as it propagates through the atmosphere. Figure 3 illustrates the absorption of electromagnetic energy by the atmospheric gases of water vapor and oxygen. At frequencies below 1 GHz, the effect of atmospheric absorption is negligible. Above 10 GHz, it becomes increasingly important.

Because of the frequency limits placed upon the electromagnetic propagation programs of TESS and IREPS, and because of the extreme difficulty in assessing aerosol concentrations both horizontally and vertically, atmospheric absorption is neglected for radar performance assessment.

Atmospheric absorption is, however, considered in assessing FLIR performance ranges. FLIR performance is seriously reduced by rain, snow, fog, clouds, haze, and smoke. These effects are extremely difficult to predict because they depend upon particle size, density, local variations, and discontinuous altitude distributions, which are themselves difficult to predict, or even to measure. Thus, within the FLIR model, they are crudely represented by the distribution of relative humidity with altitude and a simple function of surface horizontal visibility.

While absorption reduces the signal level, it also has an additional effect upon a FLIR system. These absorbing agents later re-emit the absorbed energy in all directions. This tends to produce a "veiling" radiation, which mixes with the desired signal power, thereby reducing the FLIR system sensitivity.

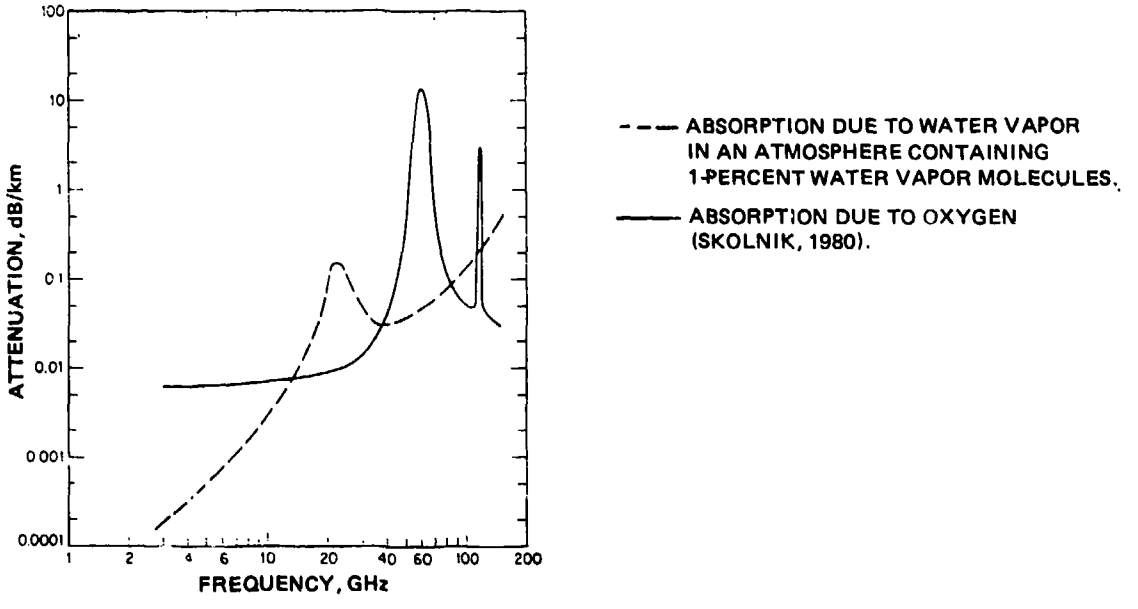

Figure 3. Attenuation of electromagnetic energy by atmospheric gases in an atmosphere at 76-cm pressure.

2.5 SCATTERING

Scattering is the diffusing of radiation in all directions within the atmosphere. For the purposes of TESS and IREPS, scattering takes two forms, based upon the mechanism causing the scattering.

The first mechanism of scattering is by small particles suspended in the atmosphere. This type of scattering tends to be a broadband phenomenon. Figure 4 is a typical aerosol scattering curve. Scattering varies as a function of the ratio of the particle diameter to the wavelength of radiation. The falloff at greater wavelengths is related to the fact that larger particles tend to fall out of the air; hence, long-IR and millimeter-wave radiation is much less affected by haze, smoke, etc., than shorter wavelengths.

Aerosol scattering has an additional effect upon FLIR systems. Since any absorbed energy is re-radiated by the absorbing agent, this radiant power may be scattered "into" as well as "out of" the line of sight of a FLIR sensor. This scattering "into" enhances the "veiling" of radiation, reducing the FLIR system's sensitivity.

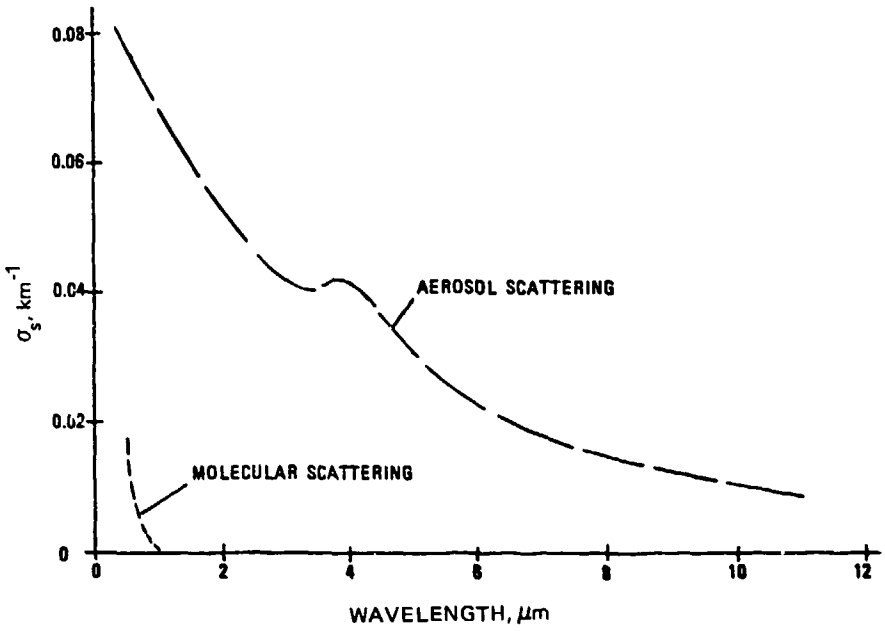

Figure 4. Typical aerosol scattering effect (Greening, 1987).

A second mechanism of scattering is by small inhomogeneities within the atmosphere which bend the energy away from the path of the radar beam. For ranges much beyond the horizon, this type of scattering, called troposcatter, becomes the dominating factor in determining detection ranges. The loss of energy from the radar beam is so great, in fact, that it is difficult for any known radar system to detect targets. Scattering is also an important consideration for certain communications systems and electronic support measures (ESM) system where the receivers are much more sensitive than a normal radar receiver.

3.0 REFRACTION

3.1 INDEX OF REFRACTION

The term refraction refers to the property of a medium to bend an electromagnetic wave as it passes through the medium. The degree of bending is determined by the index of refraction, n, defined as the velocity, c, of propagation in free space (away from the influence of the earth or other objects) to the velocity, v, in the medium.

$$n = \frac{c}{v} \tag{4}$$

3.2 STRUCTURE AND CHARACTERISTICS OF THE EARTH'S ATMOSPHERE

The earth's atmosphere is a collection of many gases together with suspended particles of liquid and solids. Excluding variable components such as water vapor, ozone, sulfur dioxide, and dust, the gases of nitrogen and oxygen occupy about 99 percent of the volume, with argon and carbon dioxide being the next two most abundant gases. From the earth's surface to an altitude of approximately 80 kilometers, mechanical mixing of the atmosphere by heat-driven air currents evenly distributes the components of the atmosphere. At about 80 kilometers, the mixing decreases to the point where the gases tend to stratify in accordance with their weights.

The lower, well-mixed portion of the atmosphere is called the homosphere; while the higher, stratified portion is called the heterosphere.

The molecules of atmospheric gases are composed of atoms which consist of a positively charged nuclei surrounded by shells of negatively charged electrons. In a stable atom, these charges are balanced. Should a stable atom absorb electromagnetic radiation or collide with another atom, the electric balance may be upset such that an electron may be "knocked off" or separated from the atom. This process produces a positively charged atom (an ion) and a free floating electron. The separation of charged particles is known as "ionization." The number of free electrons per unit volume is called "electron density" which is a measure of the extent of ionization. Because the peak of the ionization process occurs within the heterosphere, the heterosphere is commonly referred to as the "ionosphere."

Since human activity is confined to the lowest part of the homosphere, it is convenient to divide the homosphere into layers so one may talk about the lowest part or the highest part. By using temperature gradients, the homosphere may be divided into three layers: the troposphere, closest to the ground; the stratosphere, lying above the troposphere; and the mesosphere, lying between the stratosphere and the heterosphere.

The refractive index is quite different in the ionosphere and the troposphere; therefore, electromagnetic wave propagation through each region is examined separately.

3.2.1 Ionosphere

3.2.1.1 Ionization.

As mentioned above, a molecule of gas may be split into atoms or an electron may be separated from an atom only with a specific amount of energy. In other words, a given gas absorbing radiation will be ionized if the radiation frequency is in excess of a certain critical value. This value is known as ionization frequency or ionization wavelength.

While the sun continues to radiate energy at all wavelengths of the electromagnetic spectrum, a radiation peak occurs within the ultraviolet wavelengths. These ultraviolet wavelengths contain the necessary energy to ionize the nitrogen and oxygen of the heterosphere, thereby producing atomic nitrogen and oxygen, ions of nitrogen and oxygen, and free electrons. In addition to electromagnetic radiation, the sun also produces its own ions of hydrogen and helium and electrons which are projected into space with speeds near that of light. This flow of ions and free electrons from the sun is known as the solar wind. These ions and free electrons have sufficient energy (velocity) so that their collision with the nitrogen and oxygen of the earth's heterosphere will also produce ionization.

The output of radiation and solar wind is not constant with time. The intensity of the radiation and solar wind is directly proportional to the intensity of sunspots, solar flares, and other solar-magnetic disturbances. Other agents, such as electromagnetic radiation from stars and cosmic dust entering the earth's atmosphere, also play a part in ionizing the heterosphere but not to the extent of the sun.

With a constant input of radiation over time, the entire atmosphere should become ionized. This does not happen however. Only a portion of the earth's atmosphere is receiving radiation at any time (the portion facing the sun). In their travels, the free electrons, ions, molecules, and atoms will collide with each other, recombining back into various forms of stable atoms or molecules. The rate of recombination is inversely proportional to the square of the electron density. Thus, the rate of recombination will be very quick with the fall of night and will slow down as the night progresses.

The peak effect of ionization does not occur at all altitudes of the atmosphere. At the earth's surface, significant ionization does not occur since the ionizing radiation is expended before it penetrates the entire depth of the atmosphere. At the top of the atmosphere, even though the radiation level is at its peak, there are so few atoms present that even if they all were ionized, the effect they would produce would be

inconsequential. Exploration of the heterosphere with rockets, satellites, and dispersion interferometers have shown that there is a rather well-defined region or layer, called the F2 layer, and several rather ill-defined regions or layers, called the D, E, and F1 layers, where electron density shows a peak. These layers are ill-defined in altitude and intensity because, as discussed earlier, electron density depends upon solar activity (flares and storms), duration of radiation (day versus night), and the recombining activity of the ions and free electrons. For example, after nightfall, the D layer disappears because of the high rate of recombination.

3.2.1.2 Refractive Index of an Ionized Medium in the Presence of a Permanent Magnetic Field.

The permanent geomagnetic field of the earth makes the ionized gases of the heterosphere an anisotropic medium, that is, one having different properties in differing directions. The geomagnetic field exerts an additional force (the Lorentz force) upon a traveling electron, causing it to travel not in a straight line but in a complicated spiral in a plane which is normal (at right angles) to the direction of propagation. Therefore, a linearly polarized wave, spiraling in relation to the geomagnetic field, will be split into two waves: an ordinary wave where the electric field is parallel to the geomagnetic field, and an extraordinary wave where the electric field is at right angles to the geomagnetic field. The ordinary wave will propagate as though no magnetic field were present. The extraordinary wave, however, is accelerated by the magnetic field, thus propagates with a greater velocity than the ordinary wave. With a change of velocity, the frequency of the extraordinary wave also changes. The index of refraction, equation 4, defined in terms of velocity, now becomes a function of frequency.

Waves traveling with variable velocities, variable energy losses occurring by collisions between different sized particles, and the variable energy absorption associated with ordinary and extraordinary waves further complicate the refractive index within the ionosphere.

3.2.1.3 Refraction and Reflection of Electromagnetic Waves in the Ionosphere.

Since the refractive index within the ionosphere is frequency dependent, only a wave with a frequency below a critical value (approximately 20 megahertz) will be refracted within the ionosphere. Wave propagating from a nonionized atmosphere (originating from the earth's surface) into one which is ionized and stratified, will bend in the direction of greatest density. If its penetration angle is sufficiently shallow, it will achieve a path which is parallel to the stratum. If, however, the penetration angle is steep, the wave will escape through the ionosphere into space. Once the wave path becomes parallel to the stratum, it is not obvious why a wave will return to a region of lesser density, or in other words, why a wave will return to the earth's surface. It has been found that as the electron density increases with height and the vertical gradient of the density is not less than a certain critical value,

the propagating wave will be *reflected* back toward the earth's surface. In addition to electron density, the reflection of an electromagnetic wave is a function of frequency. Therefore, as electron densities change with changing solar activities, the frequency of a reflected wave will change. Waves of different frequencies will be reflected at different altitudes within the ionosphere resulting in different paths as shown in figure 5, which illustrates the paths of the ordinary and extraordinary wave. For long-range, over-the-horizon, high frequency (HF) communications, it is generally necessary to continually shift the frequencies transmitted to insure continuous communications.

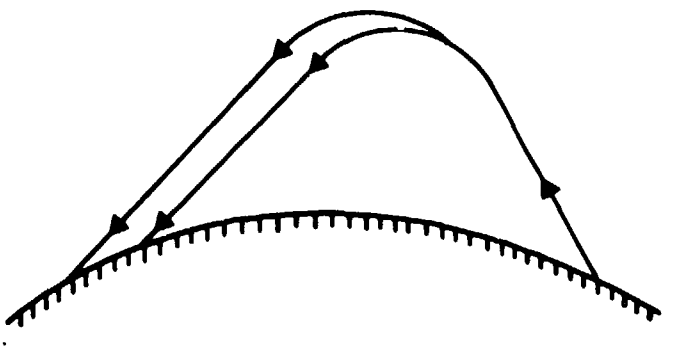

Figure 5. Path of ordinary and extraordinary waves.

TESS and IREPS are designed to assess the performance of radars, ultrahigh frequency (UHF) communications, and electronic warfare (EW) systems. Because the frequencies of these systems are above those affected by the ionosphere, propagation within the ionosphere is not considered. The Propagation Forecasting Terminal (PROPHET) system developed at the Naval Ocean System Center (NOSC) does consider propagation through the ionosphere. A description of the PROPHET system and its use is presented in NOSC Technical Document 848.

3.2.2 Troposphere

Within the troposphere, the process of ionization does not take place to a significant degree. Therefore, the magnetic field of the earth does not affect electromagnetic wave propagation. The troposphere is an isotropic medium, that is, one having the same properties in differing directions. Thus, the frequency dependency is removed from the refractive index. Throughout the entire homosphere, the atmosphere's effects upon wave propagation are the same.

The troposphere extends from the earth's surface to an altitude of 8 to 10 kilometers at polar latitudes, 10 to 12 kilometers at middle latitudes, and up to 18 kilometers at the equator. It is characterized by a temperature decrease with height. The point at which the temperature ceases to decrease with height is known as the tropopause. The average vertical temperature gradient of the troposphere varies between 6 and 7°C per kilometer.

The concentrations of gas components of the troposphere vary little with height, except for water vapor. The water vapor content of the troposphere comes from evaporation of water from oceans, lakes, rivers, and other water reservoirs. Differential heating of land and ocean surfaces produces vertical and horizontal wind circulations which distribute the water vapor throughout the troposphere. The water vapor content of the troposphere rapidly decreases with height. At an altitude of 1.5 kilometers, the water vapor content is approximately half of the surface content. At the tropopause, the content is only a few thousandths of what it is at the surface.

In 1925, the International Commission for Aeronavigation defined the "international standard atmosphere." This is a hypothetical atmosphere having an arbitrarily selected set of characteristics reflecting an average condition of the real atmosphere. Assessment systems such as TESS and IREPS will present propagation resulting from standard conditions and propagation which results from nonstandard conditions.

3.3 REFRACTIVITY

The normal value of n for the atmosphere near the earth's surface varies between 1.000250 and 1.000400. For studies of propagation, the index of refraction is not a very convenient number; therefore, a scaled index of refraction, N, called refractivity, has been defined. At microwave frequencies, the relationship between the index of refraction n and refractivity N for air which contains water vapor is given as:

$$(n-1)\ 10^6 = N = \frac{77.6\ p}{T} + \frac{3.75 \times 10^5\ e}{T^2} \qquad (5)$$

where e = partial pressure of water vapor in millibars or

$$e = -\frac{rh}{100} \times 6.105 \exp(a) \qquad (6)$$

$$a = 25.22 \times \frac{(T - 273.2)}{T} - 5.31 \times \log_e \left(\frac{T}{273.2}\right) .$$

p = atmosphere's barometric pressure in millibars

T = atmosphere's absolute temperature in degrees Kelvin

rh = atmosphere's relative humidity in percent

Thus, the atmospheric refractivity near the earth's surface would normally vary between 250 and 400 N units.

Since the barometric pressure and water-vapor content of the atmosphere decrease rapidly with height while the temperature decreases slowly with height, the index of refraction and, therefore, refractivity normally decreases with increasing altitude.

3.4 REFRACTION IN THE TROPOSPHERE

3.4.1 Standard Refraction

In free space, an electromagnetic wave will travel in a straight line because the index of refraction is everywhere the same. Within the earth's atmosphere, however, the velocity of the wave is less than that of free space and the index of refraction decreases with increasing altitude. Therefore, the propagating wave will be bent downward from a straight line. It is more convenient, however, to compute refractivity in terms of waves traveling in straight lines. This may be approximated by replacing the actual earth's radius with one approximately four-thirds as great (often referred to as the effective earth's radius) and replacing the actual atmosphere by one that is homogeneous in nature. The refractivity in this orientation is called modified refractivity and is expressed in M units where the relationship between N and M units is

$$M = N + 0.157\,h \qquad \text{for altitude h in meters}$$
$$M = N + 0.048\,h \qquad \text{for altitude h in feet.} \qquad (7)$$

The refraction occurring in the standard troposphere is referred to as "standard refraction." The refractivity and modified refractivity profiles for this condition are illustrated in figure 6. Figure 7 shows the wave path under various refractive conditions.

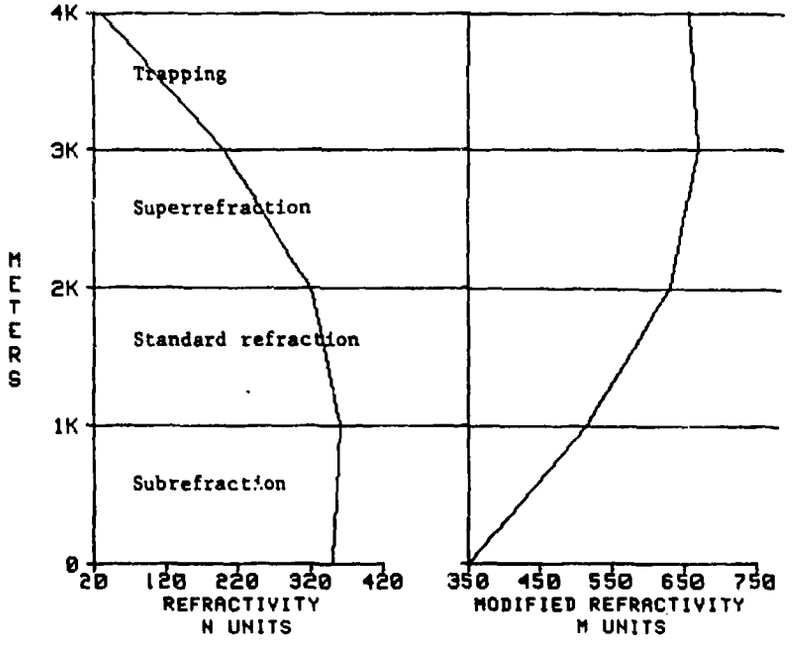

Figure 6. Refractivity N and modified refractivity M versus altitude for various refractive conditions.

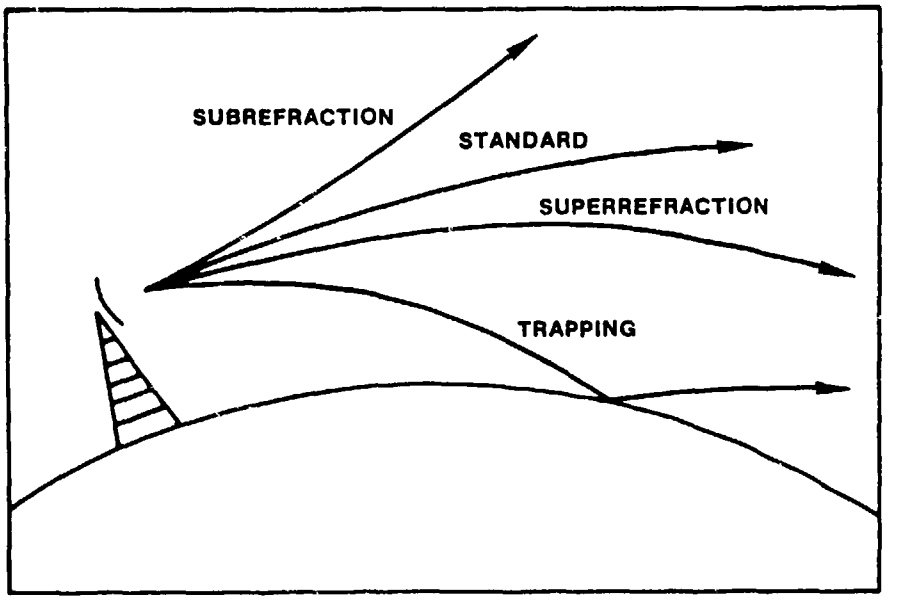

Figure 7. Wave paths for various refractive conditions.

3.4.2 Subrefraction

If the motions of the atmosphere produce a situation where the temperature and humidity distribution creates an increasing value of N with height, the wave path would actually bend upward and the energy would travel away from the earth. This is termed negative refraction or subrefraction. Although this situation rarely occurs in nature, it still must be considered when assessing electromagnetic system's performance. Figures 6 and 7 illustrate the refractivity profiles and the wave path for subrefraction.

3.4.3 Superrefraction

As discussed in section 3.4.1, a standard atmosphere has a refractivity gradient which causes waves to bend downward from a straight line. If the troposphere's temperature increases with height (temperature inversion) and/or the water vapor content decreases rapidly with height, the refractivity gradient will decrease from the standard (equation 5). The propagating wave will be bent downward from a straight line more than normal. As the refractivity gradient continues to decrease, the radius of curvature for the wave path will approach the radius of curvature for the earth. The refractivity gradient for which the two radii of curvature are equal is referred to as the "critical" gradient. At the critical gradient, the wave will propagate at a fixed height above the ground and will travel parallel to the earth. Refraction between the normal and critical gradients is known as superrefraction. Figures 6 and 7 illustrate the refractivity profiles and the wave path for superrefraction.

3.4.4 Trapping

Should the refractivity gradient decrease beyond the critical gradient, the radius of curvature for the wave will become smaller than that of the earth's and the wave will either strike the earth and undergo surface reflection, or enter a region of standard refraction and be refracted back upward, only to reenter the area of refractivity gradient which causes downward refraction. This refractive condition is called trapping since the wave is confined to a narrow region of the troposphere. The common term for this confinement region is a tropospheric "duct" or a tropospheric "waveguide." It should be noted that a tropospheric waveguide is not a waveguide in the true sense of the word since there are no rigid walls which prevent the escape of energy from the guide. Figures 6 and 7 illustrate the refractivity profiles and the wave path for trapping.

Table 2 summarizes the refractivity gradients and their associated refractive conditions.

Table 2. Relation of N and M gradients to refraction.

	N–Gradient	M–Gradient
Trapping	$\leq$ −157 N/km	$\leq$ 0 M/km
	$\leq$ − 48 N/kft	$\leq$ 0 M/kft
Superrefractive	−157 to − 79 N/km	0 to 79 M/km
	− 48 to − 24 N/kft	0 to 24 M/kft
Standard	− 79 to 0 N/km	79 to 157 M/km
	− 24 to 0 N/kft	24 to 48 M/kft
Subrefractive	> 0 N/km	> 157 M/km
	> 0 N/kft	> 48 M/kft

4.0 ELECTROMAGNETIC WAVE PROPAGATION MECHANISMS

4.1 STANDARD PROPAGATION

Standard propagation mechanisms are those propagation mechanisms and processes that are independent of the existing refractivity conditions. These propagation mechanisms are free-space propagation, optical interference (or surface reflection), diffraction, and tropospheric scatter.

4.1.1 Free-Space Propagation

The simplest case of electromagnetic wave propagation is the transmission of a wave between a transmitter and a receiver in free space. Free space is defined as a region whose properties are isotropic, homogeneous, and loss-free, i.e., away from the influences of the earth's atmosphere. In free space, the electromagnetic wave front spreads uniformly in all directions from the transmitter. If a particular point on a wave front is followed over time, the collection of point positions would define a ray. The ray would coincide with a straight line from the transmitter to the receiver. Often wave propagation is illustrated with the aid of rays such as in figure 7.

While the total amount of energy transmitted does not vary, i.e., no losses to absorption, etc., the energy is distributed over an ever enlarging surface. Thus the energy level along any one ray decreases inversely with the square of the sphere's radius. This is called the free-space path loss. The power density, (W/m^2), over a sphere at any point in free-space, P_a is

$$P_a = \frac{P_t}{4\pi r^2} \tag{8}$$

where P_t is the power radiated by the transmitter in watts and r is radius of the sphere in meters.

In free space, the power density at a loss-free, isotropic receiving antenna is the power density over the entire sphere's surface times the area of the sphere covered by the receiver antenna, also called the antenna's effective aperture, A_e. The effective aperture is related to the wavelength (λ) of radiation by

$$A_e = \frac{G \lambda^2}{4\pi} \tag{9}$$

where G is the antenna's gain (section 5.3). For a loss-free, isotropic antenna, G is unity. Thus, the power at the receiver, P_r, is

$$P_r = P_a A_e = \frac{P_t \lambda^2}{(4 \pi r)^2} \tag{10}$$

The free-space path-loss is expressed as

$$\text{Loss}_{fs} = \frac{P_t}{P_r} = \frac{(4\pi r)^2}{\lambda^2} \qquad (11)$$

where r and λ are in the same units. Sometimes the free-space path loss is expressed in logarithmic terms (by using equation 3) and in frequency ($f = c/\lambda$). Thus

$$\text{Loss}_{fs} = 32.44 + 20\log_{10}(r) + 20\log_{10}(f) \qquad (12)$$

for r in kilometers and f in MHz.

4.1.2 Optical Interference and Surface Reflection

When an electromagnetic wave strikes a nearly smooth, large surface, such as the ocean, a portion of the energy is reflected from the surface and continues propagating along a path that makes an angle with the surface equal to that of the incident ray, as illustrated by figure 8.

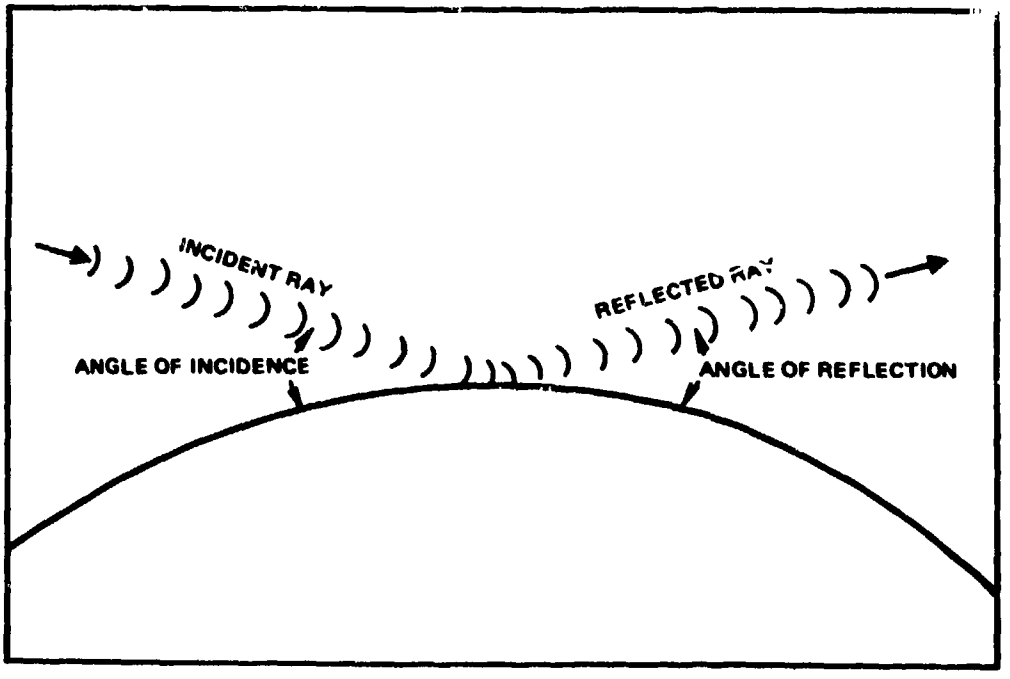

Figure 8. Incident ray and reflected ray illustrating equal angles of reflection.

The strength of the reflected wave is determined by the reflection coefficient, a value which depends upon the frequency and polarization of radiation, the angle of incidence, and the roughness of the reflecting surface.

Typical values of the reflection coefficient for shallow incidence angles and smooth seas are 0.99 (i.e., the reflected wave is 99 percent as strong as the incidence wave). As the wind speed increases, the ocean surface grows rougher and the reflection coefficient can decrease to about 0.15. For a transmitter near the surface, the reflection process results in two paths to a receiver within the line of sight, as illustrated by figure 9.

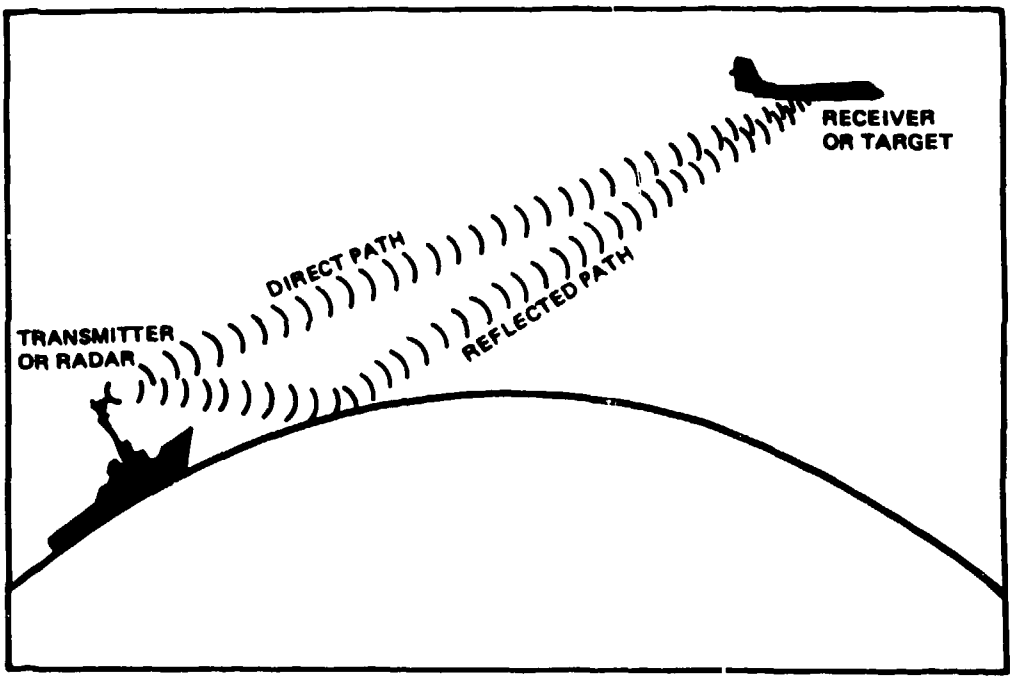

Figure 9. Surface-to-air geometry illustrating direct and sea-reflected paths.

Not only is the magnitude of the reflected wave reduced, but the phase of the wave is also altered. For horizontally or vertically polarized waves at low grazing angles, there is a 180-degree phase change upon reflection. Whenever two or more wave trains traveling over different paths intersect at a point in space, they are said to interfere. If two waves arrive at the same point in phase, they constructively interfere and the electric field strength is greater than either of the two component waves taken alone. If the two waves arrive together out of phase, they destructively interfere and the resultant field strength is weakened.

As the geometry of figure 9 changes, the relative lengths of the direct path and reflected path also change, which results in the direct and reflected wave arriving at the receiver in varying amounts of phase difference. The received signal strength, which is the vector sum of the signal strengths of the direct and reflected wave, may vary up to 6 dB above and 20 dB or more below the free-space value. This fluctuation in power is known as "fading."

4.1.3 Diffraction

Energy tends to follow along the curved surface of an object. Diffraction is the process by which the direction of propagating radiation is changed so that it spreads into the geometric shadow region, figure 10, of an opaque or refractive object which lies in the radiation field. In the earth-atmosphere system, diffraction occurs where the straight-line distance between the transmitter and receiver is just tangent to the earth's surface. This point of tangency with the earth is referred to as the geometrical, or optical, horizon. This is also the radar horizon and is given by equation 13.

$$\text{horizon} = 3.572 \left((k H_t)^{.5} + (k H_r)^{.5} \right) \qquad (13)$$

where k is the effective earth radius and H_t and H_r are the electromagnetic system's transmitter and receiver/target heights, respectively, in meters.

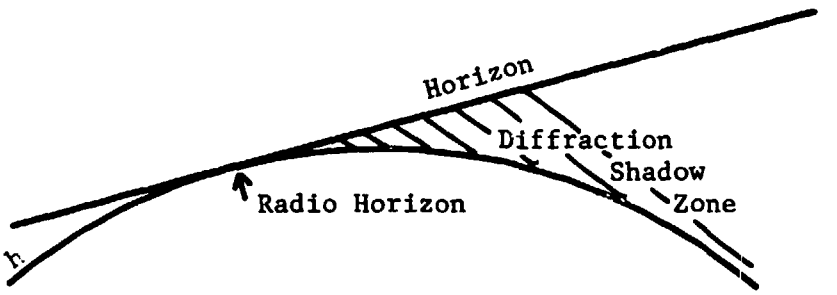

Figure 10. Radar horizon and diffraction region shadow zone.

The ability of the electromagnetic wave to propagate around the earth's curvature by diffraction is highly dependent upon frequency. The lower the frequency, the more the wave is diffracted. Diffraction, in addition to ionization, is important at very low frequencies (VLF) where it assists in providing world-wide communications. At radar frequencies the wavelength is small when compared to the earth's dimensions and little energy is diffracted. At optical frequencies or very short radar wavelengths, the optical horizon represents the approximate boundary between regions of propagation and no propagation.

The electric field strengths within the diffraction region can be determined by summing the power along all the different geometries (modes) that a wave may take, assuming the atmosphere acts like a waveguide in the diffraction region. Or in other words, finding the solution to the fundamental equation of mode theory. For a standard atmosphere, an acceptable solution may be represented by a single mode. However, at the horizon (the intermediate region between the optical region and the diffraction region), a single mode is not sufficient and the equation must be solved for a large number of possible modes. This calculation is extremely labor intensive. To speed the calculation in this intermediate region, a "bold interpolation" between the last path-loss value of the optical region and the first path-loss value in the single mode diffraction region is made.

4.1.4 Tropospheric Scatter

At ranges far beyond the horizon, the path loss is dominated by troposcatter. Propagation in the troposcatter region is the result of scattering as discussed in section 2.5. The calculation of path loss in the troposcatter region is quite easily performed by using semiempirical formulations. The rate at which the path loss increases with range, within the troposcatter region, is considerably less than the rate in the diffraction region.

4.1.5 Atmospheric Path Loss

For assessment systems such as TESS or IREPS, a system's performance in the atmosphere is often compared to its performance in free space. As seen above, the path loss (or the decrease of energy along the path from the transmitter to the receiver) is a function of path interference within the optical horizon, the diffraction of energy around the curvature of the earth, the scattering of energy in regions well beyond the horizon, and, of course, the refractive condition of the atmosphere.

A convenient form to display system performance is by plotting a performance threshold upon a path loss versus range display. Figure 11 shows a plot of path loss versus range for a 5000-MHz transmitter located 60 feet above the sea surface, a receiver at 100 feet above the sea surface, and standard refractive conditions. For comparison purposes, the path loss in free space is also illustrated. The regions are labeled to indicate the primary physical mechanism which dominates the propagation in the region, i.e., interference, diffraction, and scattering. As stated in section 4.1.2, the depth of the nulls (maximum destructive interference) and the height of the peaks (maximum constructive interference) depend very much on the surface roughness related to the wind speed. The example here is for a smooth sea surface associated with zero wind speed, but, as the wind speed increases, the path loss in the nulls would approach the free-space value. A system would be able to successfully operate at ranges where the path loss did not exceed the threshold. It would not be able to successfully operate at ranges where the path loss exceeded the threshold.

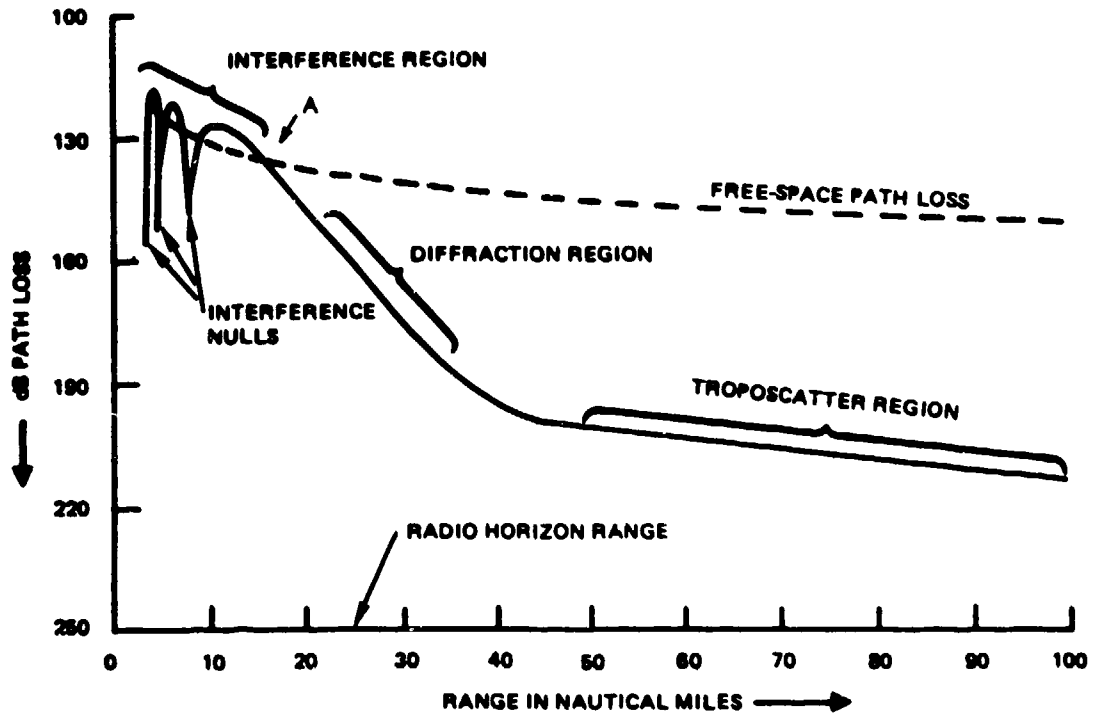

Figure 11. Path-loss curve for a 5000-MHz transmitter at 60 feet, a receiver at 100 feet above the surface, and standard refractive condition.

As discussed in section 2.5, troposcatter may be a significant method of energy propagation, particularly for communication and ESM intercept ranges. Figure 12 illustrates a plot of free-space path loss, standard atmosphere path loss considering troposcatter, and standard atmosphere path loss without considering troposcatter. As can be seen, an ESM receiver with a threshold of 212 dB would only be able to intercept the transmitter at a range of 37 nautical miles (nmi) without the aid of troposcatter. With the aid of troposcatter propagation, however, the transmitter's signal would be intercepted at a range of 85 nmi, a very significant increase in the intercept range.

Sometimes, a more convenient form to display the performance capability of an electromagnetic system is the vertical coverage diagram, which shows those areas on a height versus range plot where the path-loss values are always less than some specified value. Figure 13 illustrates the vertical coverage diagram associated with the path loss curve of figure 11. The shaded area in the diagram represents the area in which detection or communications is expected. The display clearly shows the effects of the interference region.

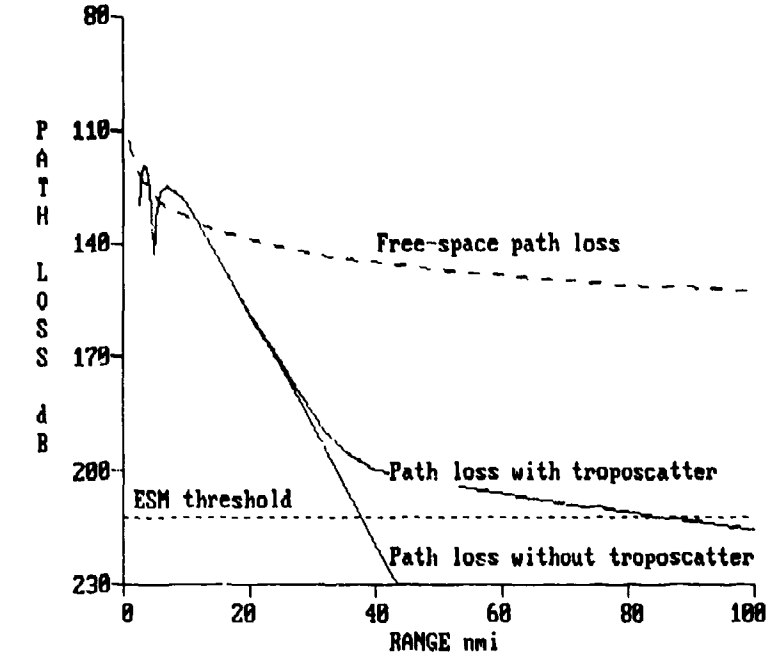

Figure 12. Free-space and standard atmosphere path loss, with and without troposcatter propagation.

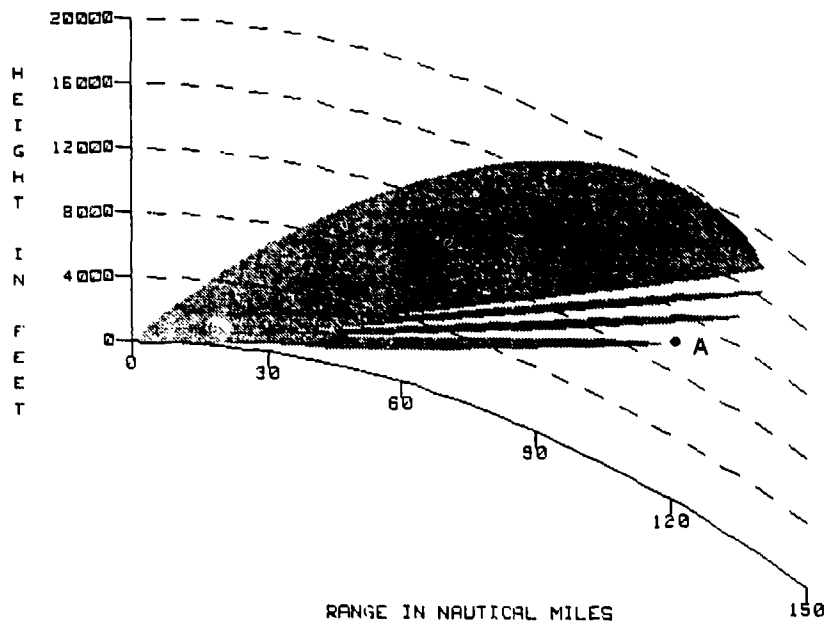

Figure 13. Coverage diagram for a 5000-MHz transmitter at 60 feet and standard refractive conditions.

The TESS/IREPS models used with the coverage and loss products for an airborne system do not include interference effects. Surface systems are the only systems in which the coverage and loss products include the effects from a sea-reflected ray. For graphics drawing convenience, a coverage display for a surface system will show three lobes of the interference pattern, starting with the lowest elevation angle. For angles above the third lobe, the spacing between lobes becomes very small on the display and only the maximum detection envelope is shown. A loss display for a surface system will show the interference null locations until the position when the spacing between the nulls is less than one-twentieth of the maximum range. At close ranges, the minimum path loss, or the interference peak, is plotted to provide an envelope to the tightly spaced null positions.

As stated above, upon reflection, a portion of the energy is propagated in the direction of initial wave motion. A portion of energy is also reflected backward toward the transmitter. This backward reflected energy is also received by the radar and may interfere with the radar's ability to distinguish a desired target. This backward reflected energy is called clutter (see section 5.2). The TESS/IREPS models do not include any effects produced by sea or land clutter in the calculation of detection ranges. This shortcoming may be of importance for air-search radars in the detection of airborne targets.

4.2 ANOMALOUS PROPAGATION

A deviation from the normal atmospheric refractivity leads to conditions of subrefraction, superrefraction, and trapping as explained in sections 3.4.2, 3.4.3, and 3.4.4 respectively. The term anomalous propagation, or nonstandard propagation, applies to any of the above listed conditions, but it is most often used when describing those conditions which lead to radar ranges or ESM intercept ranges well beyond the normal. Anomalous propagation conditions are also commonly referred to as "ducting" conditions, although the term ducting only applies to trapping refractivity gradients.

4.2.1 Subrefractive Layers

As stated in section 3.4.2, a subrefractive layer of the troposphere would cause the propagating energy to bend upward or away from a flat earth's surface, thereby leading to decreased detection ranges and shortened radio horizons. Altitude errors for height-finding radars will also become evident in a subrefractive environment.

Subrefractive layers may be found both at the earth's surface or aloft. In areas where the surface temperature is greater than 30°C and relative humidities are less than 40 percent (i.e., large desert and steppe regions), solar heating will produce a very nearly homogeneous surface layer, often several hundreds of meters thick. Since this layer is absolutely unstable, the resultant convective processes tend to concentrate any available moisture near the top of the layer. This in turn creates a

positive N gradient or subrefractive statum aloft. This layer may retain its subrefractive nature into the early evening hours, especially if a radiation inversion develops, trapping the water vapor between two stable layers.

For areas with surface temperatures between 10 and 30°C and relative humidities above 60 percent, i.e., the western Mediterranean, Red Sea, Indonesian Southwest Pacific, etc., surface-based subrefractive layers may develop during the night and early morning hours. It is characteristically caused by advection (blowing horizontally) of warm, moist air over a relatively cooler and drier surface. While the N gradient is generally more intense than that described above, the layer is often not as thick. Similar conditions may also be found in regions of warm frontal activity.

4.2.2 Superrefractive Layers

Superrefractive conditions, as defined in section 3.4.3, are largely associated with temperature and humidity variations near the earth's surface. Inversions aloft, due to large-scale subsidence (slow sinking air) will lead to superrefractive layers aloft. Superrefractive layers will lead to increase radar detection ranges and extensions of the radio horizon.

The effects of a superrefractive layer upon a surface-based system is directly related to its height above the earth's surface. For airborne systems, the effects of a superrefractive layer depend upon the position of the transmitter and receiver relative to the layer. Both of these factors are related to the electromagnetic wave's angle of layer penetration. The steeper the penetration angle, the less of an effect the layer will have upon propagation. For example, refractive effects are practically inconsequential for penetration angles greater than 2°. Trapping is an extension of superrefraction because the meteorological conditions for both are the same. Additional features of superrefractive layers will be presented in the following section.

4.2.3 Atmospheric Ducts

As defined in section 3.4.4, a duct is a channel in which electromagnetic energy can propagate over great ranges. To propagate energy within a duct, the angle the electromagnetic system's energy makes with the duct must be small, usually less than one degree. Thicker ducts in general can support trapping for lower frequencies, but there is no simple relationship between the vertical thickness or strength of a duct and the frequencies most affected. The vertical distribution of refractivity for a given situation must be considered as well as the geometrical relationship of transmitter and receiver to the duct in order to assess the duct's effect at any particular frequency.

Ducts not only give extended radar detection, UHF communications, and ESM intercept ranges for systems within the duct, they may also have a dramatic effect upon transmitter/receiver systems which transcend duct boundaries. For example, an air target which would normally be detected may be missed if the radar is within or just below the duct and the target just above the duct. This area of reduced coverage is known as a radar or radio "hole" or shadow zone and is illustrated by figure 14. Height finding radars use the standard refractivity gradient as the basis for height calculations. Should the refractivity be anomalous, an error in height calculations will result. This is also illustrated in figure 14. It should be emphasized that although the duct acts like a waveguide for the energy, this waveguide does not have rigid and inpenetrable boundaries except for the earth's surface in the case of surface-based ducts. Therefore energy is continually "leaking" from the duct. While the energy level within a radar hole may be insufficent for radar detection, it may be sufficient for ESM intercept.

In a discussion of ducting conditions upon electromagnetic wave propagation, the usual concern is propagation beyond the normal horizon. Within the horizon, however, ducting also has an effect. Ducting can alter the normal lobing pattern caused by the interference of the direct ray and the surface-reflected ray as illustrated in figure 13. The relative phase between the direct and reflected path may be changed as well as the relative amplitudes of the two rays. The effect of the duct on the line-of-sight propagation is to reduce the angle of the lowest lobe, bringing it closer to the surface.

There are a number of meterological conditions which will lead to the creation of ducts. Should these conditions occur close to the earth's surface such that the base of the duct is located at the surface, the duct is referred to as a surface-based duct. If the base of the duct is above the surface, the duct is referred to as an elevated duct. A nearly permanent ducting mechanism created at the air-sea interface is known as the evaporation duct, which is very important for near-surface propagation paths at frequencies above 2 GHz.

Within TESS/IREPS, a complete climatological description of propagation conditions for ocean areas of the world is available within the historical electromagnetic conditions summary (which is fully described within section 10.6). This information is also available within NOSC Technical Document 573 (Revision 1). The following is a brief description of the three duct types and the meteorological conditions which lead to their creation.

4.2.4 Surface-Based Ducts

Surface-based ducts occur when the air aloft is exceptionally warm and dry in comparison with the air at the earth's surface. There are several meteorological conditions which may lead to the formation of surface-based ducts.

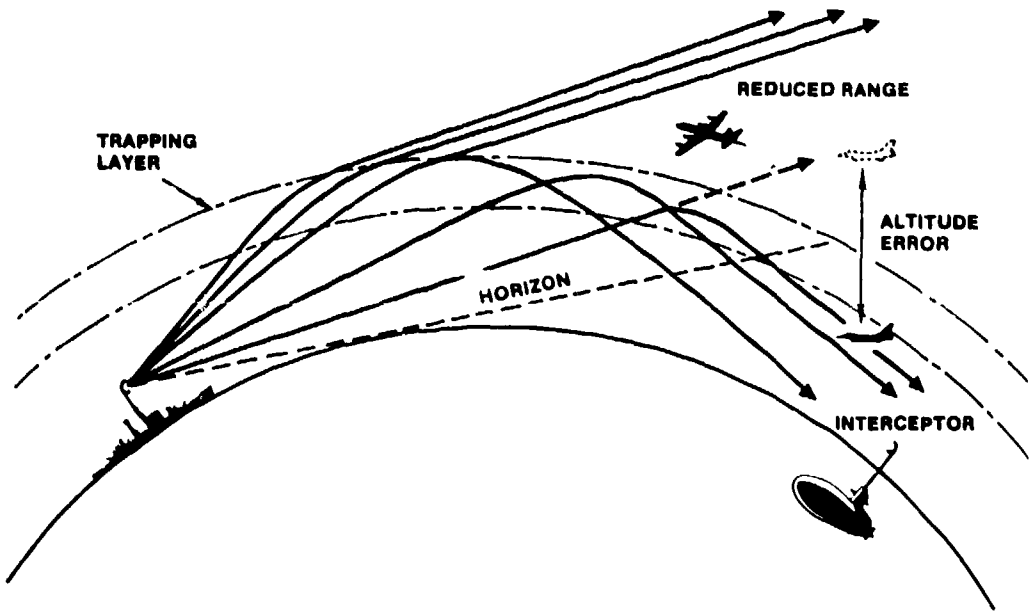

Figure 14. An example of extended detection/ESM Intercept for a surface-based radar with its associated radar hole and height error.

Over land, ducting is usually caused by radiation of heat from the earth on clear nights, especially in the summer when the ground is moist. The earth loses heat and its surface temperature falls, but there is little or no change in the temperature of the troposphere a few tens of meters above the surface. This leads to a temperature inversion at the ground with a sharp decrease in the moisture with height. Therefore, over land masses ducting is most noticeable at night and usually disappears during the warmer parts of the day. It must be noted that while ducting occurs over land, TESS/IREPS model limitations preclude the use of these assessment systems over land.

Over the ocean, the nighttime radiational cooling of the surface is not observed like that over land. Near land masses, however, warm dry continental air may be advected over the cooler water surface. Examples of this type of advection are the Santa Ana of southern California, the sirocco of the southern Mediterranean, and the shamal of the Persian Gulf. This will lead to a temperature inversion at the surface. In addition, moisture is added to the air by evaporation, producing a moisture gradient to strengthen the ducting conditions. Surface-based ducts tend to be on the leeward side of land masses and may occur both during the day or at night. In addition, surface-based ducts may extend over the ocean for several hundred kilometers and may be very persistent (lasting for days).

Another method of producing surface-based ducting conditions is by divergence (spreading out) of relatively cool air under a thunderstorm. While this method may not be as frequent as the other methods, it may still enhance surface propagation during the thunderstorm activity, usually on the order of a few hours.

With the exception of thunderstorm conditions, surface-based ducting is associated with fair weather, with increased occurrence of surface-based ducts during the warmer months and in more equatorial latitudes. Anytime the troposphere is well mixed, such as with frontal activity or with high wind conditions, surface-based ducting is decreased.

Assessment of the surface-based duct can be made with a standard radiosonde or with a microwave refractometer. A detailed discussion of these measurement techniques and associated problems is contained within sections 10.2 and 10.3. Figure 15 illustrates the refractivity and modified refractivity profile versus altitude for a surface-based duct. Of particular note is the distinction between the actual layer of the troposphere with the trapping gradient and the resulting duct.

Due to the lack of sea-surface or land clutter modeling, for surface-based ducts the actual detection capability at some ranges for air targets flying just above the duct may be reduced.

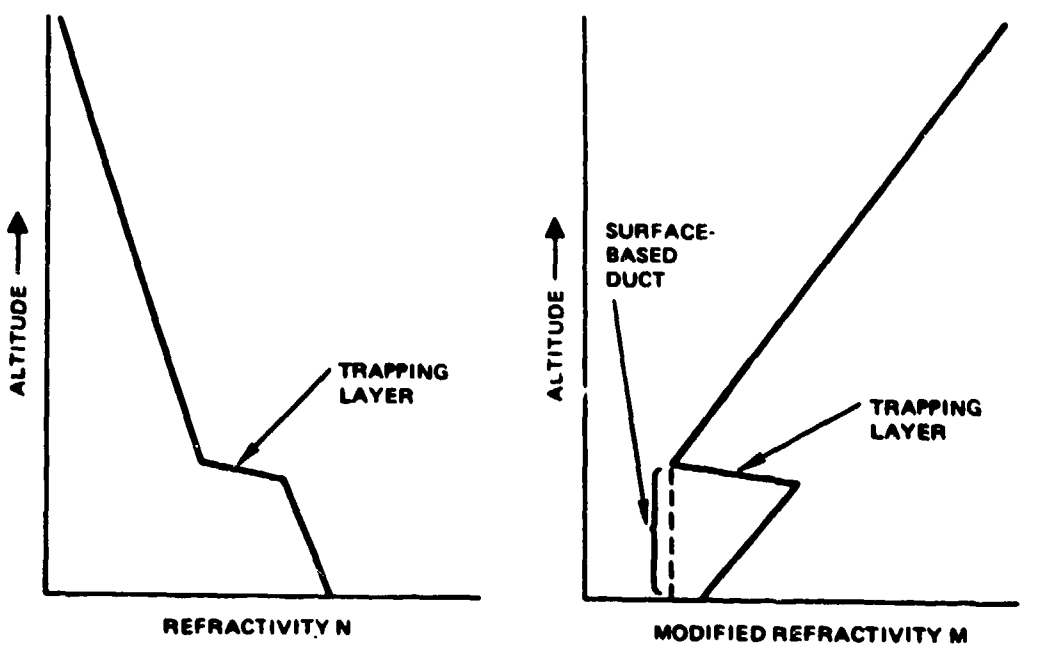

Figure 15. Refractivity N and modified refractivity M versus altitude for a surface-based duct created by an elevated trapping layer.

4.2.5 Elevated Ducts

Great semipermanent surface high-pressure systems, centered at approximately 30°N and 30°S latitudes, cover the ocean areas of the world. Poleward of these systems lay the midlatitude westerly winds and equatorward, the tropical easterlies or the "tradewinds." Within these high-pressure systems, there is large-scale subsidence of air which is heated as it undergoes compression. This leads to a layer of warm, dry air overlaying a cool, moist layer of air (often called the marine boundary layer). The resultant inversion is referred to as the tradewind inversion and may create a strong ducting condition at the top of the marine boundary layer. Elevated ducts may vary from a few hundreds meters above the surface at the eastern part of the tropical oceans to several thousand meters at the western part. There is also a general decrease in refractivity from east to west. For example, along the southern California coast, elevated ducts occur an average of 40 percent of the time with an average top elevation of 600 meters. Along the coast of Japan, elevated ducts occur an average of 10 percent of the time with an average top elevation of 1500 meters.

It should be noted that the meteorological conditions necessary for a surface-based duct are the same as those for an elevated duct. In fact, a surface-based duct may slope upward to become an elevated duct as warm, dry continental air glides over cool, moist marine air. The tradewind inversion may also intensify, thereby turning an elevated duct into a surface-based duct.

Assessment of the elevated duct can be made with a standard radiosonde or with a microwave refractometer. A detailed discussion of these measurement techniques and associated problems is contained within sections 10.2 and 10.3. Figure 16 illustrates the refractivity and modified refractivity profiles versus altitude for an elevated duct.

The TESS/IREPS models account for low-elevated ducts and surface-based ducts provided the transmitter or radar antenna is within the duct. The models do not, however, properly account for the over-the-horizon regions for low-elevated ducts when the bottom of the duct is just above the transmitter or radar antenna. The calculated ranges for the coverage display will generally be less, and the path-loss values for the loss display will be greater than the corresponding actual ranges and path-loss values. The error becomes less the higher the elevated duct is above the transmitter or antenna and should be insignificant when the separation exceeds a few thousand feet. The interference region calculations are correct for low-elevated ducts.

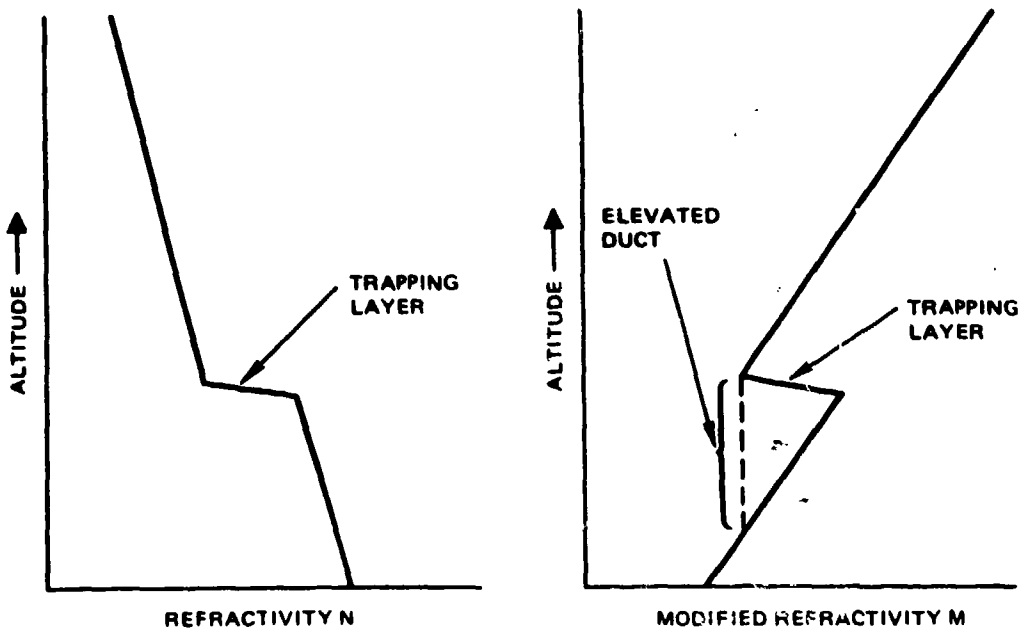

Figure 16. Refractivity N and modified refractivity M versus altitude for an elevated duct created by an elevated trapping layer.

4.2.6 Evaporation Ducts

As can be seen from equation 5, a change in the moisture distribution without an accompanying temperature change can also lead to a trapping refractivity. The air in contact with the ocean's surface is saturated with water vapor. A few meters above the surface, the air is not usually saturated so there is a decrease of water vapor pressure from the surface to some value well above the surface. This decrease in water vapor pressure tends to be logarithmic, figure 17, leading to a logarithmic decreasing refractive index. The duct which results is known as an evaporation duct.

Evaporation ducts exist over the ocean, to some degree, almost all of the time. The height varies from a meter or two in northern latitudes during winter nights to as much as 40 meters in equatorial latitudes during summer days. On a world average, the evaporation duct height is approximately 13 meters. It should be emphasized that the evaporation duct "height" is not a height below which an antenna must be located in order to have extended propagation, but a value which relates to the duct's strength or its ability to trap radiation. The duct strength is also a function of wind velocity. Stronger winds generally result in stronger signal strengths (or less propagation loss) than do weaker winds.

To illustrate the concept of a variable evaporation duct height effect upon a fixed height antenna, figure 18 shows the relationship between detection range and evaporation duct height for a C-band surface-search radar. The radar antenna in this case is at 33.5 meters above the sea surface and the target is a ship of destroyer size. Both multimode and single-mode model (that of TESS/IREPS) behavior is shown.

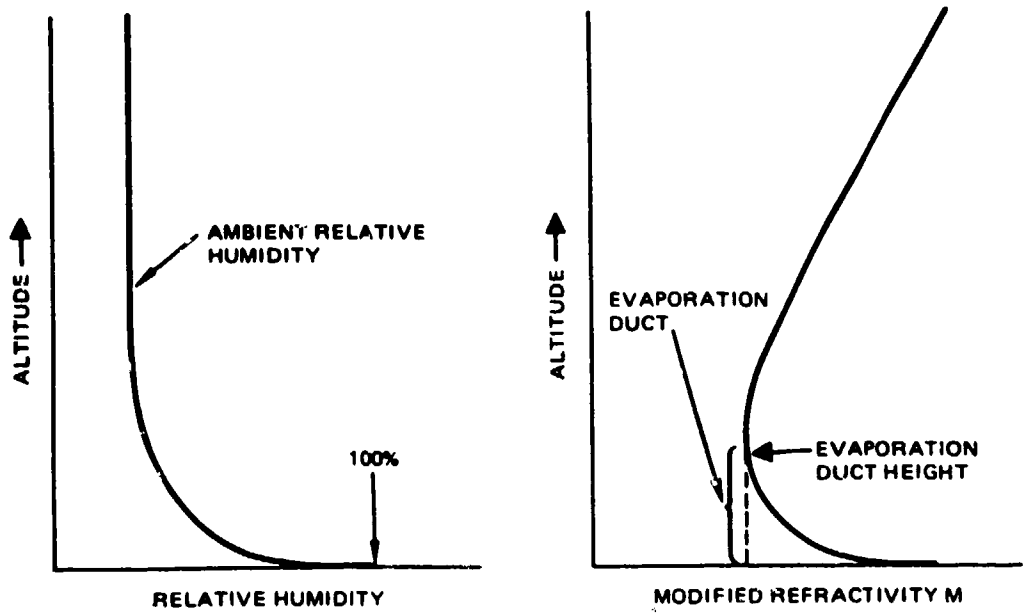

Figure 17. Relative humidity and modified refractivity M versus altitude for an evaporation duct.

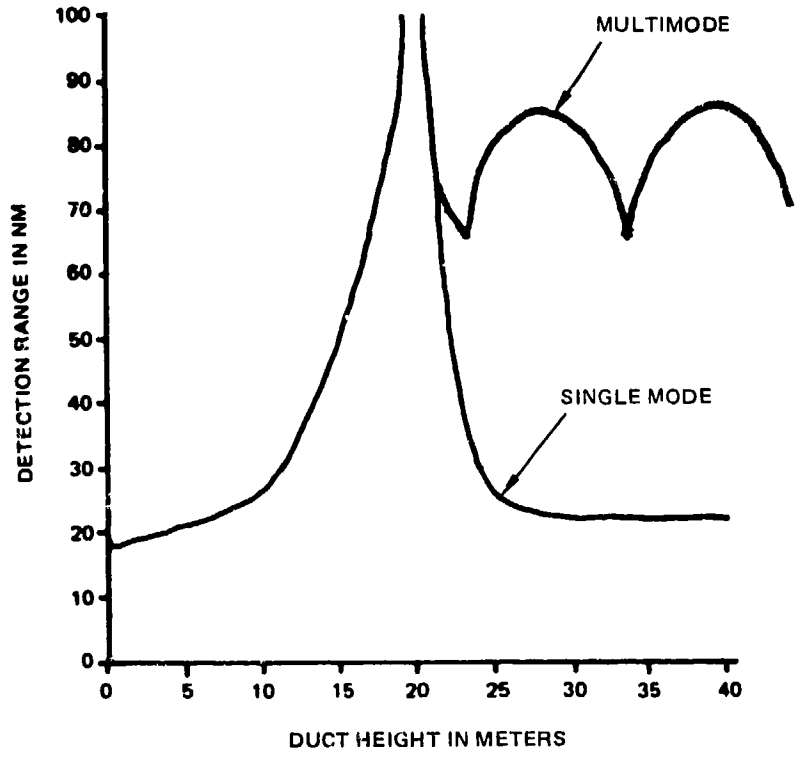

Figure 18. Detection range versus evaporation duct height for a C-band radar with an antenna height of 33.5 meters and 90-percent probability of detection of a destroyer-sized surface target.

From figure 18, it can be seen that for an evaporation duct height of zero, the detection range is approximately 19.5 nmi (corresponding to the normal radar horizon). As the evaporation duct height increases, the detection range increases until the duct height reaches approximately 19 meters. As the duct height increases beyond 19 meters, the detection range decreases until a minimum of approximately 26 nmi is reached. The detection range decrease between the multimode and single-mode model is due to the interaction between the height-gain of the antenna and the attenuation rate. This interaction exaggerates the actual modal interference effects.

Since the evaporation duct is much weaker than the surface-based duct discussed in section 4.2.4, its ability to trap energy is highly frequency dependent. Generally, the evaporation duct is only strong enough to affect electromagnetic systems above 2 GHz. The peak in detection range of figure 18 would occur at higher duct heights for lower frequencies and at lower duct heights for higher frequencies.

The proper assessment of the evaporation duct can only be performed by making surface meteorological measurements and inferring the duct height from the meteorological processes occurring at the air/sea interface. The evaporation duct height cannot be measured using a radiosonde or a microwave refractometer. With the advent of newer, high-resolution sondes which may be lowered to the surface from a ship, the impression is given that the evaporation duct may be measured directly. For practical applications, however, this impression is false and a direct measurement should not be attempted. Due to the turbulent nature of the troposphere at the ocean surface, a refractivity profile measured at one time would most likely not be the same as one measured at another time, even when the two measurements are seconds apart. Therefore, any measured profile would not be representative of the *average* evaporation ducting conditions that assessment systems such as TESS/IREPS must consider. A discussion of measurement techniques and associated problems appears in section 10.1.

5.0 BASIC PRINCIPLES OF RADAR

Radar detection of a target is based on the transmission and reception of electromagnetic waves. By measuring the time required for the wave to travel to the target and return from a reflection (echo), the distance to the target can be computed. By focusing the transmitted waves into a directional beam (like that of a searchlight) and by using the same focusing principle on reception, the direction of the target can be determined, both in the horizontal plane and the vertical plane. By observing the target's change of position with time, its velocity can be computed. The radial component of the target's velocity (moving away from or toward the transmitter) can also be determined by measuring the Doppler (a shift in frequency) of the received signal relative to the transmitter signal. A radar which measures range, elevation (vertical) angle, and azimuth (horizontal) angle is called a 3D or "height-finder" radar. A radar which measures range and only one angle (usually azimuth) is called a 2D radar.

A block diagram for a simple radar system is illustrated in figure 19. It consists of a transmitter which generates power; a receiver which amplifies the weak echo signals picked up by the antenna to a level sufficient to display them; a duplexer which connects the transmitter to the antenna during the transmission of the radiated pulse and connects the receiver to the antenna during the time between radiated pulses; an antenna which concentrates the radiated power into a shaped beam which points in the desired direction and collects the echo signal for delivery to the receiver; a signal processor which evaluates the signal from the receiver; and a visual display unit which presents the information contained in the echo signal to an operator for interpretation and action.

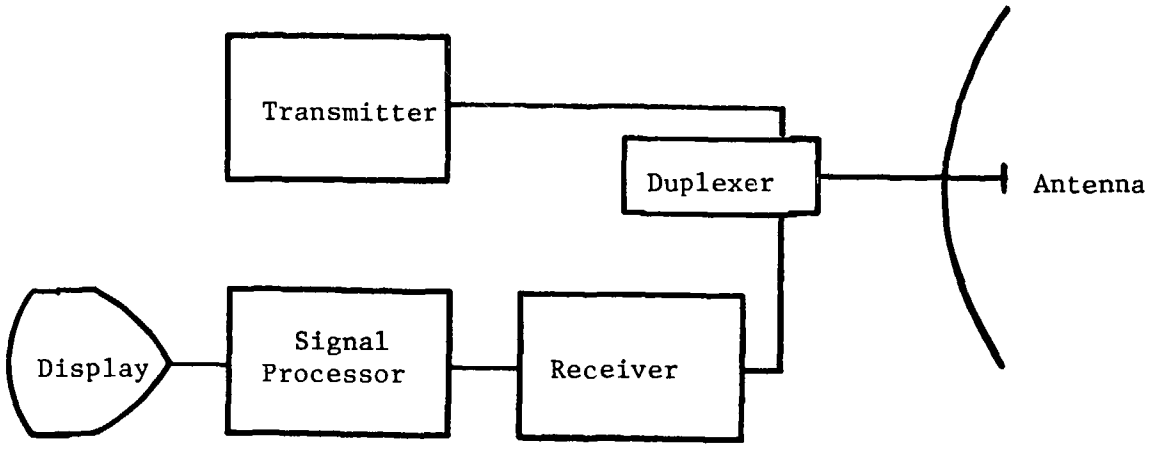

Figure 19. Block diagram for a monostatic (transmitting and receiving antenna at the same location) pulse radar system.

Since the TESS/IREPS operator must provide information specific to the radar whose performance is being assessed, it is appropriate to discuss the important parameters of the major components.

5.1 TRANSMITTERS

Over the years, many different types of transmitters have been developed to perform special demands of the radar such as moving target indication (MTI), pulse Doppler, continuous waveforms (CW), phased-array radar, electromagnetic compatibility (EMC), and electronic counter-countermeasures (ECCM). The basic demand of the transmitter, however, is to generate power in the form of shaped waves. A number of terms associated with the transmitter are of concern to the TESS/IREPS operator. These are as follows:

a. Frequency of the produced electromagnetic wave in megahertz.

b. Peak power in kilowatts. In electromagnetic systems, there are several definitions of power which may be considered. These are (1) the power output of the transmitter (peak power), (2) the power delivered by the transmitter to the antenna terminals, and (3) the power actually radiated (effective radiated power). The first and second differ by the amount of any power lost in the transmission line connecting the transmitter to the antenna. The second and third differ by the amount of power lost in the elements of the antenna itself. While the third definition is the most desirable, in addition to considering transmission and dispersive losses, the antenna gain must also be considered.

c. Pulse length in microseconds. In nature, energy is typically transmitted in the form of a simple sinewave. A radar transmitter will generate, in short bursts or pulses, this sinewave and then vary (or modulate) its frequency or phase, thereby shaping the waveform. A shaped waveform will increase the information which may be obtained from the returned echo. The pulse length is the length of time between the start and end of the pulse. Long pulse lengths have the advantage that large amounts of energy can be applied to a target in order to enhance its detectability. Long pulse lengths will lead to the longest range of detection and are, therefore, used in long-range search radars. Long pulses have the disadvantage that fine details within the return echo will be lost, thereby reducing target resolution. For example, a long pulse width may be used to detect the presence of a harbor within a coast line but will be unable to detect a pier within the harbor.

d. Pulse repetition frequency (pulse rate) in pulses per second, or in other words, how many pulses the transmitter generates each second.

e. Unambiguous range. After the transmitter sends out a pulse, it turns off and allows the receiver to "listen" for an echo. It may happen that a pulse will travel to a target and back, only to arrive while the transmitter is in the process of sending out another pulse. In this case, the pulse is not received and the target is not detected. It may also happen that the pulse will return at some time after the transmitter has sent out a second pulse. In this case, the target will appear closer to the transmitter than it really is. Echo signals received after an interval exceeding the pulse repetition period are call "multiple-time-around" echoes. Multiple-time-around echoes are often referred to as "radar ghosts." The range that a pulse can travel to and back in the time interval between pulses is known as the "maximum unambiguous range" or the "maximum instrumented range." The time between pulses is commonly "jittered" or constantly varied so that multiple-time-around echoes will bounce around in range on the display. This variation in range alerts the operator to the true nature of the target.

Often the maximum unambiguous range will not be available in publications. It may be estimated (in kilometers) with the following:

$$R_u = \frac{c}{2\ prf} \qquad (14)$$

where c = speed of light (meters per second)

prf = pulse repetition frequency (pulses per second)

f. Height-finder radars employ antennas which steer the transmitted energy upward in angle. While the power necessary to detect a target 200 miles away in the horizontal is desired, the same power directed upward at 30 degrees would detect a target at approximately 530,000 feet. Since targets are not expected at this height, the power of the transmitter is reduced as the elevation angle increases. In addition, there is a reduction in how long the receiver waits for a return echo. This has the advantage of reducing the strain on the transmitter and allows for better utilization of the radar's time.

5.2 RECEIVERS

The function of the receiver is to detect electromagnetic radiation within a certain frequency band. As in the human ear example of section 2.1, the receiver is designed to recognize a signal which exceeds a certain minimum power level. This minimum power level is the receiver's sensitivity. Any signal which exceeds the sensitivity will be registered. Not all signals with power exceeding the sensitivity are desirable, however. Nondesirable signals are referred to as noise. Noise is unwanted energy which interferes with the ability of the receiver to detect wanted signals. It may come from within the receiver itself (called receiver noise), from the environment (called environmental noise), or from a transmitter such as a radar jammer.

Receiver noise is generated from thermal radiation and mechanical motions within the receiver. A quantitative measure of the noise is the "receiver noise figure." Environmental noise is composed of cosmic radiation from our own galaxy, our sun, and other "radio stars"; blackbody radiation from atmospheric absorbers; lightning strokes; and energy radiated by manmade objects such as car ignitions, power tools, fluorescent lights, etc.

No matter where or how the noise is generated, the total noise power at the input of the receiver must be less than the power of the desired signal, or in other words, the signal-to-noise ratio must exceed a certain value, commonly called a detection threshold. Since noise is a random process (except for jamming), the signal-to-noise ratio must be described in statistical terms, that is, probabilities. The probability of detection, therefore, depends upon the probability of the desired signal power exceeding the detection threshold.

Receivers are designed with a high enough detection threshold that most receiver or environmental noise will not exceed it. On occasion, however, a particular noise will have sufficient power to exceed the threshold, resulting in a "false alarm." A tolerable rate at which false alarms occur depends upon the nature of the radar application. False-alarm probabilities for most practical radars are quite small, on the order of 10^{-6} or smaller. The TESS/IREPS operator must specify a false-alarm rate which is appropriate to the radar being used.

Many receivers also perform sophisticated signal processing to aid the operator in identifying a true target or gaining additional information about the target. In the presence of jamming for example, a receiver may employ frequency band-filters which will block out radiation of a particular frequency. There are techniques to integrate the power of a signal over time, thereby improving the signal-to-noise ratio.

Another processing technique is called "pulse compression." By modulating a wave's frequency or phase, the echo may be compressed in time by the receiver. Pulse compression achieves the benefit of high target resolution that comes from using a short pulse length yet uses the energy of a long pulse, gaining longer range detectability. In addition, pulse compression also reduces the influence of clutter.

5.3 ANTENNAS

The purpose of the radar antenna is to transfer power from the transmitter to the environment and from the environment to the receiver. During the time the transmitter is active, the antenna shapes the energy into beams and directs it toward a desired direction in space. When the transmitter turns off, the antenna collects returning energy and directs it to the receiver.

The most commonly used antenna type employs some sort of reflective surface which rotates horizontally and/or nods up and down. These antennas are referred to as parabolic-reflector antennas. The beam is formed by directing the energy from a "horn" or "feed" against a parabolic shaped reflecting surface, much like that of an automobile headlight. Newer antenna designs employ a series of fixed radiating surfaces. These surfaces are radiated electronically at different times, thereby forming the beam and changing its direction. This type of antenna is called a "phased-array" antenna.

The distribution of energy into space relative to the antenna's axis of symmetry is called the "antenna pattern," its "power pattern," or its "radiation intensity pattern." While the distribution of energy is three dimensional, it is most commonly displayed as a series of two-dimensional planar patterns. Figures 20 and 21 illustrate the antenna patterns known as sin(x)/x and cosecant-squared respectively. The major concentration of energy is along the axis of symmetry and is known as the main beam or "lobe." The beamwidth, both horizontally and vertically, is most commonly expressed in degrees. Normally the beamwidth is the width between half-power points. The additional lobe structure of the antenna pattern outside the region of the main beam is called "sidelobes." Sidelobes cause problems in target detection because they allow energy from outside the desired direction to enter the system. This leads to false targets or increased susceptibility to radar jamming.

A TESS/IREPS input is antenna type, or more correctly, antenna pattern. The choices are omni (an antenna uniformly radiating in all directions), sin(x)/x, cosecant-squared, or height-finder. While height-finder is not a radiation pattern as such, the software will construct an antenna pattern appropriate to the specific height-finder radar being assessed. In addition to the antenna pattern, the operator must also provide the vertical and horizontal beamwidths of the antenna and the vertical angle of the antenna's axis of symmetry, that is, the antenna's elevation angle.

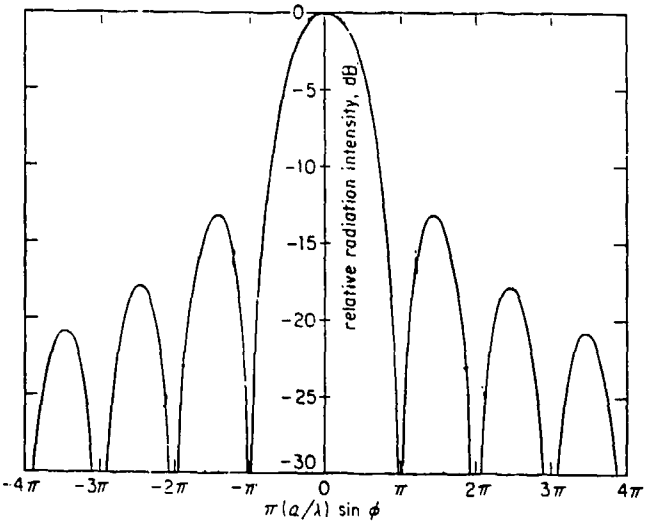

Figure 20. Sin(x)/x antenna radiation pattern (a = width of aperture in the z direction).

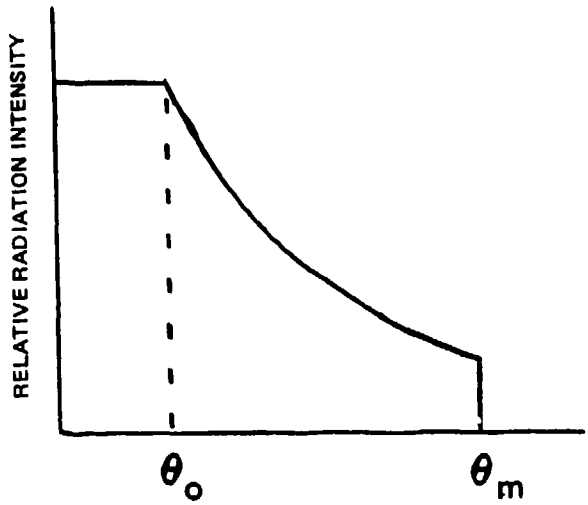

Figure 21. Cosecant-squared antenna radiation pattern (θ_0 = vertical beamwidth, θ_m = elevation angle).

The ability of an antenna to concentrate energy into a particular pattern or be more sensitive to energy arriving from a specific direction is called antenna "gain." The gain of the antenna is a function of the antenna's aperture (the physical area of the antenna face), any losses of energy from processes such as resistance and radiational heating, and the wavelength. As the aperture of the antenna increases, the wavelength of energy decreases and the antenna gain increases. Greater antenna gains, of course, mean better target detection. While most radars are fixed in size and, therefore, have corresponding fixed gains, it is possible to use the relative motion between the radar and the target to electronically increase the aperture of the radar, thereby improving the gain and resolution. These radars are called "synthetic aperture" radars (the motion of the radar is used to increase the gain or spatial resolution) or "inverse synthetic aperture" radars (the motion of the target is used to increase the spatial resolution).

As discussed in section 5.2, in order to detect a target, an acceptable signal-to-noise ratio must be obtained. One way to accomplish this is by applying more energy on the target. Applying more energy on the target may be accomplished by increasing the number of times the antenna points the beam in the target's direction. Simple rotating antennas will illuminate the target only once for each revolution of the antenna. Nonrotating antennas, such as those associated with fire-control systems, may continually illuminate the target. Sophisticated phased-array antennas are able to point a beam toward a target in addition to scanning a beam in some other predetermined search pattern. The TESS/IREPS operator must specify the number of antenna revolutions per minute for circular scanning antennas or must specify the number of energy pulses which will strike the target as the radar beam scans over the target (called hits-per-scan).

In order to take advantage of surface reflections or to help the radar "see" through weather disturbances, the direction of the electric field of the antenna may be changed. This is called antenna "polarization." Most radar antennas are linearly polarized or, in other words, the direction of the electric field is either horizontal or vertical with respect to the earth's surface. Polarization may also be elliptical or circular. Elliptical polarization is the combination of two linearly polarized waves of the same frequency, traveling in the same direction, which are perpendicular to each other. The relative amplitude and phase relationships between the two may be of any value. If the two wave amplitudes are equal and they are 90 degrees out of phase, the polarization is circular. The operator must specify the polarization of the antenna, either horizontal, vertical, or circular.

The operator must specify a height for the antenna. The model which calculates the coverage display for surface-based systems is valid only for antenna heights between 1 and 100 meters, and the program will not accept heights outside these bounds. This should not be a restriction on any normal application of ship-based systems, including submarines operating at periscope depth. The antenna heights for airborne systems are limited to the maximum height of the coverage display that has been requested.

5.4 VISUAL DISPLAY UNITS

The purpose of the display is to visually present the information contained within a return echo to an operator for interpretation and action. If the display is connected directly to the receiver, the display is called "raw" video. If the display is connected to some sort of signal processor, the display is called "synthetic video." The most commonly used display device is the cathode-ray tube (CRT). Raw video is seen on the CRT as an intensity-modulated spot or "blip." Sophisticated synthetic video may show specialized symbols or even text to aid the operator.

The ability of the operator to detect targets from a CRT display depends upon many factors such as display brightness, scan rate of the antenna, blip size, viewing distance, operator fatigue, etc. The probability of detection input required by TESS/IREPS is used to determine the signal-to-noise ratio and other factors as discussed in section 5.2. It does not contain allowances for display factors. That is, the probability of detection would apply to automatic systems. It is incumbent upon the operator to explain this to a product user.

6.0 RADAR TARGETS

In addition to the electronic characteristics of the radar system and the refractive effects of the troposphere upon the propagating electromagnetic wave, the detectability of an object depends upon the nature of the object itself. While there are hundreds of ways to classify a target, the TESS/IREPS operator is required to describe the radar target by it radar cross section and its Swerling case.

6.1 RADAR CROSS SECTION

A target's radar cross section is a term used to describe the signal scattering efficiency of the target.

A target's radar cross section is a function of its shape, the materials it is made of, the angle the target is viewed (which implies a range dependency), the radar frequency, and the polarization of the transmitting and receiving antennas. While it is commonly held that the radar cross section is independent of range, this is only true when the range is sufficiently great, or the target is sufficiently small (such as a missile nose cone), so as to cause the incident wave to be in the same plane as the receiver. This is often referred to as the "far-field" assumption or the target a "point-source" target. For short ranges, or for a very large target (such as a ship), the viewing angle becomes important. The target in this case is known as a "distributed target."

The units of radar cross section are units of area. In early work, the common unit was the square foot but presently the accepted unit is the square meter. By referencing the radar cross section to a selected "standard" cross section, it also may be expressed in decibels relative to this "standard." Most commonly, the "standard" is a 1-square-meter target. Thus, a target's radar cross section may be expressed in decibels relative to 1 square meter.

The most direct way to determine the radar cross section is to illuminate the target, or a scale model of it, with a radar and measure the return signal. Other ways are by direct solution of Maxwell's equations for the boundary conditions appropriate to the object (usually impossible for all but the simplest shapes) or by some approximation technique based upon electromagnetic theory.

For the purposes of TESS/IREPS, an air target is considered a "point-source" target and the operator must specify the radar cross section directly. NOSC Technical Document 1195, *Selected Electromagnetic Systems Parameters for Use in the Tactical Environmental Support System*, contains a listing of measured radar cross sections for various aircraft targets. A ship target is considered a "distributed target" and the radar cross section (σ) is approximated by

$$\sigma = 52\, f^{.5}\, D^{1.5} \qquad (15)$$

where f is the frequency in megahe. z and D is the ship's full load displacement in kilotons. Because the target's radar cross section is a function of so many variables, a target's radar cross section should never be extrapolated, inferred, or "guessed" from the cross section of another target.

The typical example of radar cross section in relation to target aspect is illustrated in figure 22. The three lines plotted on the polar diagram are the 20, 50, and 80 percentile values of the cross section distribution function, inner to outermost curves respectively. The cross-section values are plotted in decibels above 1 square meter, or in other words, the number of decibels above that corresponding to a 1-square-meter target. The fluctuations with aspect of 10 dB or greater can cause the detection range to vary an order of magnitude between the minimum and maximum values under the appropriate ducting conditions.

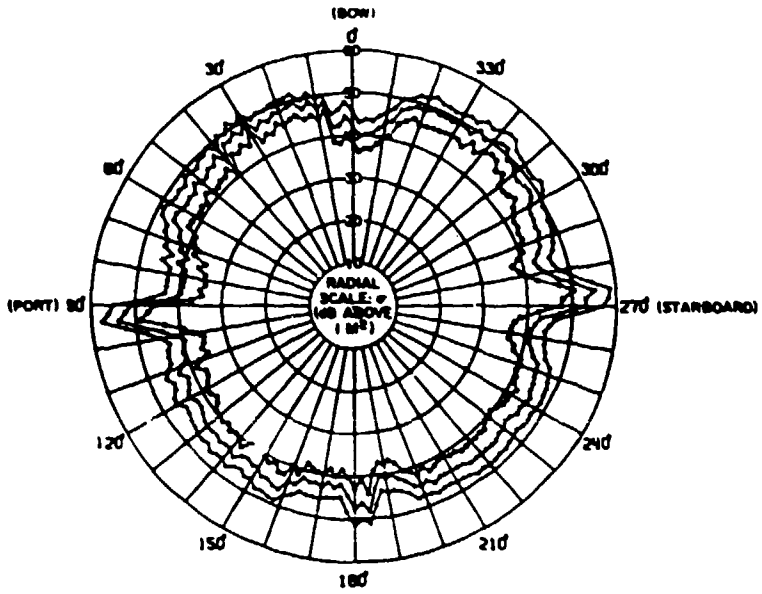

Figure 22. Variations of radar cross section with aspect for grazing angle incidence.

6.2 SWERLING CASE

Since the instantaneous radar cross section of the target is a function of aspect angle, any target that is in relative motion with the transmitter will have a fluctuating radar cross section. This fluctuation must be considered when computing the signal-to-noise ratio (and ultimately probability of detection) as discussed in section 5.2.

In 1960, Swerling proposed four models for these fluctuations in radar cross section. These models assume a time dependency or differing rates of fluctuation: a slow rate in which the fluctuation will be independent of the scan rate of the antenna

but will be the same between pulses within one beamwidth; and a fast rate in which the fluctuations will be independent from pulse to pulse. A second dependency of the model is the probability of finding any particular value of target radar cross section between two specified values. This probability is also referred to as the "probability-density" function.

These models are referred to as cases 1 through 4. Cases 1 and 2 employ one method of determining the probability-density function for a slow and fast fluctuating target respectively. Cases 1 and 2 may be applied to a complex target consisting of many independent scattering surfaces, all of which are approximately the same size. Cases 3 and 4 employ an alternate method of determining the probability-density function for a slow and fast fluctuating target respectively. Cases 3 and 4 may be applied to targets which consist of one large reflecting surface together with other small reflectors.

It is extremely difficult to determine which case to apply for any particular target. Within TESS/IREPS, the four target cases are combined into two, either a fluctuating target or a nonfluctuating target. Unless the target characteristics are known exactly, it is recommended that the fluctuating target case be used. For example, an aircraft target would normally be a fluctuating target. This selection will provide the most conservative value and will not produce an unreasonably high signal-to-noise ratio.

7.0 NONRADAR ELECTROMAGNETIC SYSTEMS

There is a large array of electromagnetic systems with varied uses but which may be grouped together for the purposes of performance assessment. These "communications" systems range from simple radiosonde or sonobuoy transmitters, to systems such as information friend or foe (IFF) or radio communications or ESM receivers, to extremely sophisticated systems such as electronic countermeasures (ECM) jammers which receive a signal, alter it to achieve a designed effect, and retransmit it. Most of these systems employ an omnidirectional antenna. However some, such as the multichannel Jezebel relay (MCJR), have a directionality capability.

No matter the design of the system, the basic concepts of transmitters, receivers, and antennas, such as transmitter power and frequency, receiver sensitivity, and antenna polarization (as discussed in sections 5.1 through 5.3), also apply to these systems. Any two-way transmission path consideration such as an unambiguous range, does not apply however.

The environmental effects upon propagation of waves transmitted from or received by these systems are the same as for radars. Some transmitters, such as a sonobuoy, have additional considerations which do not apply to radars and which are not accounted for in the TESS/IREPS assessment. For example, a sonobuoy antenna is subject to ocean wave overwash or motions which rapidly and randomly alter the antenna's orientation (and hence, its actual antenna pattern). While TESS/IREPS assumes a relatively smooth earth surface (no land terrain) for radars, this assumption is invalid for a sonobuoy whose antenna may be well below the crest of an ocean wave, thus providing a physical barrier to the electromagnetic wave. For these reasons, the user must understand the assessment of a sonobuoy systems is an optimistic assessment. In actuality, signal fading problems may often occur.

8.0 FORWARD LOOKING INFRARED SYSTEMS (FLIR)

Images, as seen by the human eye, are produced primarily by reflection of energy from objects. It is the intent of the thermal imaging system to make visible to the human eye, by presentation on a television-type monitor, the naturally emitted (self-generated) energy of objects. This energy occurs within the infrared portion of the electromagnetic spectrum (figure 2). Early airborne thermal imaging systems were pointed down to view the sea or land surface. When they were first used to view objects in the near horizontal plane, the term FLIR or Forward Looking Infra-Red was introduced.

Rather than thinking of energy in radiometric terms (frequencies and wavelengths), the relationships discussed in section 2.3 may be used to express the intensity of emitted energy in terms of temperature. Therefore, within a particular scene (or field of view), all of the sensible (felt by the human body) heat, the reflections, and emissions by bodies within the scene can be combined so that each point within the scene may be represented by an "effective" temperature. The variations in effective temperature throughout the scene tend to correspond to the details in the visual scene, that is, the radiations of a human body would take a form recognizable by the eye as a human body. It is not the intent of the FLIR assessment product of TESS/IREPS to indicate a range at which an object is recognizable however. Rather, this product is used to assess the range of first detection.

Generally, the detection of objects such as a ship or an aircraft, depends upon the ability to distinguish between the temperature of the object and the temperature of its background, that is, the ocean and the air. This is often referred to as the minimum detectable temperature difference (MDTD). Calculation of a detection range requires the knowledge of the object's MDTD as a function of range to the object. For ship targets, the apparent contrast is greatly dependent upon the ship's design and construction; operating conditions such as the internal heat transfer associated with power plants, stacks, and air-conditioning systems; and weather conditions such as direct and reflected radiant exchanges with the sun, sea, sky, clouds and thermal convection between the sea and the air.

Since every object (even within the same class of objects) has its own unique MDTD, in order to obtain a true MDTD, it should be measured. If it is measured, the target is already detected and a need for an assessment model would be moot. In practice, therefore, it is appropriate to define a fixed MDTD. For this reason, each target within the TESS/IREPS model has been assigned an experimentally determined MDTD. The MDTD is designed for a target that is well inside the horizon and has an essentially blackbody sea background. In other words, the FLIR model does not account for changes in viewing angle resulting in a new target background.

For use within TESS/IREPS, the MDTD is defined as

$$MDTD(\gamma) = a_1 + a_2 \gamma \left(\left(1 + (2 \gamma_x e_x)^2 \right)^{.5} \left(1 + (2 \gamma_y e_y)^2 \right)^{.5} \right) \qquad (16)$$

where the coefficients a_1, a_2, e_x, and e_y are characteristics of a particular FLIR, and the parameter γ is a characteristic of the target. These coefficients have *no physical meaning* and, as stated above, must be determined by experimentation. NOSC and others have determined coefficients for several specific FLIR systems which are available with NOSC Technical Document 1195. Use of the TESS/IREPS FLIR function is not recommended for systems other than those specified within TD 1195 until such time as additional polynominal coefficients can be determined.

Since atmospheric absorption (section 2.4) and scattering (section 2.5) are also a major consideration for FLIR performance assessment, it is important to know the vertical distributions of moisture and aerosols. For this reason, a FLIR assessment may only be made when the environment is measured with a radiosonde. In addition, a determination of horizontal visibility is required.

Figure 23 illustrates a sample FLIR range display. For calculation purposes, the targets are modeled as a rectangular block of fixed dimensions. Some versions of TESS/IREPS will display detection ranges for only three target sizes: large (such as a cruiser); medium (such as a destroyer); and small (such as a frigate). Other versions will display detection ranges for six target sizes, i.e., cruiser, destroyer, frigate, surface submarine, snorkeling submarine, and a submarine periscope. For submarine targets, an estimated wake length is included in the dimension of the target.

In addition to two classes of target sizes, several different altitude ranges exist between TESS/IREPS versions. An attempt at combining the two altitude ranges into one has been made. Since the FLIR model is empirically formulated for a specific FLIR system, this attempt has resulted in an interpolation artificiality at a height of 5000 feet. This may be evident as an increase of range at an altitude just below 5000 feet, to a rapid decrease of range at an altitude just above 5000 feet. Within figure 23, this artificiality is highlighted by a darkened arrow (the arrow will not be present in the actual FLIR product). The operator must recognize this range variation is not a true representation of the actual FLIR detection range at an altitude of 5000 feet.

LOCATION: ACTUAL DATA
DATE/TIME: RADIOSONDE

FLIR ONE

FLIR ALTITUDE FEET	NOMINAL FLIR RANGE(NM) FOR TARGET DETECTION — CHARACTERISTIC TARGET TYPE		
	CRUSIER	DESTROYER	FRIGATE
500	15.1	13.7	11.9
1000	15.5	14.0	12.2
1500	15.6	14.2	12.2
2000	15.7	14.3	12.3
2500	15.7	14.2	12.3
3000	15.8	14.3	12.3
3500	16.3	14.7	12.7
4000	17.0	15.3	13.2
5000	18.0	16.2	13.9
7500	17.1	15.5	13.3
10000	18.5	16.7	14.4
15000	21.5	19.1	16.4
20000	23.3	21.2	18.7
25000	25.6	23.4	20.6
30000	27.6	25.2	22.1

	SURFACE SUB	SNORKEL SUB	PERISCOPE
500	8.4	3.2	1.6
1000	8.5	3.2	1.7
1500	8.6	3.3	1.7
2000	8.6	3.3	1.9
2500	8.6	3.3	2.0
3000	8.6	3.3	2.1
3500	8.9	3.6	2.2
4000	9.1	3.8	2.3
5000	9.6	4.1	2.3
7500	9.2	4.4	2.0
10000	10.3	4.6	1.8
15000	12.4	4.5	0.0
20000	13.8	3.8	0.0
25000	14.8	9.6	0.0
30000	15.5	0.0	0.0

MTDT coefficient A1 = 0
MTDT coefficient A2 = 0
MTDT coefficient EX = 0
MTDT coefficient EY = 0

Figure 23. FLIR performance range display.

9.0 FREE-SPACE RANGES

9.1 RADAR SYSTEMS

For assessment of a radar's performance, the most important factor to consider is the radar's free-space detection range or, in other words, the range at which a specific target may be detected in an isotropic, homogeneous, lossless environment. This range serves as an optimum range (or figure of merit) for a particular radar/target combination and allows for a comparison with nonstandard refractive conditions.

The free-space range may be determined in several ways, the first being by calculation (A.E. Barrios, NOSC, personal communication, 1985). The free-space range in kilometers is given by

$$R_{fs} = 58 \left[\frac{x \; P_t \; \sigma \; \tau}{f^2} \right]^{.25} \qquad (17)$$

where $x = 10^{0.1 \left(2G - N_f - \left(\frac{S}{N} \right)_{min} - L \right)}$

G = antenna gain (dB)

N_f = receiver noise figure (dB)

$\left(\frac{S}{N} \right)_{min}$ = minimum signal-to-noise ratio (db)

L = system loss (db)

P_t = maximum radiated power (kilowatts)

σ = target's radar cross section (square meters)

τ = pulse length (microseconds)

f = transmitter frequency (megahertz)

The signal-to-noise ratio [Blake, 1980] is given as:

$$\left(\frac{S}{N} \right)_{min} = \frac{X_o}{4 N_p} \left[1 + \left(1 + \frac{16 N_p}{X_o} \right)^{.5} \right. \qquad (18)$$

where $X_o = (g_{fa} + g_d)^{.5}$

$g_{fa} = 2.36 \left(- \log_{10} P_{fa} \right)^{.5} - 1.02$

$$g_d = 1.231 \frac{t}{(1 - t^2)}$$

$$t = .9 (2 P_d - 1)$$

N_p = number of pulses

P_{fa} = probability of false alarms

P_d = probability of detection

For height-finder radars, the number of pulses is the same as the number of hits per scan. For nonheight-finder radars, the number of pulses may be given as

$$N_p = \frac{\zeta_h \; p_r}{6 h_s}$$

where

ζ_h = horizontal beamwidth

p_r = pulse rate

h_s = horizontal scan rate

The signal-to-noise ratio given by equation 18 is valid for a steady target. In the case of a fluctuating target, the fluctuation loss, a ratio between the signal-to-noise levels of a fluctuating and nonfluctuating target, must be added to equation 18. This fluctuation loss is given as

$$L_f = [(- \ln P_d \; (1 + \frac{g_d}{g_{fa}})]^{-1} \quad .$$

The free-space range (equation 17) uses the system's peak power expressed in kilowatts. As discussed in section 5.1, there are several definitions of power when considering electromagnetic systems. Often in publications, the system's power given will be the effective radiated power expressed in dBW (decibel relative to a watt). It will be necessary, therefore, to convert the power to the proper quantity. For conversion purposes, the effective radiated power may it be defined as

$$P_{eff} = 10 \log_{10}(P_t) + G - L_{tl} \qquad (19)$$

where P_t = peak power (watts)

G = antenna gain (dB)

L_{tl} = transmission line loss (dB)

For the purpose of free-space range calculations, equation 19 may be used to calculate the peak power required by equation 17. Care must be taken, however, to insure reasonable values are used when making this calculation. For most practical radars, the transmission line loss will be in the order of 1 or 2 dB (Barton). An order of magnitude error in antenna gain will make an order of magnitude difference in the power obtained (recall equation 3). For example, assuming a transmission line loss of 0 dB, an antenna gain of 30 dB, and an effective radiated power of 100 dBW, the resultant maximum radiated power will be 10,000 kilowatts, an impracticable number. If the antenna gain was 40 dB, however, the resultant radiated power would be 1,000 kilowatts, a more reasonable value.

Recall from section 5.2 that the signal-to-noise ratio is probabilistic in nature because it includes a false-alarm rate and probability of detection. In addition, the target's radar cross section is also probabilistic in nature because it includes the Swerling case of the target. A calculated free-space range also assumes the radar is operating at design specifications.

As can be seen, the calculation of free-space range involves a number of uncertainties, often leading to an overly optimistic range. The most accurate method of establishing the free-space range is by observation of the actual maximum detection range of known targets at angles above a few degrees from the horizontal, where effects of refraction are minimized. In the case of surface-based 2D air-search radar systems, the free-space detection range is one-half the maximum observed range at high altitudes because of the influences of the interference region. For surface-based height-finder and all airborne radar systems, the free-space detection range is the maximum observed range at high altitudes. Both TESS and IREPS contain a utility program which will calculate the radar free-space detection range.

9.2 COMMUNICATIONS AND ESM SYSTEMS

As with radar systems, the best method of determining a range for UHF communications or ESM intercept is by observation. While this method is easily employed for communications systems, an observed range for an ESM intercept is very rare.

For occasions where making an observation is impractical, the free-space range may be calculated. The path loss in free space is determined by the geometrical spreading of the power over the surface of an expanding sphere centered at the transmitter (section 4.1.1). The maximum sustainable path-loss for an UHF communications or ESM receiver (path-loss threshold) is simply the difference between the transmitter power and antenna gain and the sensitivity of the receiver. The free-space range communications or ESM intercept range, in nautical miles, is, therefore

$$R_{fs} = 10^{((10\log_{10}(P) - 20\log_{10}(f) + G - S + 22.2) / 20)} \quad (20)$$

where P = maximum radiated power (kilowatts)

f = transmitter frequency (megahertz)

G = transmitter's antenna gain (dB)

S = receiver sensitivity (dBm)

For the purposes of communications and ESM intercept, the receiver gain generally includes the gain of the receiving antenna. Note that the probabilistic nature of the radar free-space detection range is not seen in the communications or ESM intercept free-space range; this is usually taken into account in establishing the sensitivity of the receiver.

The free-space range can be extremely large, on the order of many thousands of kilometers, which would be the ESM receiver's capability in free space. However, the influence of the earth and other factors such as atmospheric absorption and scattering limit the actual intercept range to a value much less than the free-space range. It may happen, however, that the calculated free-space range exceeds the limits of TESS/IREPS inputs. In this case, the path-loss threshold in decibels may be calculated as

$$PL_{threshold} = 60 + 10\log_{10}(P) + G - S \qquad (21)$$

where P = transmitter power (kilowatts)

G = transmitter's antenna gain (dB)

S = receiver sensitivity (dBm) (decibels relative to a milliwatt)

Often a receiver sensitivity will be published in a multiple of volts. Assuming that receiver sensitivity may be defined as the minimum amount of power necessary for reception, a conversion to the proper units may be made using the following:

$$S\ (dBm) = 20\log_{10}(S\ millivolts) - 10\log_{10}(R) - 30 \qquad (22)$$

where R is the resistance in ohms. When the resistance is not known, a value of 50 ohms has proved to be a reasonable assumption for a resistance.

Because of the long free-space ranges or large free-space path-loss values, the path-loss product of TESS and IREPS, as discussed in section 13.0, is the proper assessment product for ESM applications. The free-space path loss is included in figure 11 for reference and illustrates how the path loss within the troposphere oscillates above and below the free-space value in the interference region.

Both TESS and IREPS contain a utility program which will calculate the free-space intercept range and/or the path-loss threshold.

10.0 ENVIRONMENTAL ASSESSMENT

Section 4.2 briefly describes the tropospheric conditions which would lead to anomalous propagation of electromagnetic waves. Determination of these conditions is based upon standard meteorological field observations, measurements from instruments such as a microwave refractometer, images from satellite sensors, numerical forecast fields provided by organizations such as the Fleet Numerical Oceanography Center (FNOC), Monterey, California, or from the TESS/IREPS climatological database.

Historically, a number of poor environmental observation or evaluation techniques and/or misconceptions have lead to the misapplication or unrealistic use of TESS/IREPS. While it is beyond the scope of this document to fully describe the above information gathering methods, it is appropriate to provide some additional guidelines for environmental measurement or evaluation.

10.1 SURFACE OBSERVATIONS

In the absence of warm temperature advection, the marine surface layer is typically slightly unstable due to the different heat capacities of air and water. Or, in other words, the air temperature is slightly cooler than the sea-surface temperature. This unstable condition is by far the most common situation over open ocean areas. This unstable condition may be seen in figure 24, which illustrates the annual air/sea-surface temperature difference distribution from the National Oceanic and Atmospheric Administration (NOAA) ocean buoy 42002 located at lat. 32.3°N, long. 75.2°W.

While slightly unstable atmospheric conditions are normal for ocean areas, stable conditions may occasionally occur. Advection of warm, high-humidity air over cold ocean frontal boundaries or up-welling areas, or atmospheric warm frontal activity, may lead to stable conditions far removed from land. This type of meteorological situation is also conducive to fog formation. Near land masses, advection of warm, low-humidity air over the ocean, such as occurs in the Santa Ana, will also lead to stable conditions.

Unstable conditions produce shallow evaporation duct heights, generally less than 20 meters. Stable conditions may produce a wide range of evaporation duct heights up to and in excess of 40 meters. In the case of Santa Ana type advection, the surface-to-surface propagation would most likely be dominated by a surface-based duct and the evaporation duct would have little importance. For normal conditions, however, surface-to-surface propagation is dominated by the evaporation duct. The calculation of evaporation duct within TESS/IREPS is extremely sensitive to the relative difference between air and sea-surface temperatures. Any errors in air/sea-surface temperature measurements could ultimately produce unreasonable propagation ranges.

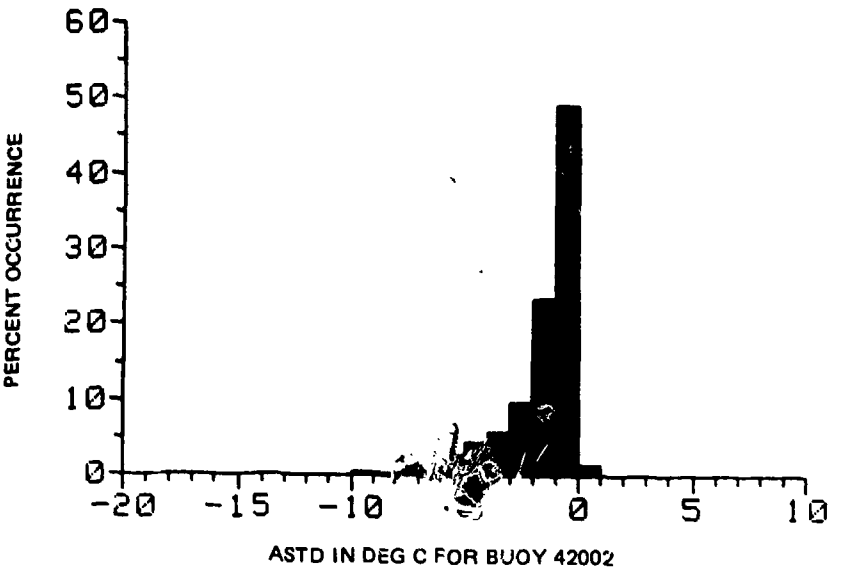

Figure 24. Annual air/sea-surface temperature difference distribution from NOAA ocean buoy 42002.

The elements of wind speed, air and sea-surface temperature, and relative humidity as measured by transiting ships have been, for the most part, sufficiently accurate for general meteorological and climatological purposes. Since the relative difference between air and sea-surface temperatures is critical, the accuracy of measurements used for evaporation duct calculations may not be sufficient. Measurement errors may be made in a number of ways. For example, air temperatures reported by ships in the tropics appear to be consistently high under sunny conditions due to poor instrument exposure. Sea-surface temperature reports are commonly seawater injection temperatures. While sea-surface temperatures obtained from expendable bathythermographs are potentially the most accurate measurements currently made by U.S. Navy ships, these instruments are often ejected into the ship's wake. Compounding the problem is the fact that air and sea-surface temperature measurements are made using two different sensors which are most likely not calibrated together.

Taken together, the errors in measurements produce an air/sea-surface temperature difference distribution such as illustrated in figure 25. Figure 25 was constructed from over 100 [illegible]s of shipboard meteorological measurements from within Marsden square 82, a 10° lat. by 10° long. square containing NOAA buoy 42002. By comparing figure 24 with figure 25, a bias toward stable, anomalous conditions by shipboard measurements becomes evident. Figure 25 also illustrates the evaporation duct height distribution calculated from the shipboard measurements. Of particular note is the large occurrence of evaporation duct heights in excess of 40 meters, which in turn lead to overly optimistic propagation ranges.

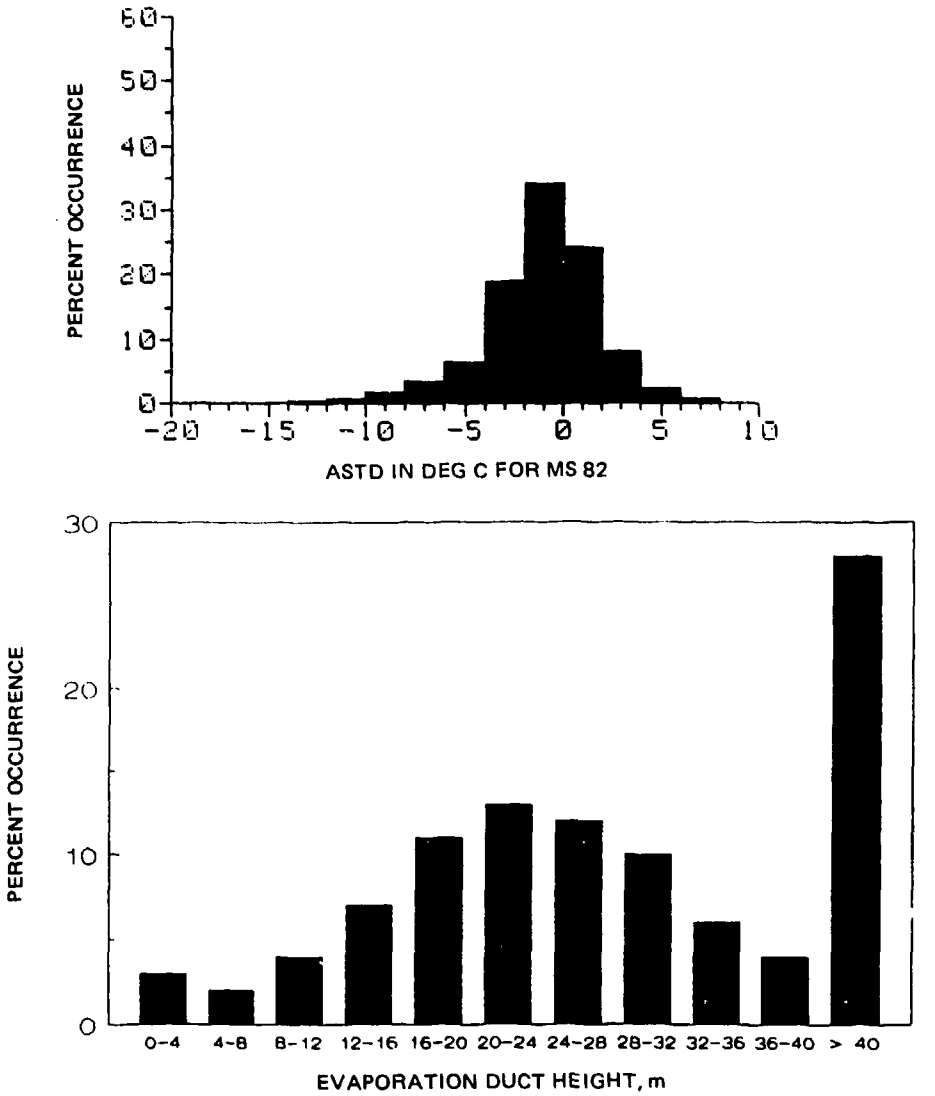

Figure 25. Annual air/sea-surface temperature difference and evaporation duct height distributions from Marsden square 82.

10.2 RADIOSONDE OBSERVATIONS

The most widely used instrument for observing the structure of the troposphere is the radiosonde. It is used in conjunction with a hand-held pyschrometer that measures surface air and wet-bulb temperature. The wet-bulb temperature is defined as the lowest temperature that air may be cooled to by evaporating water into it.

In using radiosondes to measure the vertical profiles of temperature and humidity, the absolute accuracy of the data is not as important for refractivity assessment as accurate measurement of the gradients. Sensor lag tends to reduce the gradients and increase the altitude at which gradient changes occur. The lag errors are not too serious at normal radiosonde ascension rates but can be very significant at launch. Often the radiosonde is prepared in a heated or air-conditioned space and is released without allowing for the proper acclimatization of the sensors. In other cases, the radiosonde may be exposed to direct sunlight and radiating surfaces, such as being left sitting on the ship's deck, for several minutes prior to launch.

Another factor which often contributes to spurious gradients is using psychrometric measurements for the surface level of the sounding. The psychrometer measurements are more accurate than the radiosonde's. In addition, the psychrometer is not usually co-located with the radiosonde. That is, the psychrometer is carried to the best position for measurements while the radiosonde is likely to be in a fixed position subject to the heat-island effects of the ship.

It has been shown by R.A. Paulus, NOSC (personal communication, 1987) that within the error range of the radiosonde's sensors, an error of $\pm$ 9.1 N-units at each reporting level may occur within conditions typical for the northern Indian Ocean. Psychrometric error may lead to $\pm$ 1.3 N-units per observation within the same environment. Compounding this sensor error with poor acclimatization or measurement techniques could lead to extremely abnormal low-level refractive gradients in radiosonde data over the open ocean and, ultimately, to dramatic inaccuracies in the quality of TESS/IREPS assessment products. For example, table 3 is a listing of daytime radiosonde data collected by a U.S. Navy ship on 17 July 1987.

Table 3. Radiosonde measurement and calculated refractive conditions at 41.36°N, 006.12°E for 0844 (GMT), 17 July 1987.

Level	Pressure (mbs)	Temperature (C)	Relative Humidity (%)	M-units	Refractive Condition
1	1005.4	24.3	88.0	376.6	Trapping
2	1000.0	24.8	78.8	373.4	Sub
3	975.4	22.0	98.4	411.2	Trapping
4	954.2	20.9	79.4	409.7	Super
5	933.2	22.2	56.7	413.7	Standard
6	850.0	18.5	44.5	497.8	Standard
7	758.3	10.2	57.2	622.4	

During the evening over land, formation of a temperature inversion in contact with the ground is common as is an accumulation of water vapor near the surface leading to a decrease of humidity with altitude. This inversion often results in superrefractive conditions. During the daytime, a superadiabatic layer quickly develops upward which in turns produces mechanical mixing, thereby restoring the refractive conditions back to standard. Over the open ocean there is much less variability since the sea-surface temperature may only change by a few tenths of a degree Celsius from night to day. By plotting the values of table 3 on a thermodynamic diagram such as a Department of Defense Weather Plotting Chart (DOD-WPC) 9-16-1, "USAF SKEW-T, log p Diagram," or by constructing profiles of potential temperature (θ) and specific humidity (q), as illustrated in figure 26, the nighttime conditions of surface temperature inversion with trapping conditions are evident. Since this sounding was obtained during the day, it appears to be directly opposite to the meteorologically plausible behavior of the marine boundary layer. The TESS/IREPS operator must either rationalize the refractive conditions observed with an appropriate meteorological condition or must suspect instrument error due to improper prelaunch procedures.

Even without displaying the radiosonde sounding on a thermodynamic diagram, the TESS/IREPS operator may also take warning by inspection of the height of the anomalous refractive condition. Characteristically, the top of the trapping, subrefractive or superrefractive layer, is always at a pressure of 1000 millibars when the surface pressure exceeds 1000 millibars. For surface pressures less than 1000 millibars, the anomalous refractive condition tops are at the top of the superadiabatic layer. TESS makes an attempt to compensate for these measurement problems by employing an averaging technique over the input parameters. IREPS does not try to correct for instrument errors but does warn the operator by a printed message that a superadiabatic condition exists.

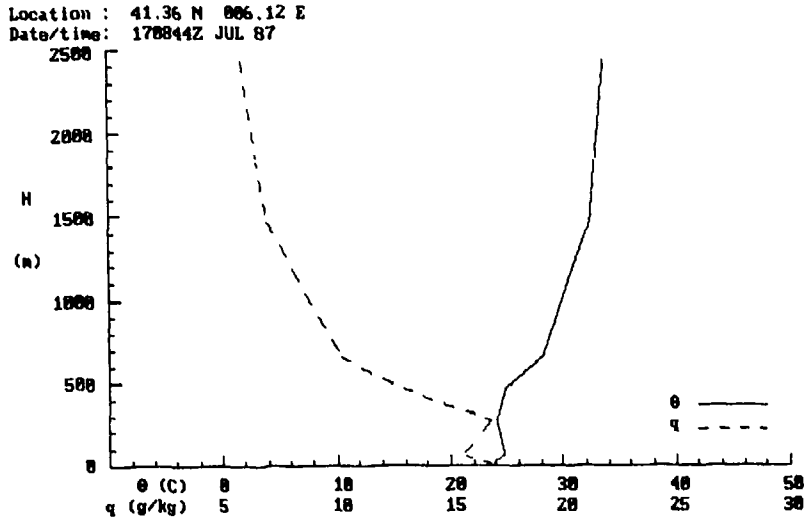

Figure 26. Profiles of potential temperature and specific humidity derived from radiosonde soundings of table 3.

Following an exhaustive study, Helvey [1982] makes the following recommendations in an attempt to eliminate instrument errors.

a. Avoid exposing the radiosonde to any environment other than ambient outdoor conditions for 5 minutes prior to release.

b. Use a portable aspirator to ventilate the sonde or place the sonde in an aspirated thermoscreen in the shade, away from large superstructures.

c. Obtain the surface data point for the sounding from the sonde itself rather than a psychrometer. Allow sufficient time to get a stable "average" surface value.

d. Select "significant levels" based on deviations in humidity of 3 percent and in temperature of 0.5°C. Preserve regions of strong gradient in either humidity or temperature.

e. Avoid any measurements between the surface and 500 feet, particularly at the top of the daytime superadiabatic layer or the top of a strong surface radiation inversion. If this is not possible, calculate a relative humidity for the desired level based upon a linear interpolation of dew point temperature or mixing ratio values at the surface and from the first available humidity contact above 500 feet.

TESS/IREPS provides for entering environmental data from a radiosonde sounding transmitted via radio in the World Meteorological Organization (WMO) format. The TESS/IREPS operator must be cautious in the use of these data for several reasons. First, the data are most often obtained from a radiosonde launched over a land mass. The changing synoptic meteorological conditions must be evaluated to insure the sounding is appropriate for the area and time of operation. For example, an operator would want to reject an early evening sea-breeze sounding if nighttime land-breeze conditions are present. Second, the actual data within the sounding should be investigated. Often, digits can be transposed either during the recording of data or during radio transmission; reporting levels which are both significant and mandatory may only be listed within the mandatory section of the message; or an obvious observation error may be made. Prior to the use of any WMO data within a TESS/IREPS product, it is highly recommended that the data be plotted on a thermodynamic diagram or be used to construct a refractivity profile with the results evaluated for meteorological consistency and accuracy.

10.3 MICROWAVE REFRACTOMETER

The AN/AMH-3 Electronic Refractometer Set, also known as an airborne microwave refractometer (AMR), is a device mounted on an aircraft and directly measures the tropospheric refractivity. When activated, the unit records static pressure, Pitot pressure, air temperature, and refractivity every 1.7 seconds and stores the data on a magnetic cassette for postflight processing. A discussion of the proper operation of the AMR, the installation and operation of the AMR cassette reader, and the method of employment within TESS/IREPS may be found in the appropriate TESS/IREPS user's manual. The following is a discussion of the various environmental considerations and data reduction techniques associated with the AMR.

The normal mode of operation for the AMR-bearing aircraft is to launch, climb to station, carry out the mission, descend, and recover. Thus the AMR would record two vertical profiles of refractivity during the flight: one on ascent and one on descent. Occasionally there may be other vertical profiles but generally the TESS/IREPS operator will select the most recent in time for analysis and use in the generation of assessment products.

A typical altitude-versus-time display resulting from a normal flight is shown in figure 27. The corresponding refractivity-versus-height profile for the time period 4:00 to 4:30 is illustrated in figure 28. Note that the AMR does not provide a smooth profile of refractivity. These variations in refractivity may happen for a variety of reasons, including minor fluctuations of refractivity that actually occur in turbulent regions of the troposphere; large fluctuations due to noise or erroneous measurements by the AMR due to water droplets in the AMR cavity; bit errors in reading the AMR tape; and apparent gradients due to horizontal changes in refractivity. It is the task of the TESS/IREPS operator to approximate the shape of the profile using linear segments, thereby removing small fluctuations which are inappropriate to an accurate refractivity profile.

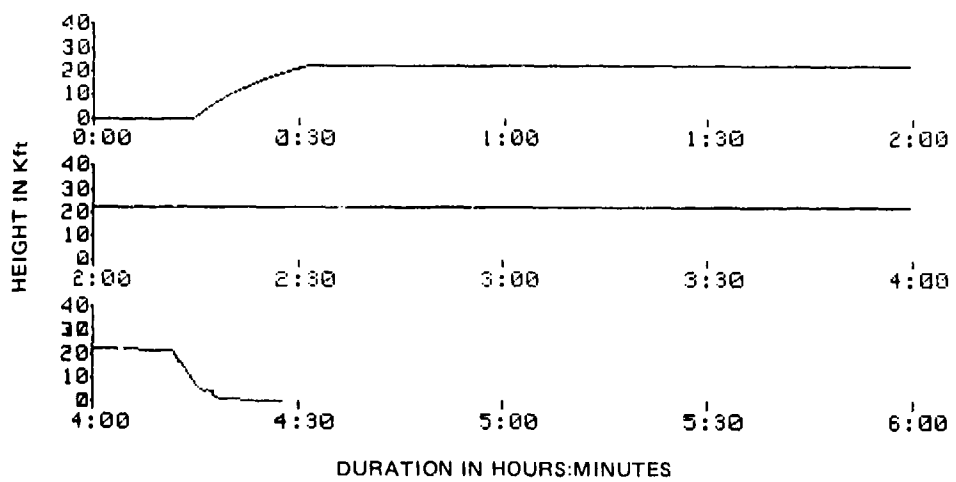

Figure 27. Refractometer altitude versus time display for a flight on 29 October 1984.

Generally, a good approximation to the shape of the profile is obtained if a straight line is drawn between neighboring data points when the data points differ by less than 4 to 6 N- or M-units. There are a number of real-world constraints that significantly impact the quality of the approximation. First, the accuracy of the AMR is plus or minus 2 N-units. Changes in refractivity of this magnitude are considered noise and are physically meaningless. Second, the AMR measures the refractivity in a very small volume of air. If this small volume is not representative of the larger scale air mass, the data are inappropriate for use. For example, on the ground prior to takeoff, the AMR sampling cavity may be exposed to hot exhaust gases from an aircraft immediately before it on the runway. Obviously, the changes measured by the AMR are localized to the airfield and not representative of the larger scale air mass surrounding the airfield and, therefore, should not be included in the analysis. Third, bit errors caused by poor quality tape or dirty read/write tape heads may indicate very large changes in either height or refractivity. Typically, a bit error will show a very abrupt change followed by yet another abrupt change which returns to nearly the same plot position as before the bit error. Lastly, TESS/IREPS has a limit to the number of data levels which may be entered into an environmental profile. A typical AMR refractivity profile from an altitude of 20,000 feet down to the surface may contain 500 data points. Experience with analyzing most profiles is that the profile can be adequately described with between 10 to 15 entries of height and refractivity pairs. A further discussion of data quantity is presented in section 10.8.

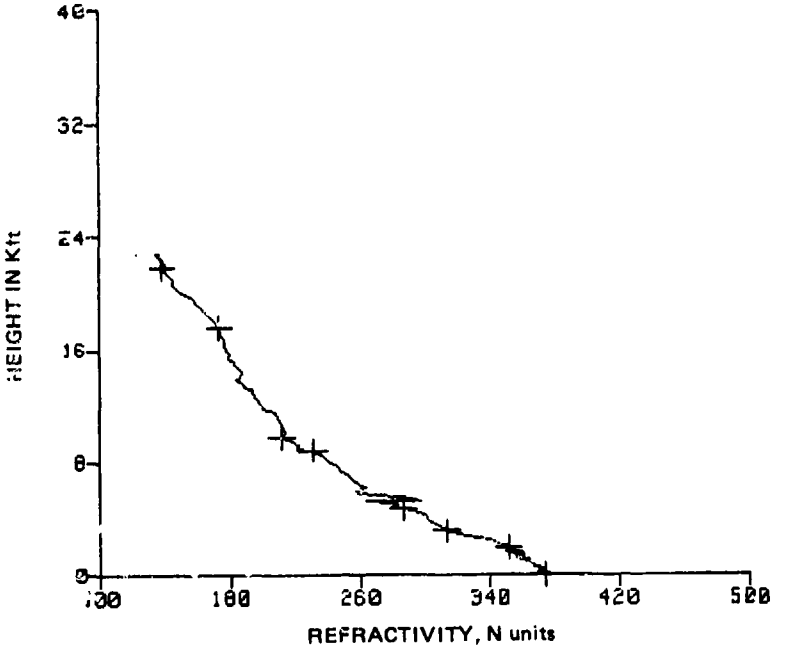

Figure 26. Refractometer refractivity profile for the time segment of 4:04:35 to 4:27:30 of figure 27.

The "+" symbols of figure 28 indicate the points the analyst has chosen to represent the profile. It is strongly recommended that a new user gain experience with refractometer data analysis by trial. By using the printing features of TESS/ IREPS, obtain a paper copy of the AMR refractivity versus height profile. With a straight edge and a pencil, draw joining lines on the hard copy such that the maximum deviation from the straight line and the plotted data are less than 3 or 4 N-units. Enter these environmental data into TESS/IREPS and produce a surface coverage diagram (section 12.0) and an airborne early warning (AEW) display (section 14.0). Repeat this procedure a number of times, but each time reduce the number of points selected on the refractivity profile, allowing greater refractivity deviations from the straight line. Compare the like system coverage and AEW products to see the effects of over- and undersampling the refractivity profile. This technique will aid in establishing subjective guidelines for approximating the refractivity profile.

Note on figure 28 that the feature between 5000 and 6000 feet has been neglected. Had this feature been included, a strong trapping layer of –94 N/kft overlain by a strong subrefractive layer of 361 N/kft overlain by another strong trapping layer of –114 N/kft would have resulted. This would be equivalent to having a strong inversion overlain by a very moist layer overlain by another strong inversion, which is meteorologically unrealistic. Another clue is that the refractivity gradients are unrealistically strong. Any subrefractive gradient greater than 100 N/kft should be considered suspicious. Any trapping layers less than –100 N/kft should also be considered doubtful. Additional information about the strengths of trapping layers in different ocean regions of the world is available in the TESS/ IREPS historical summaries (section 10.6). If one is unsure of whether or not a particular feature should be included, include it, let TESS/IREPS determine the N-unit gradient, and then delete it if it is unrealistic.

Another means to check on suspicious layers is to make comparisons with other profiles. For example, figure 29 is the refractivity versus height profile from the ascent portion of figure 27. There is no indication of the feature between 5000 and 6000 feet which leads to additional support for neglecting the layer. The analyst can get a better feel for the changes that are taking place in refractivity by plotting both ascent and descent profiles together such as illustrated in figure 30. It is apparent that the small features are indeed transient and that the gross features of the profile are consistent with the exception of the region between 3000 and 7000 feet. It is not apparent from the data alone what could be causing the discrepancy, possibly equipment problems, water droplets affecting the AMR, or erroneous data being read from the AMR tape.

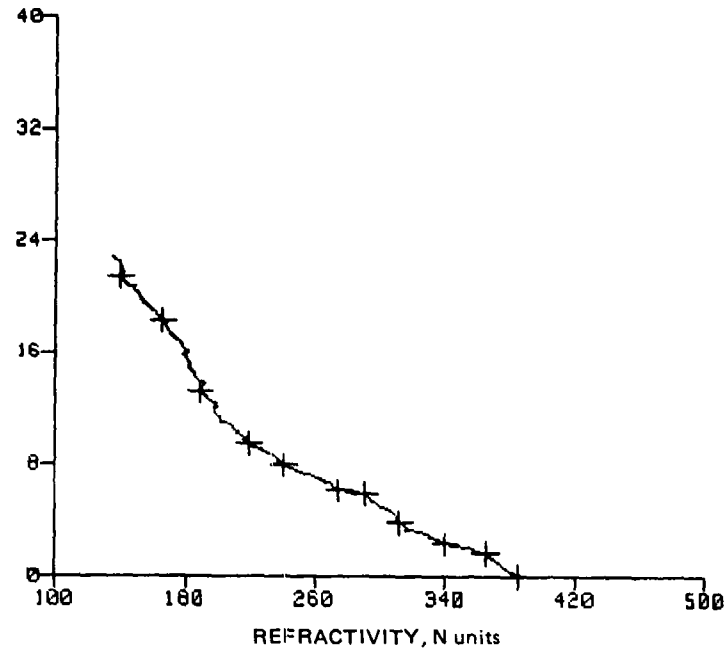

Figure 29. Ascent refractvity profile from figure 27.

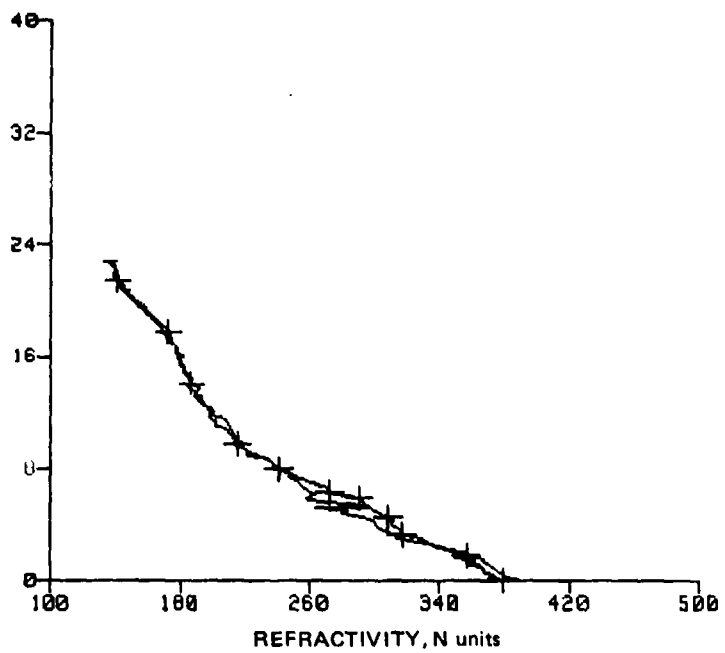

Figure 30. Combined ascent and descent refractivity profiles from figure 27.

In some cases, it may be desirable to analyze the refractivity profile in terms of the modified refractivity or M-units. The M-unit analysis greatly aids in picking out trapping layers or ducts. Normally, the M-unit profile is increasing with altitude. A trapping layer is readily observed when the M-unit profile decreases with altitude.

Analysis of a second flight, figure 31, provides additional insights.

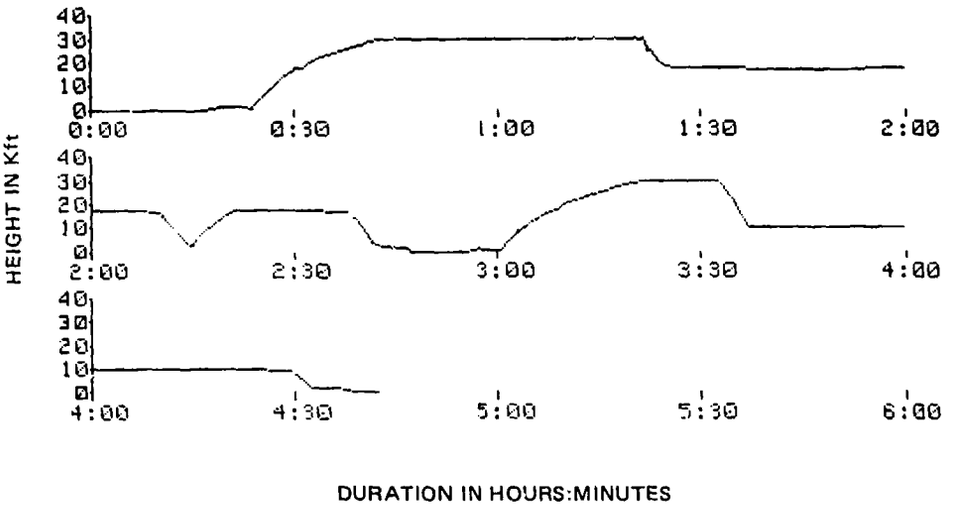

Figure 31. Refractometer altitude versus time display for a flight on 8 February 1984.

The figure 31 ascent profile from the 3:00:26 to 3:23:38 time frame and the descent profile from the 3:29:22 to 4:43:32 time frame are illustrated in figures 32 and 33 respectively. The surface point was obtained by linearly extrapolating the lowest point on the profile (about 800 feet) to the surface. The profile of figure 32 shows a typical trapping layer which lies between levels 2 and 3 and has an N gradient of about –64 N/kft.

Interestingly, the trapping layer at 4000 feet appears to have either weakened or lifted to 10,000 feet. However, the feature at 10,000 feet is suspicious in that it has a very sharp gradient. Looking again at figure 31 shows that during the time frame selected, the aircraft descended to approximately 10,000 feet and maintained that altitude for about 55 minutes before continuing the descent. At typical aircraft speeds, this could easily represent a horizontal distance of 200 to 300 nautical miles. Over these distances, the horizontal gradient of refractivity could be 15 to 20 N-units, thus introducing an offset into the profile. To compensate for this, the analyst adjusted the digitized points to the right of the actual profile above 10,000 feet. A meteorological analog to this situation would be in interpreting marine barograph traces, where the analysis of pressure changes must also include the movement of the barograph within the pressure field.

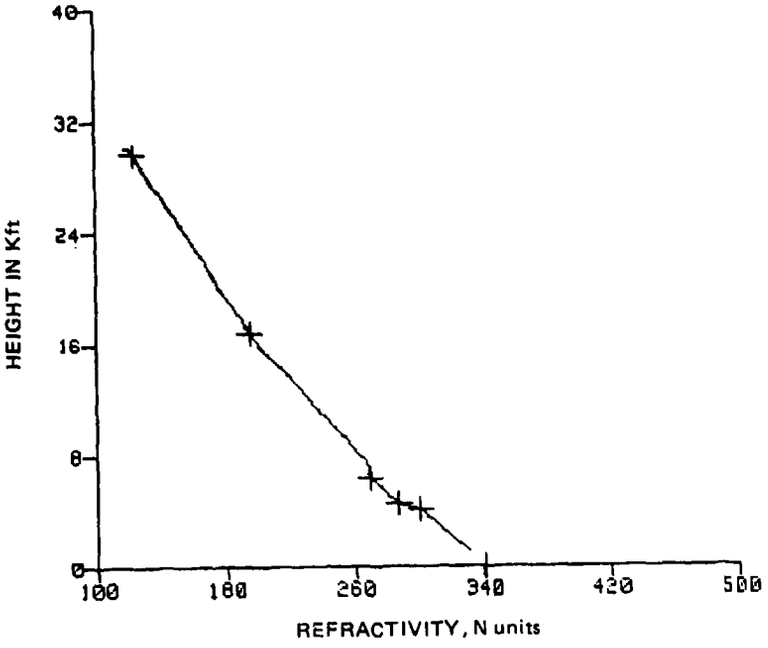

Figure 32. Refractometer refractivity profile for times between 3:00:26 and 3:23:38 hours on 8 February 1984 from figure 31.

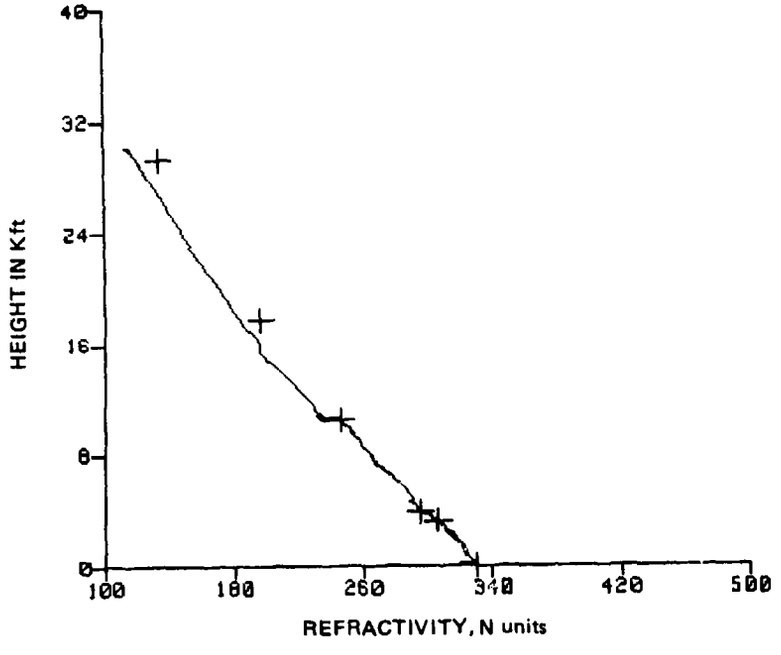

Figure 33. Refractometer refractivity profile for times between 3:39:22 and 4:43:32 hours on 8 February 1984 from figure 31.

10.3.1 Pilot Reports

Located within the aircraft cabin is a direct-read display of the AMR data. From this display, the pilot can determine the top, thickness, and strength (relative to other layers) of a trapping layer and the top of a subrefractive layer. Often times this information may be communicated via radio so that the TESS/IREPS operator is able to construct a refractivity profile without waiting for the aircraft's return and the reading of the cassette tape. While the construction of a profile requires some assumptions which may or may not be true, the profile may be used as a first approximation until actual conditions are confirmed from a radiosonde or the AMR cassette tape.

The following steps are taken to construct a refractivity profile from a pilot's report of trapping layers. The profile is constructed from the surface upward to include the total number of trapping layers. This method cannot be used to construct a profile which includes subrefractive or superrefractive layers, since the layer thickness is unavailable from the cockpit readout. Refer to figures 15 and 16 for the distinction between trapping layers and the resulting ducts.

a. Determine a surface refractivity by using equations 5 and 6, converting to modified refractivity (M-units) by equation 7.

b. Subtract the first layer's thickness from its top to obtain the layer's bottom. Examine the layer's bottom height. If it is zero, a surface-based duct created from a surface-based layer is present. By using the world-wide average modified refractivity gradient of –80.4 M/kft for a surface-based trapping layer, extrapolate the surface M-unit value up to the layer's top.

If the layer's bottom is not zero, it may or may not create a surface-based duct. By using a standard atmosphere M-unit gradient of 36 M/kft (table 2), extrapolate the surface M-unit value up to the layer's bottom. By using the world-wide average M-unit gradient of –32.4 M/kft for an elevated trapping layer, extrapolate the M-unit value at the layer's bottom up to the layer's top.

If the M-unit value at the layer's top is less than the M-unit value at the surface, the trapping layer has created a surface-based duct. If the M-unit value at the layer's top is greater than the M-unit value at the surface, the trapping layer has created an elevated duct. While it is not a necessary data point within the modified refractivity profile, the elevated duct's bottom height may be found by extrapolating the surface M-unit value, using a standard gradient, to a height which would give the M-unit calculated at the layer's top.

c. If there is more than one layer, repeat the steps outlined in (a) and (b) above but use the M-unit value at the top of the layer immediately below the one under consideration as the starting value. Since a layer's strength relative to other layers is available, the trapping gradient used may be varied to produce a more representative profile.

Rather than using the world-wide average M-unit trapping gradients, the TESS/IREPS historical database may be accessed with the latitude and longitude of the refractometer's position (section 10.6). If the listed WMO reporting station is sufficiently close to be considered within the same air mass, the more climatologically correct M-unit trapping gradients may be calculated by dividing the layers' M-unit deficits by their thicknesses.

10.4 SATELLITE IMAGERY

Visual and infrared satellite imagery reveals characteristic cloud and thermal patterns identifying fronts, airmasses, and mesoscale structure. The widespread and frequent global coverage provided by satellite imagery is most useful over the open ocean where there is an almost total void of conventional data.

With its ability to detect broad areas of stratified low clouds, satellite imagery is particularly useful in identifying suspected regions of overlying low-level inversions and, thus, low-elevated or surface-based ducts. Even though qualitative analysis of satellite imagery cannot be expected to provide a precise fix on the altitude of ducts, it does have the potential for indicating duct occurrence, probable height categories, and trends of duct strength.

Helvey and Rosenthal [1983] evaluated a number of satellite images with radiosonde soundings from the Pacific and Atlantic Ocean areas and have developed an association with meteorological processes and duct occurrence. In 1985 their work was expanded to investigate the relationship between cloud structures as seen in satellite images and refractive conditions. The principal difficulties in developing reliable predictive guidance are associated with limitations on the data available over the ocean and the measurement systems employed to gather them, the influence of small scale atmospheric and ocean features on prevailing synoptic conditions, and the imperfections in the dynamical or statistical models used in the prediction process.

It must be emphasized that any efforts in this field are still developmental, not operational. Even when an operational technique becomes available, the predictive capabilities will be intended to provide guidance in the evaluation of meteorological conditions appropriate to duct formation and will never be meant to replace the measurements of the radiosonde or AMR. Over the past several years, several refractive effects guidebooks or fleet tactical memos dealing with this topic have been published by various naval commands. While these have become obsolete or cancelled by the authors, they are still being retained and used. At the time of this document's publication, any use of schemes to derive ducting conditions and, specifically, heights and strengths from satellite imagery or synoptic parameters is not recommended.

10.5 IMPORTED METEOROLOGICAL DATA

Meteorological data, radiosonde soundings, and refractivity profiles may be obtained from the Fleet Numerical Oceanography Command (FNOC) via naval message. The *Automated Products Request User's Manual*, FLENUMOCEANCEN-INST 3140.3 (series), describes the data available and how to obtain it.

At the time of this publication, radiosonde soundings or refractivity profiles created from radiosonde soundings may be obtained only from established WMO stations or U.S. Navy ships of opportunity. All of the caveats associated with radiosonde observations as discussed in section 10.2 must be considered when using these data. At the very minimum, the data should be inspected to insure they are meteorologically reasonable.

FNOC is developing the capability to provide field points from the Navy Operational Global Atmospheric Prediction System (NOGAPS) with a vertical resolution of 40 meters, 160 meters, 368 meters, 700 meters, and 1200 meters in addition to the standard meteorological reporting levels. While this vertical resolution is insufficient for construction of a refractivity profile, it may prove valuable in assessing the meteorological conditions associated with ducting conditions. A still experimental effort is being made toward providing meteorological data with a vertical resolution sufficient for construction of a refractivity profile. This effort is entitled the Navy Operational Local Atmospheric Prediction System (NOLAPS). When these data become available, the TESS/IREPS operator is cautioned that not only may the observational errors of the input radiosonde still be present, the assumptions necessary for computer modeling of the atmosphere must also be taken into account. The operator must, at all times, inform the product user as to the reliability of the data upon which the product is based.

10.6 TESS/IREPS CLIMATOL OGY

In cases where no current environmental data are available or a planner desires sample TESS/IREPS products for a future operation, the climatology of refractive conditions may be accessed to create a refractivity profile. Figure 34 is an example of this historical propagation conditions summary. The main body of the summary consists of five tabular listings, each of which are separated into *yearly and trimonthly categories*. These categories are further subdivided into daytime, nighttime, and a combination of both day and night. An asterisk within the body of the table indicates insufficient statistical data.

The statistics displayed within the historical propagation conditions summary are derived from two meteorological data bases: the Radiosonde Data Analysis II assembled by the GTE Sylvania Corporation and the Duct63 assembled by the National Climatic Data Center.

Specified location: 15 00 N 100 00 E (*) INDICATES INSUFFICIENT DATA
Radiosonde source : 48455 13 44 N 100 30 E
Radiosonde station height: 52 Feet
Surface obs source: MS63 15 00 N 95 00 E

PERCENT OCCURRENCE OF ENHANCED SURFACE-TO-SURFACE RADAR/ESM/COM RANGES:

FREQUENCY	YEARLY			JAN-MAR			APR-JUN			JUL-SEP			OCT-DEC		
	day	nit	d&n	day	nit	d&n	day	nit	d&n	day	nit	d&n	day	nit	d&n
100 MHz	3	3	3	3	4	3	3	2	3	3	2	3	2	2	2
1 GHz	37	25	31	45	32	38	36	31	33	25	14	19	41	22	31
3 GHz	46	32	39	54	40	47	45	38	42	35	20	28	51	32	41
6 GHz	74	63	69	76	68	72	74	67	71	68	55	62	78	63	70
10 GHz	90	87	89	90	88	89	90	87	88	91	88	89	91	86	88
20 GHz	95	94	95	96	95	95	95	95	95	96	95	95	95	93	94

SURFACE BASED DUCT SUMMARY:

PARAMETER	YEARLY			JAN-MAR			APR-JUN			JUL-SEP			OCT-DEC		
	day	nit	d&n	day	nit	d&n	day	nit	d&n	day	nit	d&n	day	nit	d&n
Percent occurrence	20	18	19	16	21	19	23	19	21	26	16	21	15	15	15
AVG thickness Kft			.30			.40			.27			.20			.31
AVG trap freq GHz			.78			.47			.91			1.1			.68
AVG lyr grd -N/Kft			124			132			109			124			130

ELEVATED DUCT SUMMARY:

PARAMETER	YEARLY			JAN-MAR			APR-JUN			JUL-SEP			OCT-DEC		
	day	nit	d&n	day	nit	d&n	day	nit	d&n	day	nit	d&n	day	nit	d&n
Percent occurrence	13	7	10	26	12	19	11	5	8	3	3	3	10	8	9
AVG top ht Kft			4.5			6.0			3.6			2.8			5.6
AVG thickness Kft			.45			.47			.57			.33			.41
AVG trap freq GHz			.57			.39			.28			.92			.68
AVG lyr grd -N/Kft			56			56			60			51			57
AVG lyr base Kft			4.1			5.6			3.2			2.5			5.2

EVAPORATION DUCT HISTOGRAM IN PERCENT OCCURRENCE:

PERCENT OCCURRENCE	YEARLY			JAN-MAR			APR-JUN			JUL-SEP			OCT-DEC		
	day	nit	d&n	day	nit	d&n	day	nit	d&n	day	nit	d&n	day	nit	d&n
0 to 10 Feet	2	2	2	1	1	1	2	2	2	3	2	3	3	3	3
10 to 20 Feet	3	5	4	3	5	4	3	4	4	3	4	4	3	6	4
20 to 30 Feet	6	8	7	7	8	7	6	9	8	6	8	7	5	9	7
30 to 40 Feet	8	11	9	8	11	9	8	9	8	10	14	12	5	10	8
40 to 50 Feet	12	17	15	9	14	12	11	14	13	17	24	21	10	16	13
50 to 60 Feet	13	17	15	10	15	13	14	15	15	17	20	18	12	17	14
60 to 70 Feet	11	11	11	8	10	9	12	11	12	13	13	13	10	10	10
70 to 80 Feet	8	7	7	7	8	7	7	7	7	9	5	7	9	7	8
80 to 90 Feet	5	4	4	5	4	4	5	3	4	4	3	4	6	5	5
90 to 100 Feet	3	2	3	4	2	3	3	2	2	2	1	2	4	3	4
above 100 Feet	29	16	22	38	20	29	27	24	25	14	6	10	35	15	25
Mean height Feet	87	68	78	100	75	87	85	80	82	69	53	61	95	66	81

GENERAL METEOROLOGY SUMMARY:

PARAMETER	YEARLY			JAN-MAR			APR-JUN			JUL-SEP			OCT-DEC		
	day	nit	d&n	day	nit	d&n	day	nit	d&n	day	nit	d&n	day	nit	d&n
# Accepted sndgs	407	391	399	391	375	383	407	388	398	409	397	403	422	403	413
% occur EL&SB dcts			1.2			2.1			.64			.49			1.8
% occur 2+ EL dcts			.92			2.1			.65			0			1.0
AVG station N			381			375			387			385			375
AVG station -N/Kft			19			20			20			19			18
AVG sfc wind Kts	10	9.4	10	7.2	7.1	7.2	10	9.1	9.4	13	13	13	10	8.6	9.1

Figure 34. Historical propagation conditions summary.

GTE Sylvania, under contract by the Department of Defense, conducted a large-scale analysis of approximately 3 million worldwide radiosonde soundings during a 5-year period, from 1966 to 1969 and 1973 to 1974. Numerous statistics for tropospheric ducts, superrefractive layers and related weather parameters from 921 radiosonde stations were processed. From these statistics, a propagation conditions database was constructed to show the percent occurrence of enhanced surface-to-surface radar/ESM/communication ranges, the percent occurrence and geometries of surface-based and elevated ducts, and general meteorological parameters.

The National Climatic Data Center, Asheville, North Carolina, under contract from NOSC, produced a subset analysis of its Standard Tape Deck Family 11 (STD-11) data base. The STD-11 data base consists of over 150 years of worldwide surface meteorological observations. These observations were assembled from ship logs, ship weather reporting forms, published ship observations, automatic buoys, teletype reports, and card decks purchased from foreign meteorological services. The subset analysis, known as the the DUCT63, covers 293 Marsden squares and spans 15 years of surface observations. While the world is divided into 648 Marsden squares, only 293 squares were utilized for two reasons. First, TESS/IREPS is specifically concerned with the maritime environment. Marsden squares not containing a region of ocean are excluded from the data. Second, a requirement of at least 100 valid observations per month was imposed to reduce the effects of any spurious meteorological measurements on the distributions. The location of the Marsden squares contained within the DUCT63 analysis is shown in figure 35 as the region enclosed by the heavy border. Using these observations and the modification to evaporation duct height calculations to account for measurement error as discussed in section 10.1, an evaporation duct histogram in percent occurrence was created.

Refractivity profiles constructed from the climatological database are referenced to mean sea level; however the profile information contained within the database is referenced to the actual station height. Therefore, a generated refractivity profile containing a surface-based duct may translate the surface-based duct to an elevated duct when it is referenced to mean sea level. It will always be a surface-based duct at the station height. If a surface-based duct is critical and the translation effect occurs, the profile must be edited prior to use.

Note! Products generated from climatology should always be tagged in the user's comment lines as such. In addition, the percent occurrence of the profile should be noted. To construct a radar coverage display based upon a surface-based ducting profile, which may occur only 2 percent of the time, is inappropriate and misleading unless the product's user understands this limitation.

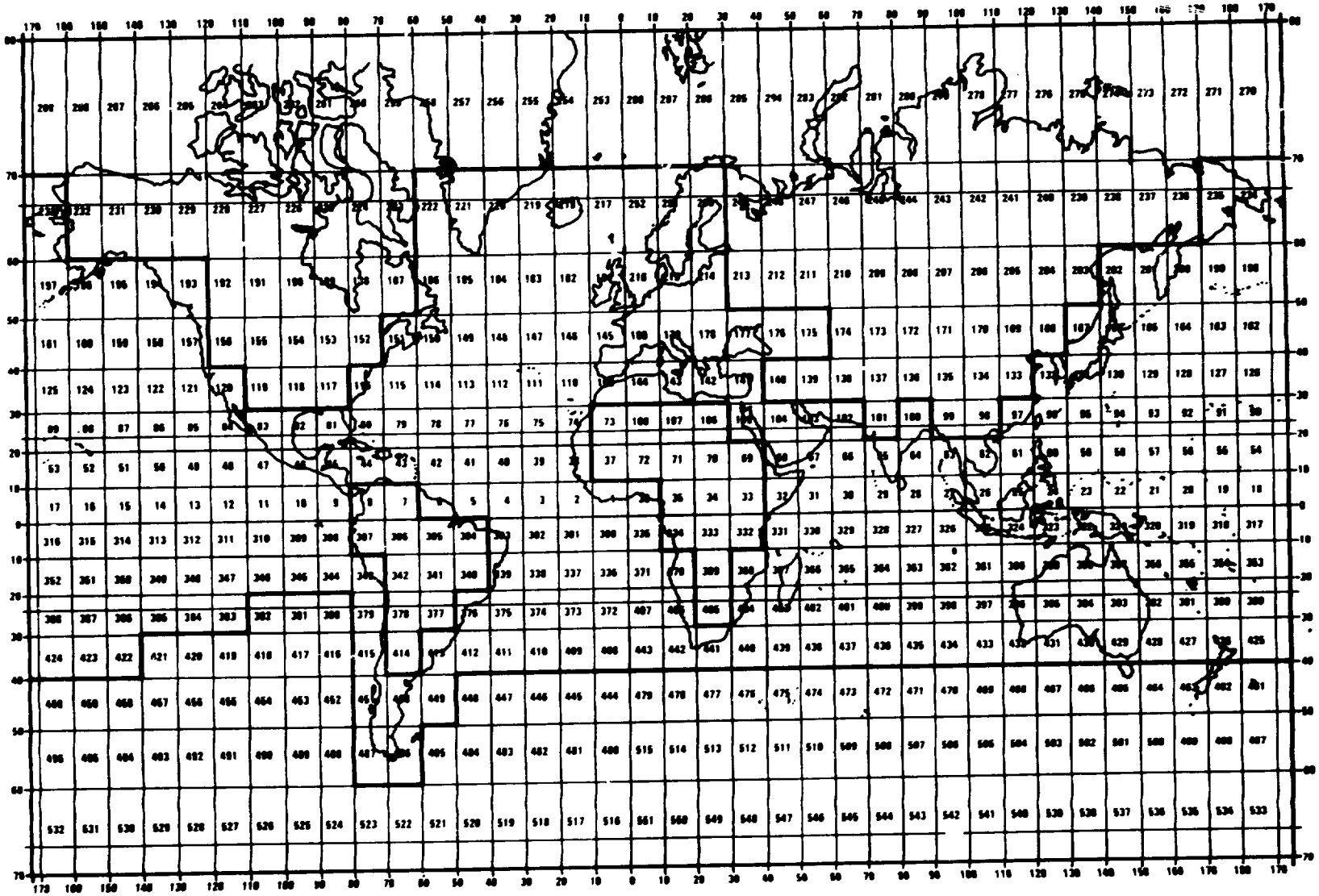

Figure 35. Marsden square numbering system for the world.

10.7 TROPOSPHERIC HORIZONTAL HOMOGENEITY

The troposphere is composed of segments of air called air masses. An air mass is often defined as a widespread body of air that is approximately homogeneous in its horizontal extent, particularly with reference to temperature and moisture; in addition, the stagnation or long-continued motion of air over a particular region, called a source region, of the earth's surface permits the vertical temperature and moisture distribution of the air to reach relative equilibrium with the underlying surface [Huschke, 1959]. A classification system known as the Bergeron classification system names these air masses according to the thermal (tropical (T), polar (P) and arctic or antarctic (A)) and moisture (continental (c) and maritime (m)) properties of the air mass's source region. Figure 36 illustrates the source regions for the major air masses of the world.

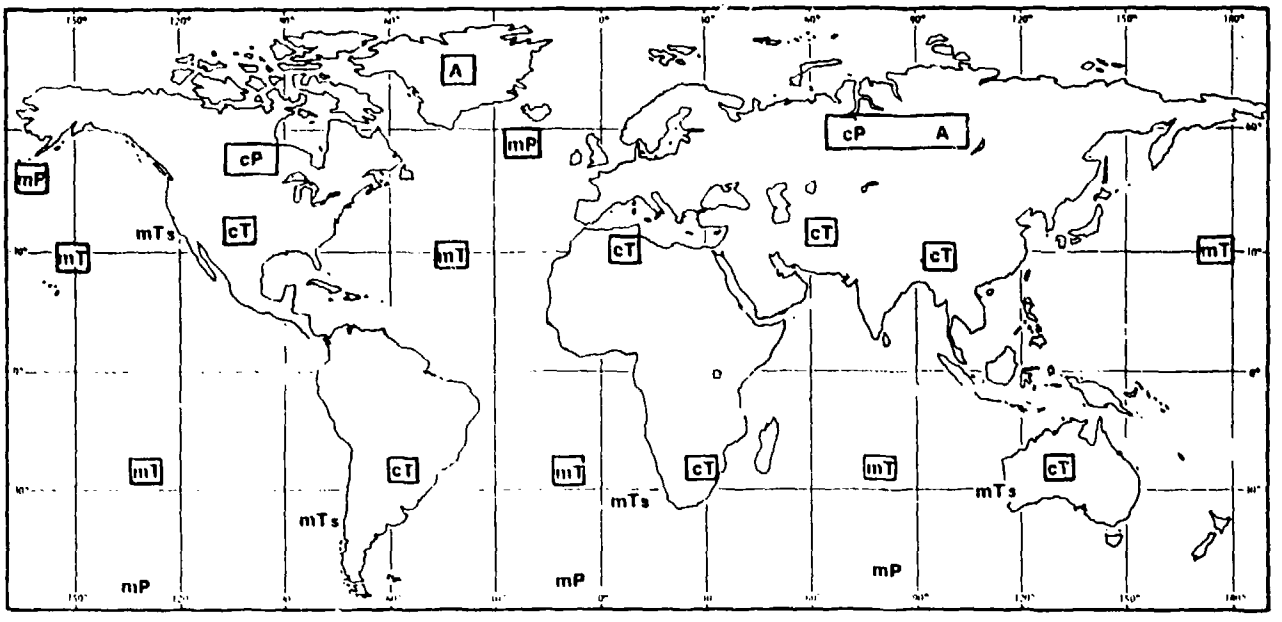

Figure 36. Air mass distribution of the world.

The boundary zone between two different air masses is referred to as a "front." When air masses are in motion relative to each other, the term "front" is modified by a temperature description, the temperature of the air mass moving into a geographical area relative to the temperature of the air mass being displaced. For example, should the cP air mass of Canada from figure 36 move southeastward into the Atlantic Ocean, the boundary zone between it and the displaced mT air mass would be called a "cold front." As can be seen from figure 36, the horizontal extent of an air mass, often in excess of 1600 kilometers, is much greater than that of a frontal zone, usually less than 200 km. In addition, the movement of air masses is generally slow, usually less than 20 knots. It is not unusual, therefore, to have a geographical

area under the influence of one air mass for several days, followed by several hours of changing conditions, returning to an air mass situation for several more days. For subtropical and equatorial latitudes, it is not unusual to have one geographical area under the influence of one air mass for months on end.

Since air masses which are horizontally homogeneous in temperature and moisture cover the majority of the earth's surface, assessment programs such as TESS/IREPS assume that the troposphere is horizontally homogeneous in the vicinity of the system being assessed. Of course, within the air mass itself, it is not unreasonable to find minor fluctuations of temperature and humidity, both horizontally and in time. The question remains, do these fluctuations have a significant influence upon electromagnetic wave propagation? Or in other words, how good is the assumption of horizontal homogeneity for assessment programs such as TESS/IREPS? Dotson [1987] compared 13 radiosonde launches taken simultaneously by two oceanographic research ships, the *R/V Endeavor* and the *R/V Oceanus*. During the period of observation, the separation distance between ships varied between 10 and 340 kilometers. For each radiosonde launch, a radar coverage diagram similar to figure 13 was produced and the height and range to the tip of each lobe (for example, point A of figure 13) was obtained. Figures 37 and 38 illustrate the height and range differences respectively of the lowest lobe for each radiosonde launch. As can be seen, the worst difference in height, 70 meters over 40 kilometers, and the worst difference in range, 1.6 kilometers over 126 kilometers, produce an assessment difference of only 0.018 percent and 0.8 percent respectively. While horizontal fluctuations of temperature and moisture do in fact occur, it would seem they are relatively unimportant for *radar assessment purposes*.

It has been demonstrated by D.F. Glevy, Naval Electronics Laboratory Center (personal communications, 1976), using actual measured signal strengths over an ocean path from San Diego to San Nicolas Island (113 nautical miles), that the troposphere is sufficiently horizontally homogenous to allow for accurate electromagnetic wave propagation assessments 85 percent of the time. This figure has also been confirmed by independent fleet operational units (Commander Third Fleet, 1979).

It is important to restate that TESS/IREPS assumes horizontal homogeneity *within an air mass*. In the vicinity of fronts, continental/ocean boundaries, ice margins, etc., horizontal homogeneity of temperature and moisture does not occur. The operator must insure the environment selected is appropriate to the mission area.

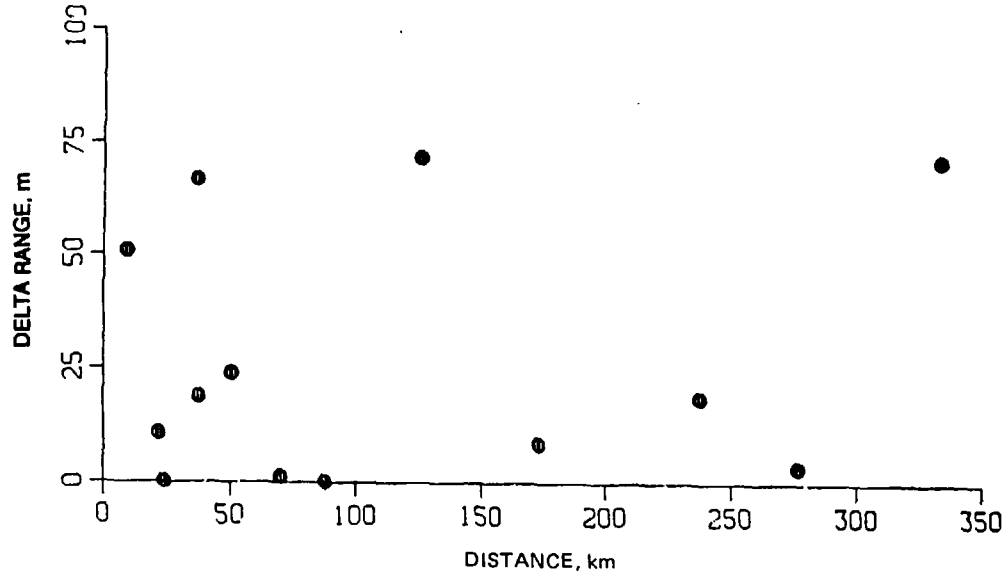

Figure 37. Difference in 50-percent probability of detection, lobe 1 heights for a surface-search radar.

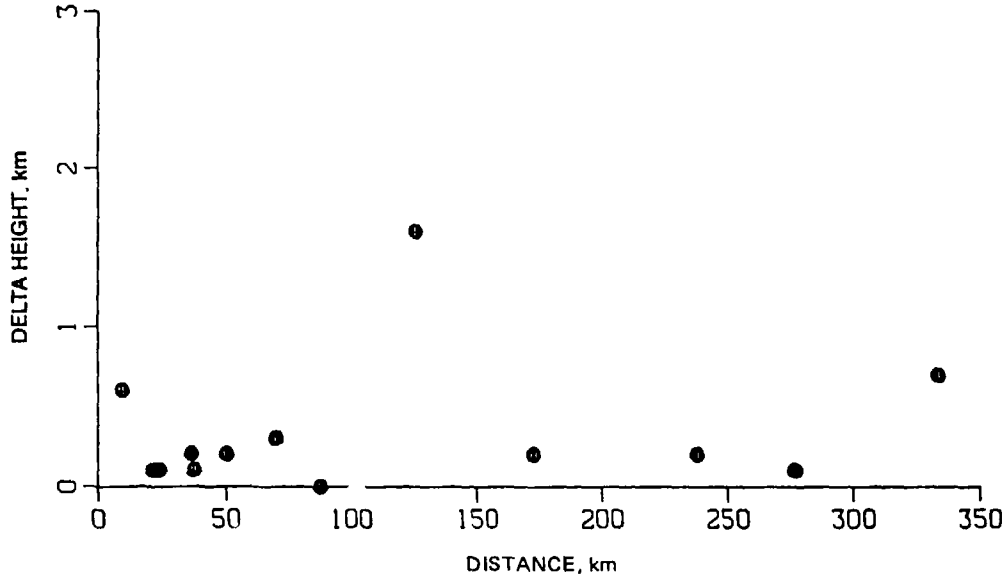

Figure 38. Difference in 50-percent probability of detection, lobe 1 ranges for a surface-search radar.

10.8 VERTICAL DATA RESOLUTION

While an air mass may be horizontally homogeneous in refractivity, it is not homogeneous in the vertical. Therefore, it is necessary to accurately define the vertical distribution of refractivity. As described within section 10.3, for most cases, the vertical profile of refractivity can be adequately described with between 10 to 15 entries of height and refractivity pairs. New high-resolution radiosondes which measure the troposphere every 1.5 seconds, using an ascent rate of 600 feet per minute, would produce 1,520 data points from the surface to a height of 23,000 feet (approximately 400 millibars). Intuitively, it would seem that the greatest vertical resolution would produce the most accurate representation of the troposphere. While this may be a true statement from a meteorological standpoint, for assessment of electromagnetic wave propagation this finely detailed refractivity structure is not necessary and may, in some cases, be misleading.

Consider figures 39 and 40. They illustrate a detailed vertical structure of temperature and humidity obtained from a high-resolution radiosonde. The "+" symbols shown in each figure define the data points selected to accurately represent the profiles. As can be seen, 22 pairs of temperature and humidity data were selected from figure 39 and 12 pairs were selected from figure 40, with both sets of data covering the same vertical extent. The height versus refractivity profiles are illustrated in figures 41 and 42 respectively.

While a difference in refractivity structure is seen, note from figures 43 and 44, typical path-loss versus range assessment products for an airborne system located at approximately 3,200 feet generated from the environments of figures 39 and 40 respectively, there is no significant difference in assessed path loss.

Figures 45 and 46 illustrate airborne radar coverage in a way appropriate to the positioning of an early warning radar (section 14.0). These two figures were generated from the environments of figures 39 and 40 respectively. Here a slight difference between products is observed, but this difference is insignificant when considering the mission of the aircraft and the purpose of the product.

Would the differences be significant for an aircraft with a different mission, such as a fighter trying to gain fire-control radar lock on with a target? It is very likely that such a multiple layered troposphere could cause radar fading problems. This is illustrated by the path-loss versus range products shown in figures 47 and 48 where both radar and target are located at an altitude of approximately 5000 feet.

Other considerations, however, such as a rapidly changing geometry between radar and target (compare figures 43 and 44 with figures 47 and 48) in relation to the anomalous propagation layers would overshadow the anomalous refractivity conditions. Regardless of the refractive significance, use of the illustrated product is inappropriate to a fighter so employed. Figures 49 and 50 illustrate the proper assessment product and it may indeed be seen that there is no significant difference between environments.

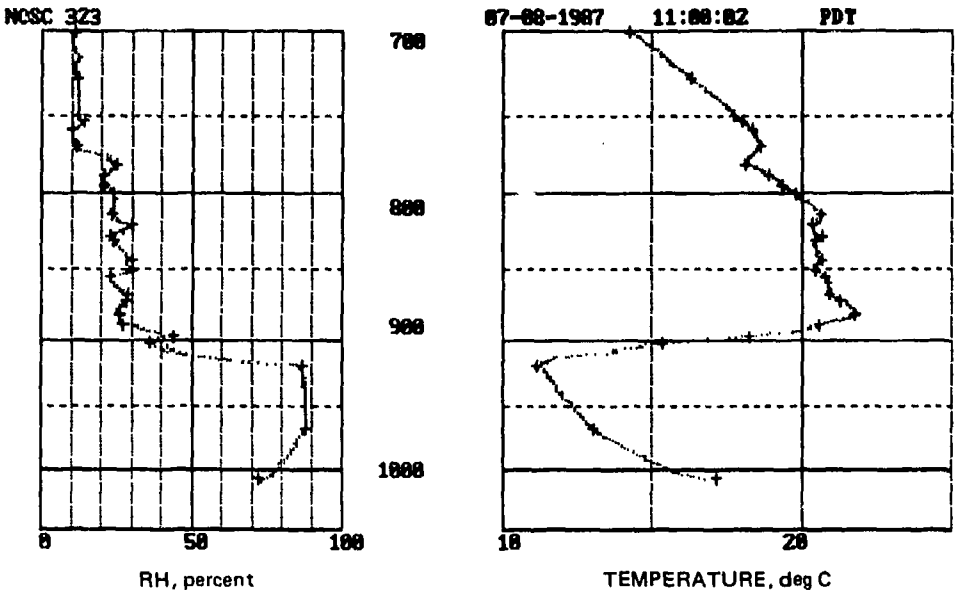

Figure 39. Temperature and relative humidity profiles of 22 pairs from rapid response radiosonde. San Diego, 8 July 1987, 1100 PDT.

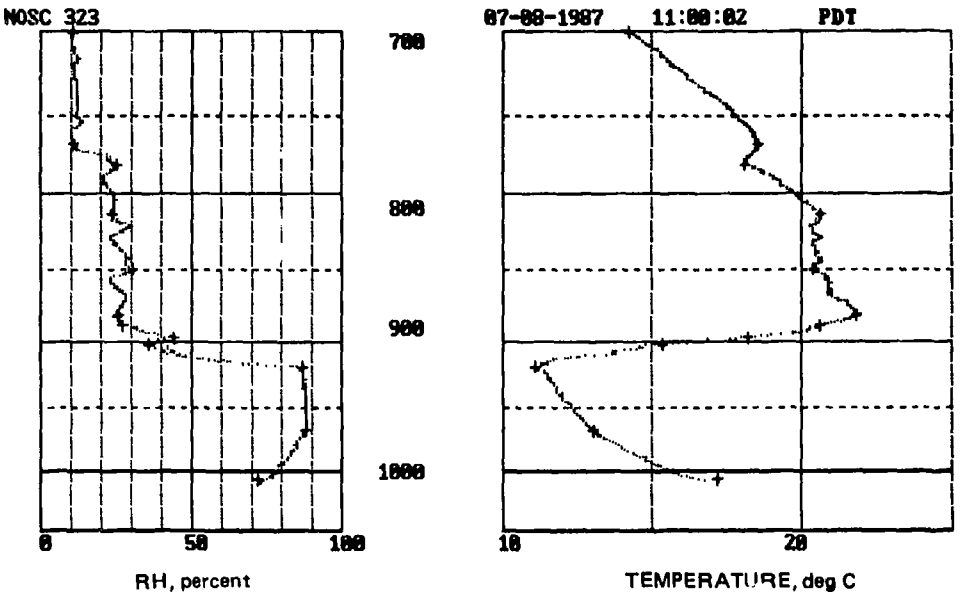

Figure 40. Temperature and relative humidity profiles of 12 pairs from rapid response radiosonde. San Diego, 8 July 1987, 1100 PDT.

LOCATION: San Diego (fine)
DATE/TIME: 07/08/87-1100PDT

WIND SPEED 3 meters per second DEFAULT EVAP DUCT HEIGHT= 13 meters
VISIBILITY is not specified

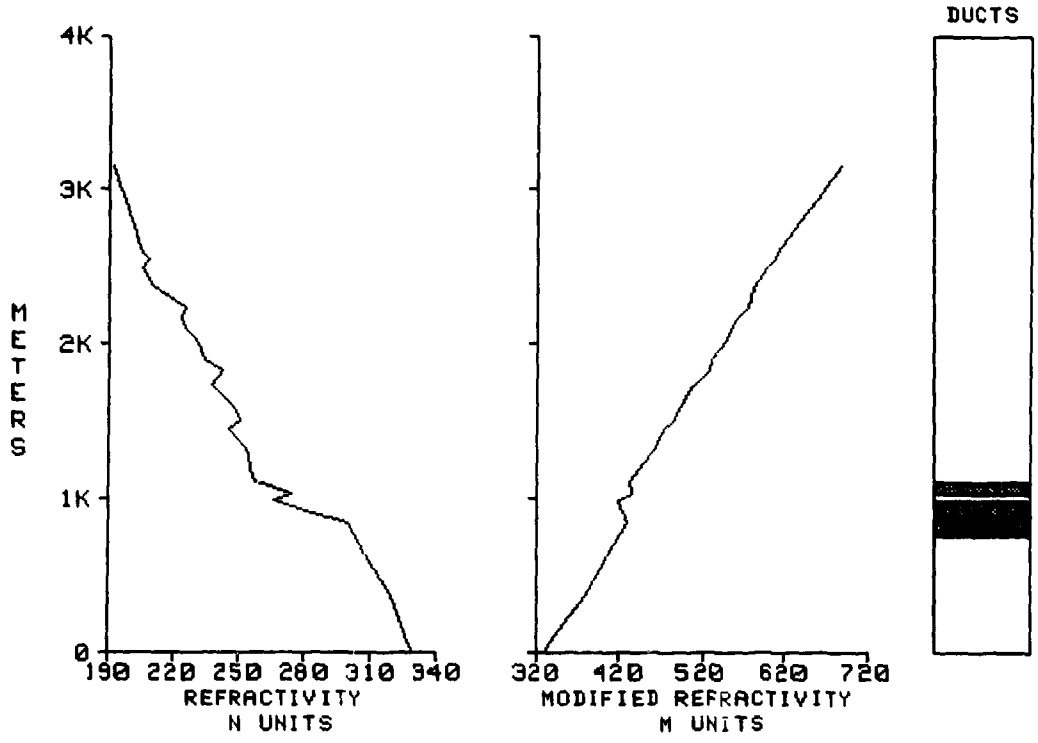

SURFACE-TO-SURFACE
   EXTENDED RANGES FOR ALL FREQUENCIES ABOVE 6 GHZ

SURFACE-TO-AIR
   NORMAL RANGES AT ALL ALTITUDES.

AIR-TO-AIR
   EXTENDED RANGES FOR ALTITUDES BETWEEN   755 AND   988 METERS
   EXTENDED RANGES FOR ALTITUDES BETWEEN 1,026 AND 1,119 METERS
   POSSIBLE HOLES FOR ALTITUDES BETWEEN   988 AND 1,026 METERS
   POSSIBLE HOLES FOR ALTITUDES ABOVE 1,119 METERS
   HOLES FROM SUB- OR SUPER- REFRACTIVE LAYERS MAY EXIST ABOVE 988 METERS

SURFACE REFRACTIVITY: 329 --SET SPS-48 TO 344

Figure 41. Propagation conditions summary derived from data of figure 39.

LOCATION: San Diego (rough)
DATE/TIME: 07/08/87-1100PDT

WIND SPEED 3 meters per second
VISIBILITY is not specified

DEFAULT EVAP DUCT HEIGHT= 13 meters

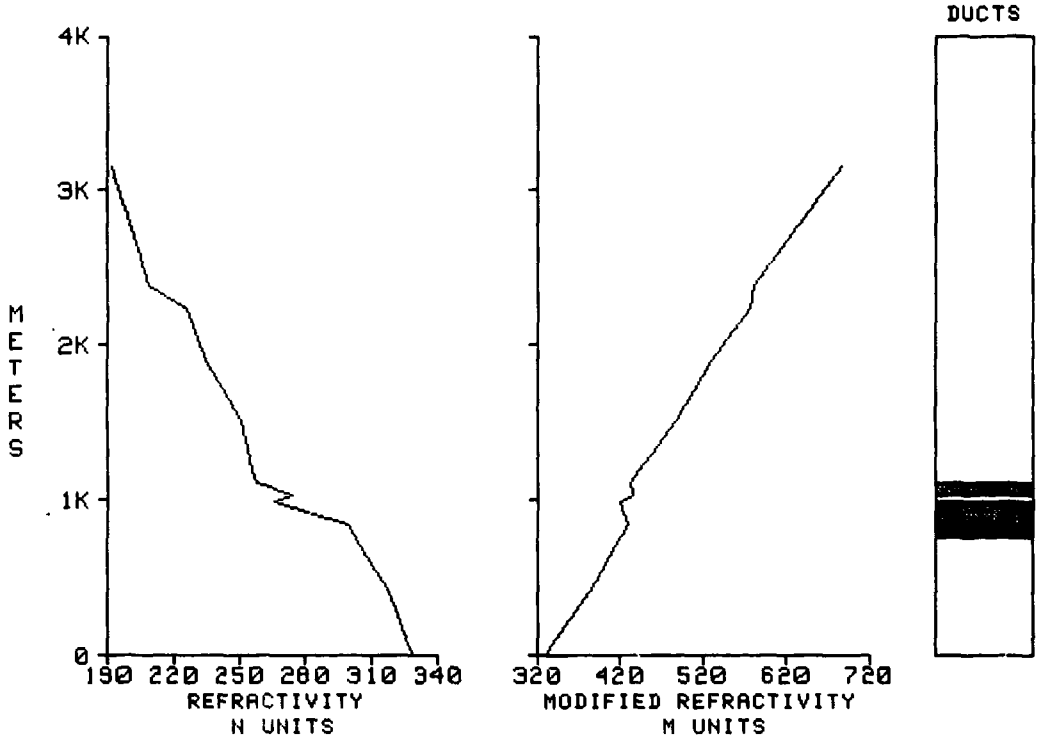

SURFACE-TO-SURFACE
EXTENDED RANGES FOR ALL FREQUENCIES ABOVE 6 GHZ

SURFACE-TO-AIR
NORMAL RANGES AT ALL ALTITUDES.

AIR-TO-AIR
EXTENDED RANGES FOR ALTITUDES BETWEEN 755 AND 988 METERS
EXTENDED RANGES FOR ALTITUDES BETWEEN 1,026 AND 1,119 METERS
POSSIBLE HOLES FOR ALTITUDES BETWEEN 988 AND 1,026 METERS
POSSIBLE HOLES FOR ALTITUDES ABOVE 1,119 METERS
HOLES FROM SUB- OR SUPER- REFRACTIVE LAYERS MAY EXIST ABOVE 988 METERS

SURFACE REFRACTIVITY: 329 --SET SPS-48 TO 344

Figure 42. Propagation conditions summary derived from data of figure 40.

LOCATION: San Diego (fine)
DATE/TIME: 07/08/87-1100PDT

200MHZ AIR OMNI

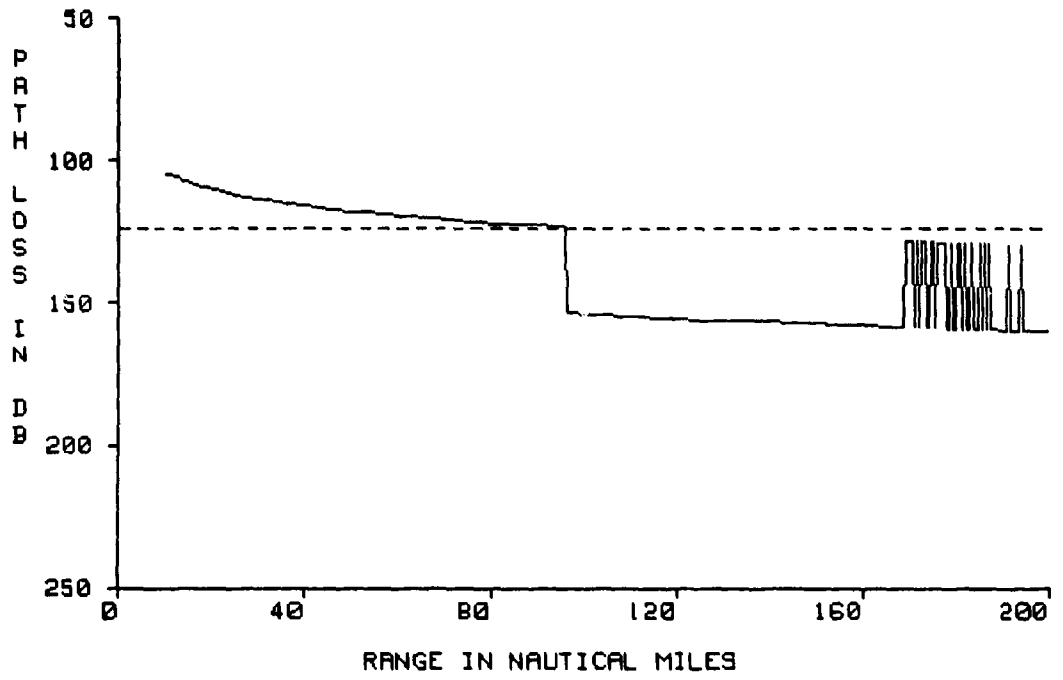

USER OPTIONAL LABEL LINE NUMBER ONE
USER OPTIONAL LABEL LINE NUMBER TWO

HORIZONTAL DASHED LINES INDICATE DETECTION, COMMUNICATION, OR INTERCEPT THRESHOLDS.

TYPE OF PLATFORM: AIRBORNE
TRANSMITTER OR RADAR ANTENNA HEIGHT: 3280.84 FEET
RECEIVER OR TARGET HEIGHT: 9842.52 FEET
FREQUENCY: 200 MHZ
POLARIZATION: HORIZONTAL
FREE SPACE RANGES: 100 NAUTICAL MILES
ANTENNA TYPE: OMNI

Figure 43. Path-loss versus range product derived from environment of figure 39.

LOCATION: San Diego (rough)
DATE/TIME: 07/08/87-1100PDT

200MHZ AIR OMNI

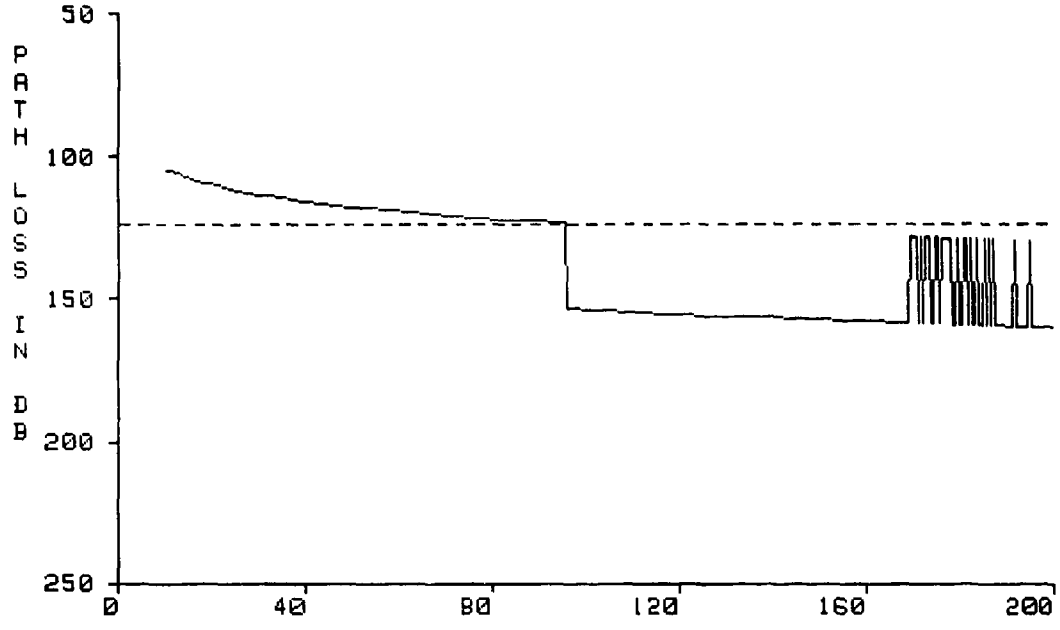

USER OPTIONAL LABEL LINE NUMBER ONE
USER OPTIONAL LABEL LINE NUMBER TWO

HORIZONTAL DASHED LINES INDICATE DETECTION, COMMUNICATION, OR INTERCEPT THRESHOLDS.

TYPE OF PLATFORM: AIRBORNE
TRANSMITTER OR RADAR ANTENNA HEIGHT: 3280.84 FEET
RECEIVER OR TARGET HEIGHT: 9842.52 FEET
FREQUENCY: 200 MHZ
POLARIZATION: HORIZONTAL
FREE SPACE RANGES: 100 NAUTICAL MILES
ANTENNA TYPE: OMNI

Figure 44. Path-loss versus range product derived from environment of figure 40.

LOCATION: San Diego (fine)
DATE/TIME: 07/08/87-1100PDT

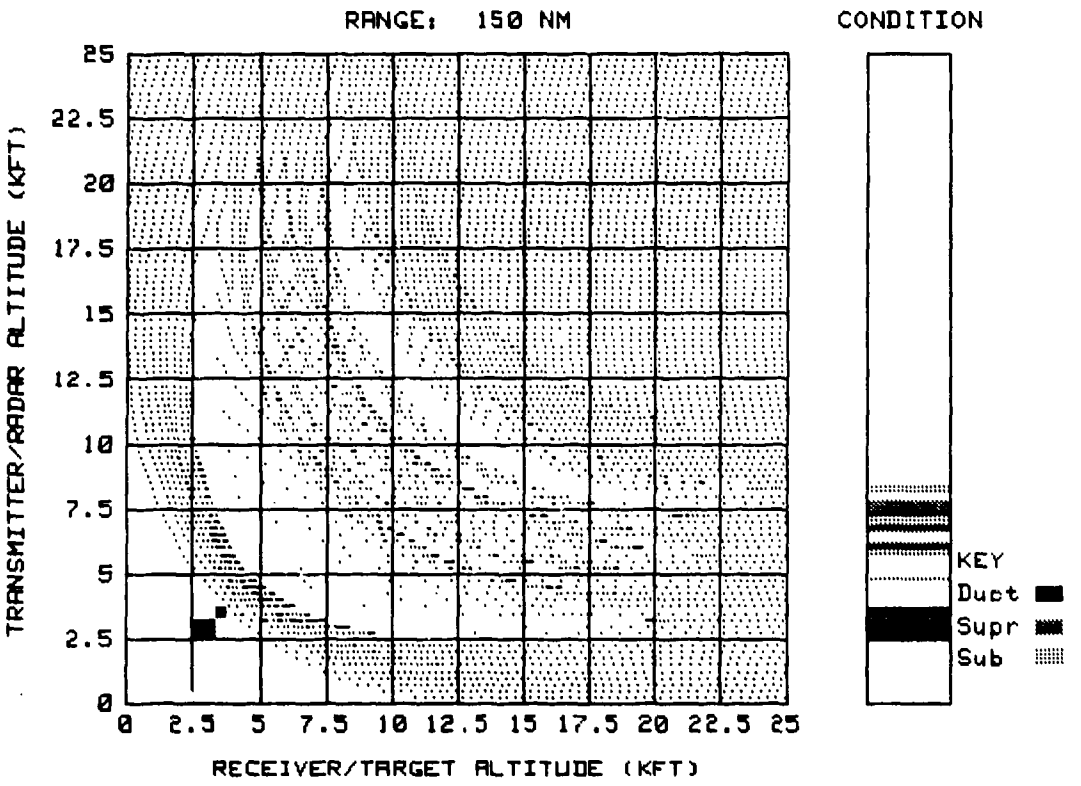

VARIATIONS IN SHADED AREA INDICATE DISTORTIONS IN PROPAGATION AT THIS RANGE

DARKEST SHADING INDICATES RAY CONVERGENCE AND MULTIPATH
LIGHTEST SHADING INDICATES RAY DIVERGENCE

Figure 45. AEW product derived from environment of figure 39.

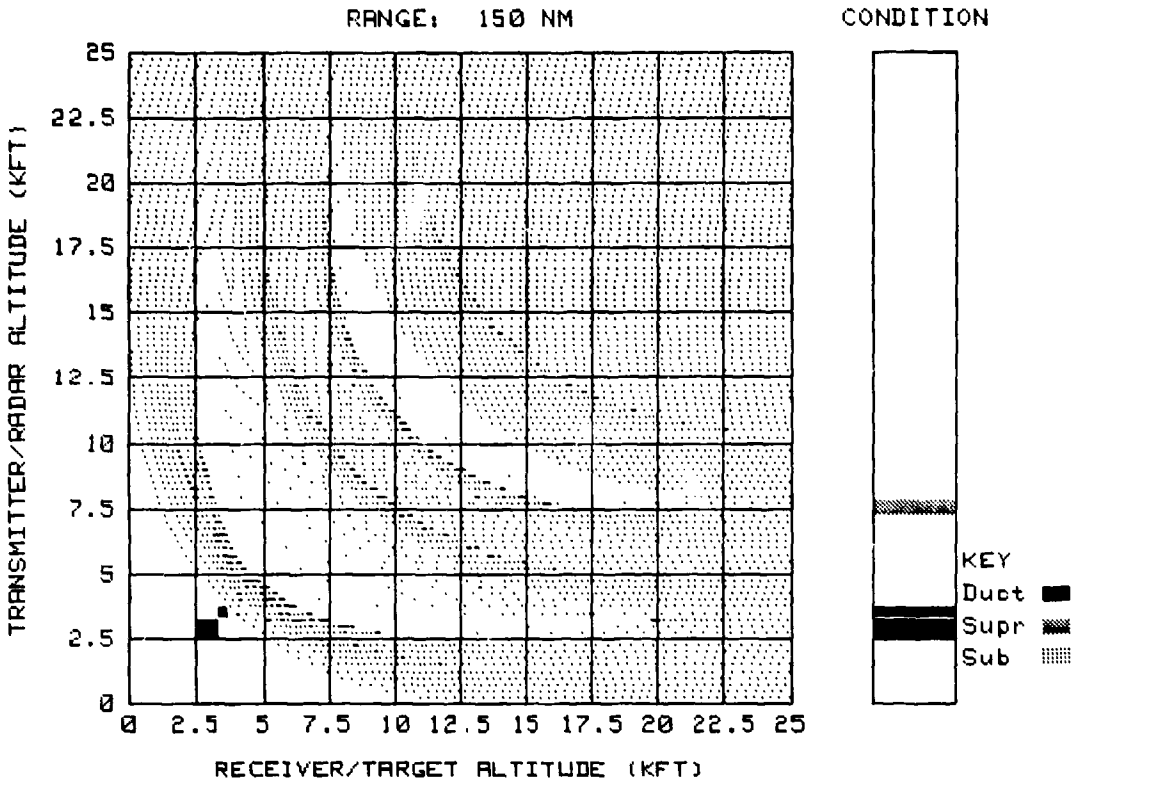

Figure 46. AEW product derived from environment of figure 40.

LOCATION: San Diego (fine)
DATE/TIME: 07/08/87-1100PDT

200MHZ AIR OMNI

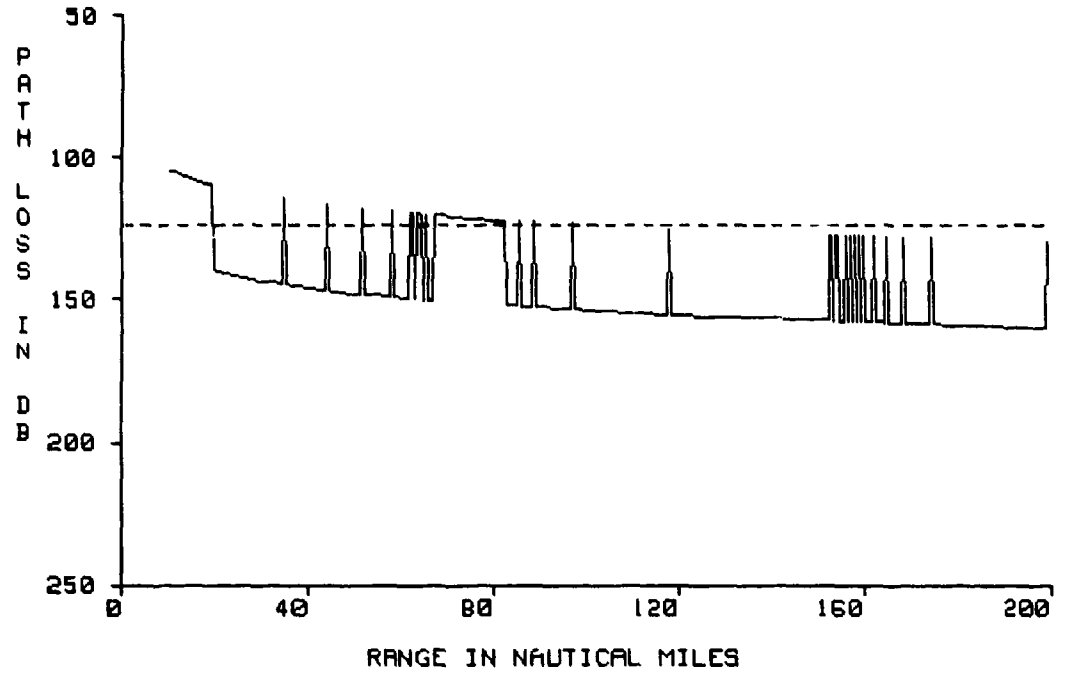

USER OPTIONAL LABEL LINE NUMBER ONE
USER OPTIONAL LABEL LINE NUMBER TWO

HORIZONTAL DASHED LINES INDICATE DETECTION, COMMUNICATION, OR INTERCEPT THRESHOLDS.

TYPE OF PLATFORM: AIRBORNE
TRANSMITTER OR RADAR ANTENNA HEIGHT: 4921 FEET
RECEIVER OR TARGET HEIGHT: 4921 FEET
FREQUENCY: 200 MHZ
POLARIZATION: HORIZONTAL
FREE SPACE RANGES: 100 NAUTICAL MILES
ANTENNA TYPE: OMNI

Figure 47. Path-loss versus range product derived from environment of figure 39.

LOCATION: San Diego (rough)
DATE/TIME: 07/08/87-1100PDT

200MHZ AIR OMNI

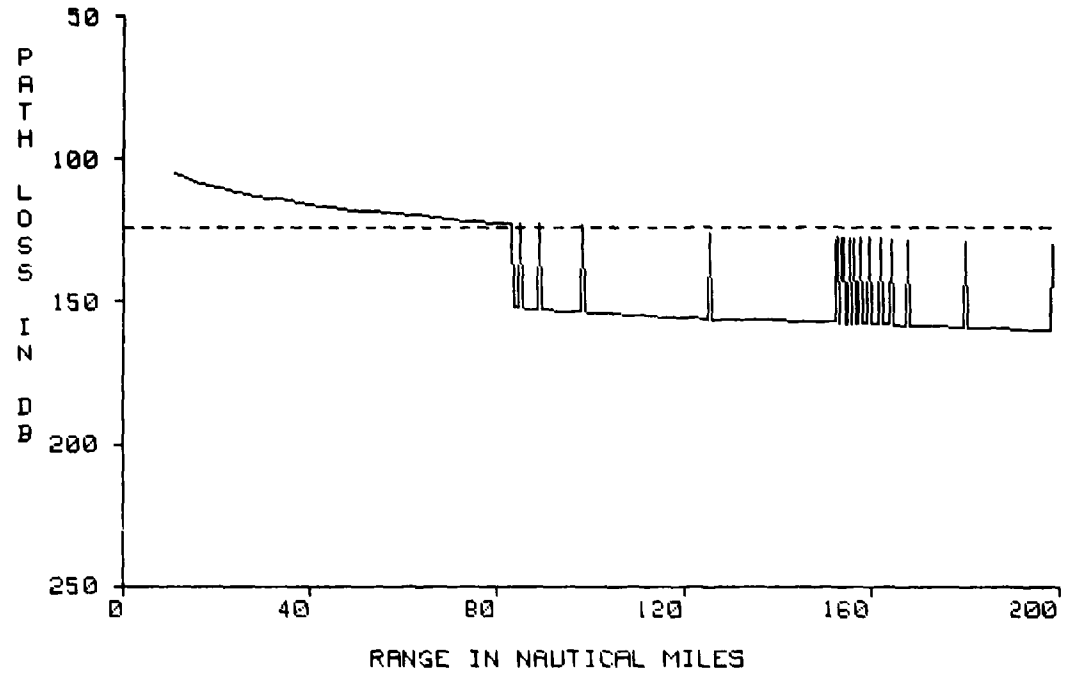

USER OPTIONAL LABEL LINE NUMBER ONE
USER OPTIONAL LABEL LINE NUMBER TWO

HORIZONTAL DASHED LINES INDICATE DETECTION, COMMUNICATION, OR INTERCEPT THRESHOLDS.

TYPE OF PLATFORM: AIRBORNE
TRANSMITTER OR RADAR ANTENNA HEIGHT: 4921 FEET
RECEIVER OR TARGET HEIGHT: 4921 FEET
FREQUENCY: 200 MHZ
POLARIZATION: HORIZONTAL
FREE SPACE RANGES: 100 NAUTICAL MILES
ANTENNA TYPE: OMNI

Figure 48. Path-loss versus range product derived from environment of figure 40.

LOCATION: San . (fine)
DATE/TIME: 07/ -1100PDT

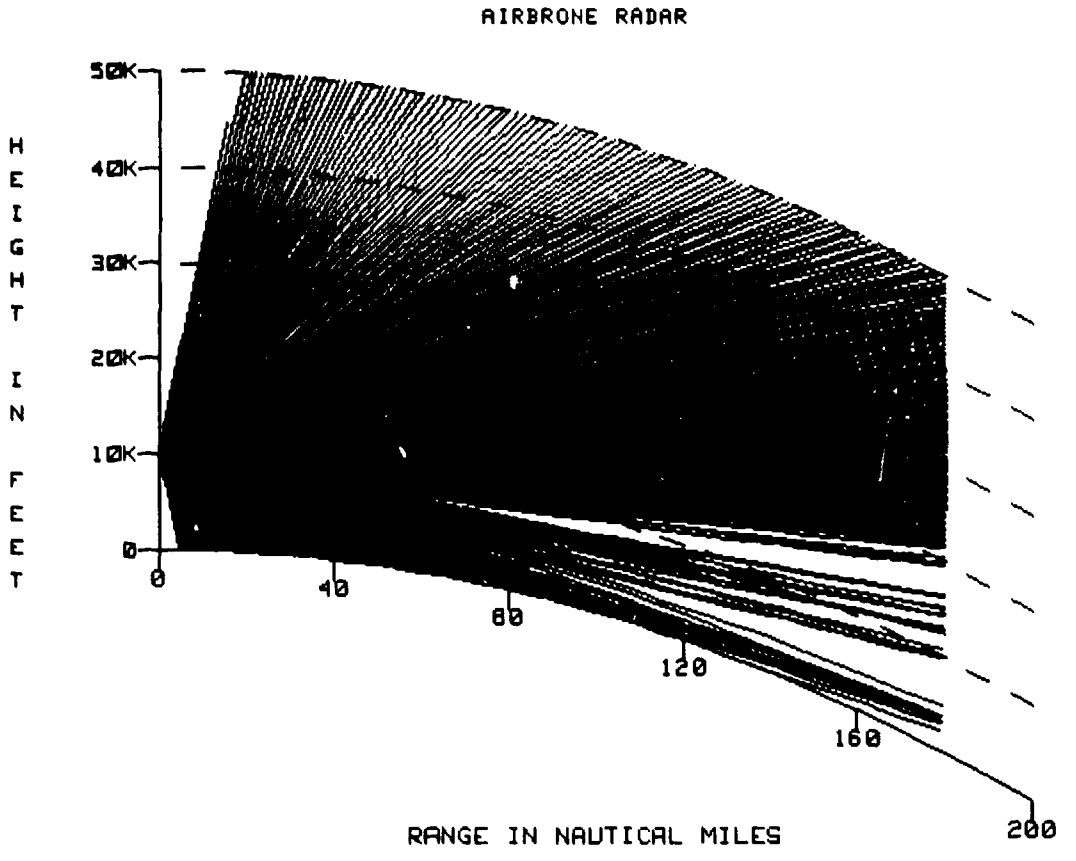

SHADED AREA INDICATES AREA OF DETECTION OR COMMUNICATION

TYPE OF PLATFORM: AIRBORNE
TRANSMITTER OR RADAR ANTENNA HEIGHT: 9842 FEET
FREQUENCY: 400 MHZ
POLARIZATION: HORIZONTAL
FREE SPACE RANGES: 180 NAUTICAL MILES
ANTENNA TYPE: SINX/X
VERTICAL BEAM WIDTH: 20 DEGREES
ANTENNA ELEVATION ANGLE: 0 DEGREES

Figure 49. Radar coverage product derived from environment of figure 39.

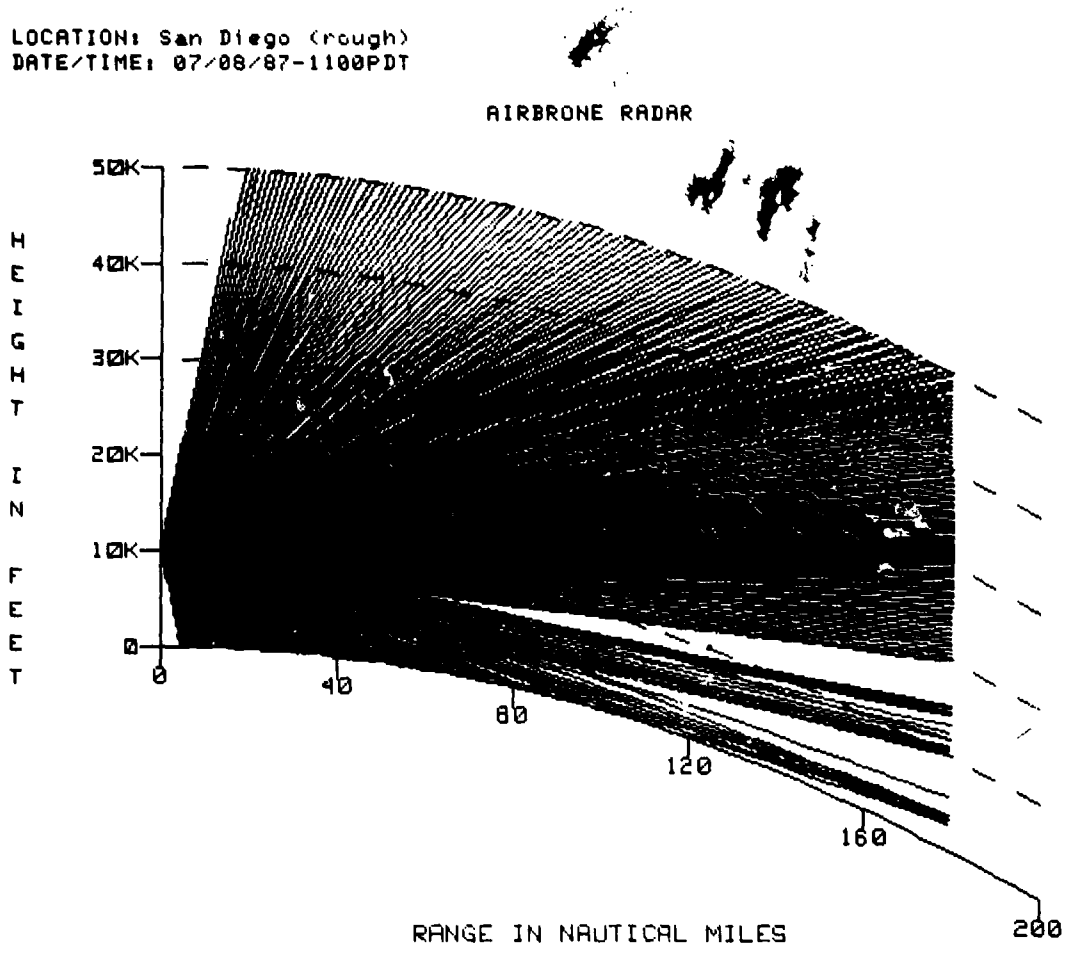

SHADED AREA INDICATES AREA OF DETECTION OR COMMUNICATION

TYPE OF PLATFORM: AIRBORNE
TRANSMITTER OR RADAR ANTENNA HEIGHT: 9842 FEET
FREQUENCY: 400 MHZ
POLARIZATION: HORIZONTAL
FREE SPACE RANGES: 180 NAUTICAL MILES
ANTENNA TYPE: SINX/X
VERTICAL BEAM WIDTH: 20 DEGREES
ANTENNA ELEVATION ANGLE: 0 DEGREES

Figure 50. Radar coverage product derived from environment of figure 40.

A final consideration is the question of data reliability. Large-scale changes of refractivity with height are easily measured and can be convincingly argued to exist. Even small-scale changes of refractivity can be measured and supported with meteorological reasoning. As time and space scales decrease, factors other than meteorological become more significant, however. Some small-scale changes in refractivity may be caused by sensor contamination, faulty instrument construction or malfunctions, computational errors during data processing, or any number of other items. Not only do these data fail to represent the true nature of the troposphere, their inclusion may lead to a tactical decision based upon erroneous information.

The TESS/IREPS operator must determine what environmental data are appropriate and what data are inappropriate *given its intended use*. As shown in the above illustrations, for the purposes of electromagnetic wave propagation as modeled within TESS/IREPS, often *more data are not necessarily better data*.

11.0 ENVIRONMENTAL AND SYSTEM ASSESSMENT PRODUCTS

At the time of this publication, there are 10 environmental or system assessment products within TESS and/or IREPS. These are

a. Propagation conditions summary
b. Radar/radio coverage
c. Radar/radio path loss
d. Stationing for airborne early warning radars
e. Surface-search radar ranges
f. ESM intercept ranges
g. FLIR performance ranges
h. ECM effectiveness
i. Platform vulnerability assessment
j. Battlegroup vulnerability assessment

The products consist of a mixture of alphanumeric labels and graphic displays which may be reproduced upon paper or within an electronic briefing package for display over closed circuit television. As TESS/IREPS undergoes the enhancement process, the display format of a particular product may change. Since the purpose of this document is to improve the understanding and usability of an assessment product, the product formats illustrated within this document are for discussion purposes only and are not meant to reflect a particular edition of TESS/IREPS.

11.1 PROPAGATION CONDITION SUMMARY

Figure 51 shows an example of a propagation conditions summary. This product is used to show the existing refractive conditions for the location and time of the environmental data set selected. In addition, the summary gives a plain-language narrative assessment of what effects may be expected on an electromagnetic system-independent basis.

The summary shows refractivity in N-units and modified refractivity in M-units as a function of altitude. The presence and vertical extent of any ducts are shown by shaded areas on a vertical bar to the right of the refractivity profiles. The quantities of wind velocity and evaporation duct height are printed numerically. Near the bottom of the product are three categories labeled SURFACE-TO-SURFACE, SURFACE-TO-AIR, and AIR-TO-AIR in which brief statements occur concerning the general performance of electromagnetic systems.

**** PROPAGATION CONDITIONS SUMMARY ****

LOCATION: X MARKS THE SPOT
DATE/TIME: HERE AND NOW

WIND SPEED 5 knots
VISIBILITY 7 nautical miles

EVAPORATION DUCT HEIGHT= 30 feet

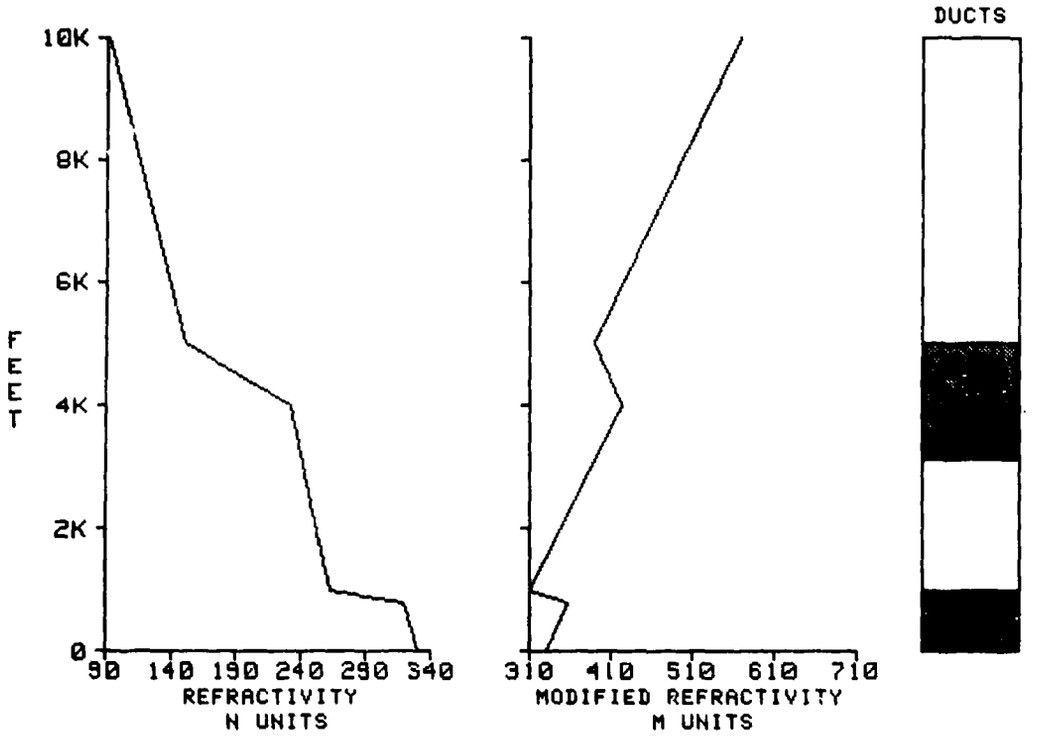

SURFACE-TO-SURFACE
EXTENDED RANGES AT ALL FREQUENCIES

SURFACE-TO-AIR
EXTENDED RANGES FOR ALTITUDES UP TO 1,000 FEET
POSSIBLE HOLES FOR ALTITUDES ABOVE 1,000 FEET

AIR-TO-AIR
EXTENDED RANGES FOR ALTITUDES UP TO 1,000 FEET
EXTENDED RANGES FOR ALTITUDES BETWEEN 3,106 AND 5,000 FEET
POSSIBLE HOLES FOR ALTITUDES BETWEEN 1,000 AND 3,106 FEET
POSSIBLE HOLES FOR ALTITUDES ABOVE 5,000 FEET

SURFACE REFRACTIVITY: 330 --SET SPS-48 TO 344

Figure 51. Typical propagation conduction summary.

The propagation condition summary may be used by the environmentalist to assess the reliability of the input data. Rapid fluctuations in refractivity or unusually sharp gradients in refractivity (outside the ranges of table 2), both of which may be caused by environmental input errors or improper environmental assessment methods, will become obvious by inspection of the refractivity profiles. In addition, the refractivity profiles may be inspected to insure meteorological consistency. For example, if a Santa Ana condition (section 4.2.4) is known to exist, there should be an indication of a surface-based duct or extended performance ranges within the profiles or narrative. The evaporation duct height should be inspected for errors as discussed within section 10.1. An evaporation duct height in excess of 30 meters should be immediately suspect.

Should input data error or meteorological inconsistency be indicated, the TESS/IREPS operator should inspect, either visually or with the use of a thermodynamic diagram (section 10.2), the input environmental data and make corrections or adjustments as necessary.

Once the refractive profiles are assessed to be accurate or meteorologically consistent, the summary may then be used as a starting point in determining which of the other assessment products should be executed for a particular electromagnetic system. For example, should the AIR-TO-AIR description state normal detection ranges are expected, it would not be necessary to produce an airborne radar coverage product for an aircraft at multiple altitudes, since a single coverage product will adequately describe the performance. Should the AIR-TO-AIR description indicate the possibility of radar holes, however, it may be necessary to produce several airborne radar coverage products to illustrate the extent of coverage degradation.

A second example could be an indication of extended detection or intercept ranges for electromagnetic systems above a certain frequency. A series of path-loss products for a whole suite of emitters may be reduced to one or two path-loss products for only the affected emitters. Not only would this greatly reduce the time and manpower efforts needed to obtain an adequate assessment, it would simplify a presentation to a TESS/IREPS customer, thereby reducing the chance of errors, confusion, or misunderstandings.

12.0 RADAR/RADIO COVERAGE DISPLAY

Figure 52 is an example of a radar/radio coverage display product that shows area of coverage on a curved-earth, range-versus height plot. The shaded area in the display corresponds to an area of expected detection or communication for the specified electromagnetic system. Multiple shading densities may be employed with various densities corresponding to variables such as target radar cross section, probability of detection, transmitter power, etc.

For airborne systems, figure 53, only one shading is employed, and the degree of shading has no relationship to the signal level expected at a point. The lines (or rays), which are drawn on a dot-matrix display, often show some patterns or distinct lines within the contour. These are called moire patterns and result from the digital nature of the display. The ray drawing technique minimizes the number of rays plotted to limit the amount of time it takes to produce an airborne system coverage display, and the ray spacing gives rise to the moire patterns.

In addition to the basic coverage display plot, this product also includes location and time labels for the environmental data set and a numeric listing of system parameters used in the generation of the product.

It is not the intent of the coverage model to calculate the maximum range for a given system but rather to show the relative performance at different altitudes as affected by the environment. It is up to the user to insure the free-space ranges being used are appropriate for the application at hand.

In addition to the various limitations of TESS/IREPS as discussed earlier, i.e., horizontal homogeneity, frequency, atmospheric absorption, antenna height, and layer height relationship, etc., the coverage product for an airborne system does not include sea-reflected interference effects (section 4.2) which could cause both reduced and enhanced coverage for low flying radar or target aircraft. The surface coverage display does account for sea-reflected interference effects. To distinguish between the two methods of calculations, the antenna height for surface-based systems is limited to between 1 and 100 meters. The antenna height for airborne systems is limited to the maximum height of the coverage display. Only the maximum range within each lobe of the interference region is plotted when the spacing between lobes becomes very close.

If a maximum unambiguous range has been specified among the system parameters, the coverage display will be terminated at this range. This range cut-off may be seen in figure 53.

The product user should be reminded about the visual distortion of the display caused by the inconsistent height and range units. The interference lobe pattern occurs only in the first couple of degrees above the horizontal.

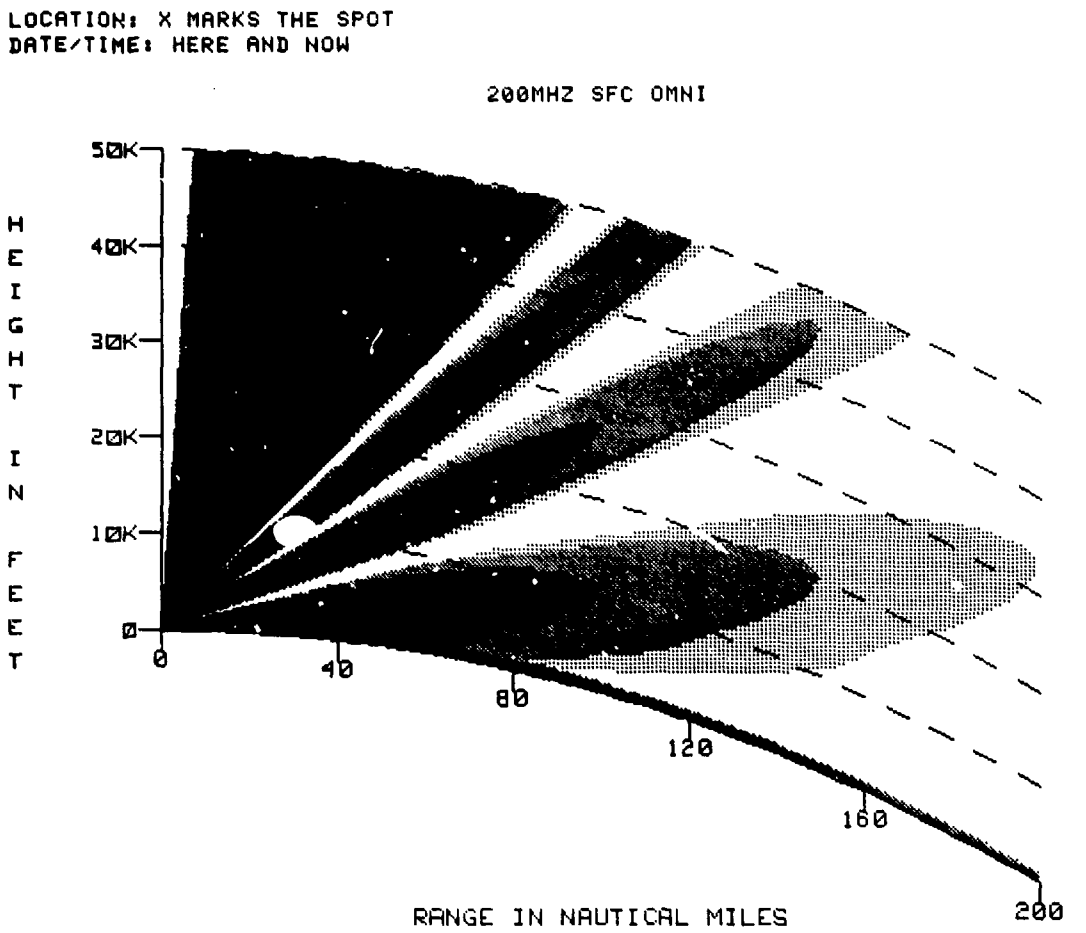

Figure 52. Typical coverage display for a surface-based electromagnetic system.

LOCATION: X MARKS THE SPOT
DATE/TIME: HERE AND NOW

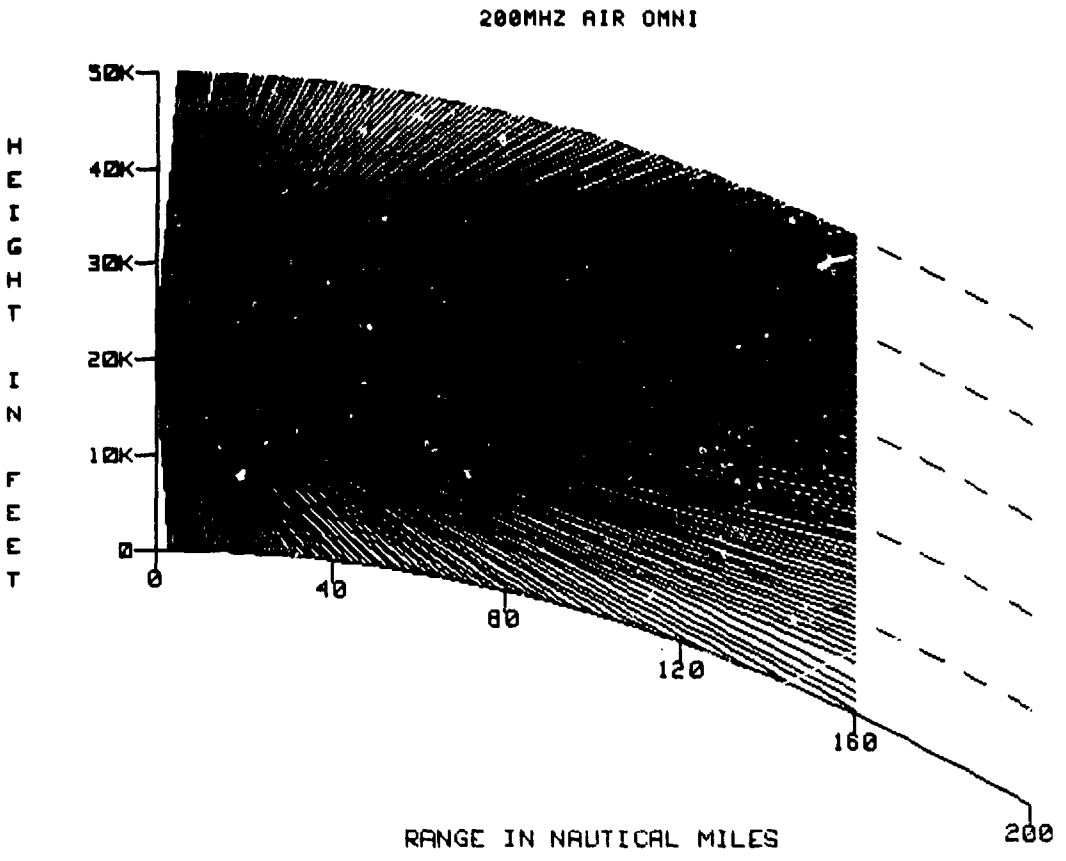

USER OPTIONAL LABEL LINE NUMBER ONE
USER OPTIONAL LABEL LINE NUMBER TWO

SHADED AREA INDICATES AREA OF DETECTION OR COMMUNICATION

TYPE OF PLATFORM: AIRBORNE
TRANSMITTER OR RADAR ANTENNA HEIGHT: 20000 FEET
FREQUENCY: 200 MHZ
POLARIZATION: HORIZONTAL
FREE SPACE RANGES: 200 NAUTICAL MILES
ANTENNA TYPE: OMNI
MAXIMUM INSTRUMENTED RANGE IN NM: 160

Figure 53. Typical coverage display for an airborne electromagnetic system.

The primary use of the coverage display is for

a. Long-range air-search radars, surface-based or airborne

b. Surface-search radars when employed against low-flying air targets

c. Surface-to-air or air-to-air communications.

12.1 USE FOR AIRCRAFT STATIONING

12.1.1 Attack Aircraft

The standard procedure for attack aircraft in penetrating an enemy target's defenses is to fly as low as possible to remain "beneath the radar coverage." This is valid during nonducting conditions. For surface-based ducting conditions, however, the enemy is given a greater detection range capability for targets flying within the duct than for a target at higher altitudes. Knowledge of the existence and height of a surface-based duct would enable the strike group or aircraft commander to select the optimum altitude for penetration. This would be just above the top of the duct, where less enemy radar energy exists for detection of targets. A standard atmosphere condition is illustrated in figure 54, and a surface-based duct condition is illustrated in figure 55.

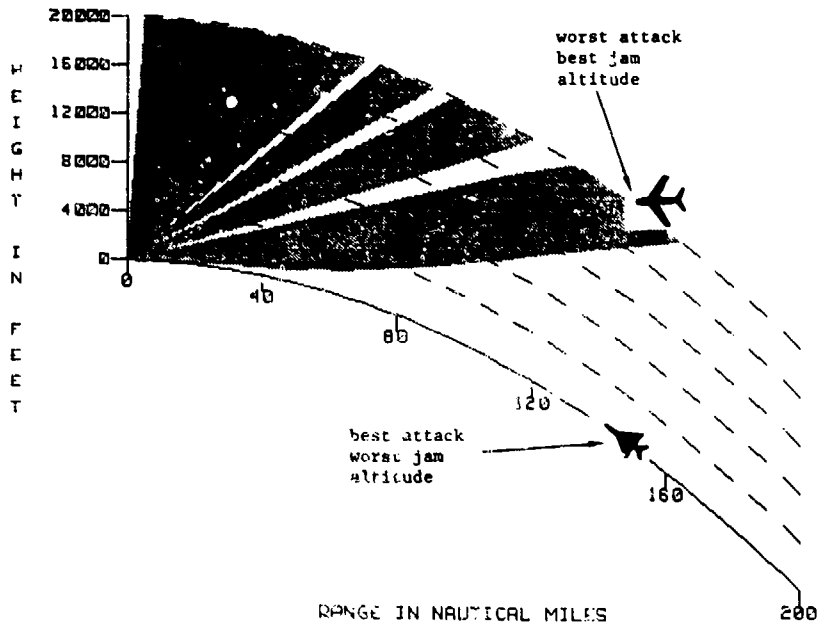

Figure 54. Stationing of attack aircraft without a surface-based duct.

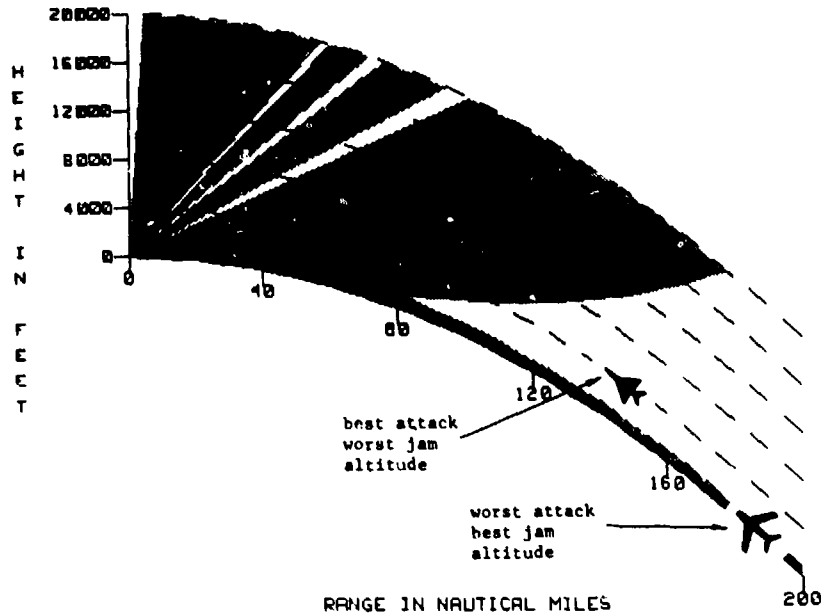

Figure 55. Stationing of attack aircraft with a surface-based duct.

While it would also be possible to avoid detection by flying down one of the interference nulls, the changing height versus range profile would be more difficult to fly and, if the aircraft were off course or the null pattern changed somewhat due to ship roll, detection would occur. In addition, ships usually have several radars, each operating at a different frequency. The lobe structure of the second radar will usually fill in the null structure of the first radar, thereby increasing the likelihood that this maneuver will be unsuccessful.

12.1.2 ECM Aircraft

In a manner similar to that described above, an ECM aircraft can adjust its position to maximize the effectiveness of its jammers by using the coverage display. By flying within a duct or lobe, the aircraft will be more easily detected but at the same time, its jamming effects will be greatly enhanced and its standoff range will be greatly extended, as illustrated in figures 54 and 55.

Figure 56(a) illustrates the jamming effects upon a radar's visual display when the jamming aircraft is flying at an altitude with a direct line of sight to the victim radar but greatly above a surface-based duct. Figure 56(b) illustrates the jamming effects upon a radar's visual display when the jamming aircraft's altitude is within the surface-based duct, even though the range to the victim radar is greatly over the horizon. Since most airborne ECM systems have a slight downward look angle, it may be necessary for the aircraft to fly a high angle of attack to optimize the coupling of energy into the duct.

12.1.3 Early Warning or Reconnaissance Aircraft

By using the proper coverage display, the optimum altitude for AEW aircraft can be determined which will minimize the effects of radar holes created by elevated ducts. Figure 57 illustrates the effect of stationing a typical AEW aircraft within an elevated duct. The aircraft will experience greatly extended detection ranges at all altitudes within the duct but at the expense of a radar "hole" or shadow zone above the duct.

For figure 58, the aircraft has increased its elevation to the top of the duct. It is seen that the region of extended range is gone and the shadow zone has widened and drawn closer to the aircraft. Positioning a surveillance aircraft at the top of a duct will result in the largest possible degradation to radar coverage. As the aircraft altitude increases above the duct, the shadow zone will again narrow and begin at increasing ranges from the aircraft, as illustrated in figure 59.

In figure 60, the aircraft has reduced its altitude to below the duct. While extended ranges are not experienced in this case, a radar shadow zone is also not experienced.

The guideline for positioning a surveillance aircraft in relation to an elevated duct is, therefore, fly as high above the duct as possible or fly anywhere below the duct, consistent with other mission objectives including radar/communication horizon, fuel usage, height assignments by traffic control, etc.

12.2 USE FOR COMMUNICATIONS

A direct tactical application of the knowledge of the presence of surface-based ducting conditions to communications procedures is found in an ASW helicopter engaged in dipping sonar operations beyond the horizon. If ducting conditions are present, the ASW helicopter can maintain both ASW surveillance and communications far beyond the normal radio horizon. If no surface-based duct exists, he must raise his sonar and increase altitude until he is within the horizon.

Figure 61 illustrates a coverage display for a communications system operating under standard atmosphere condition. Here, the aircraft would have to be at an altitude of 1000 feet in order to communicate at a range of 48 nmi on a frequency of 350 MHz. Figure 62 represents a surface-based duct condition. Here, the aircraft may be at any altitude to communicate at 48 nmi.

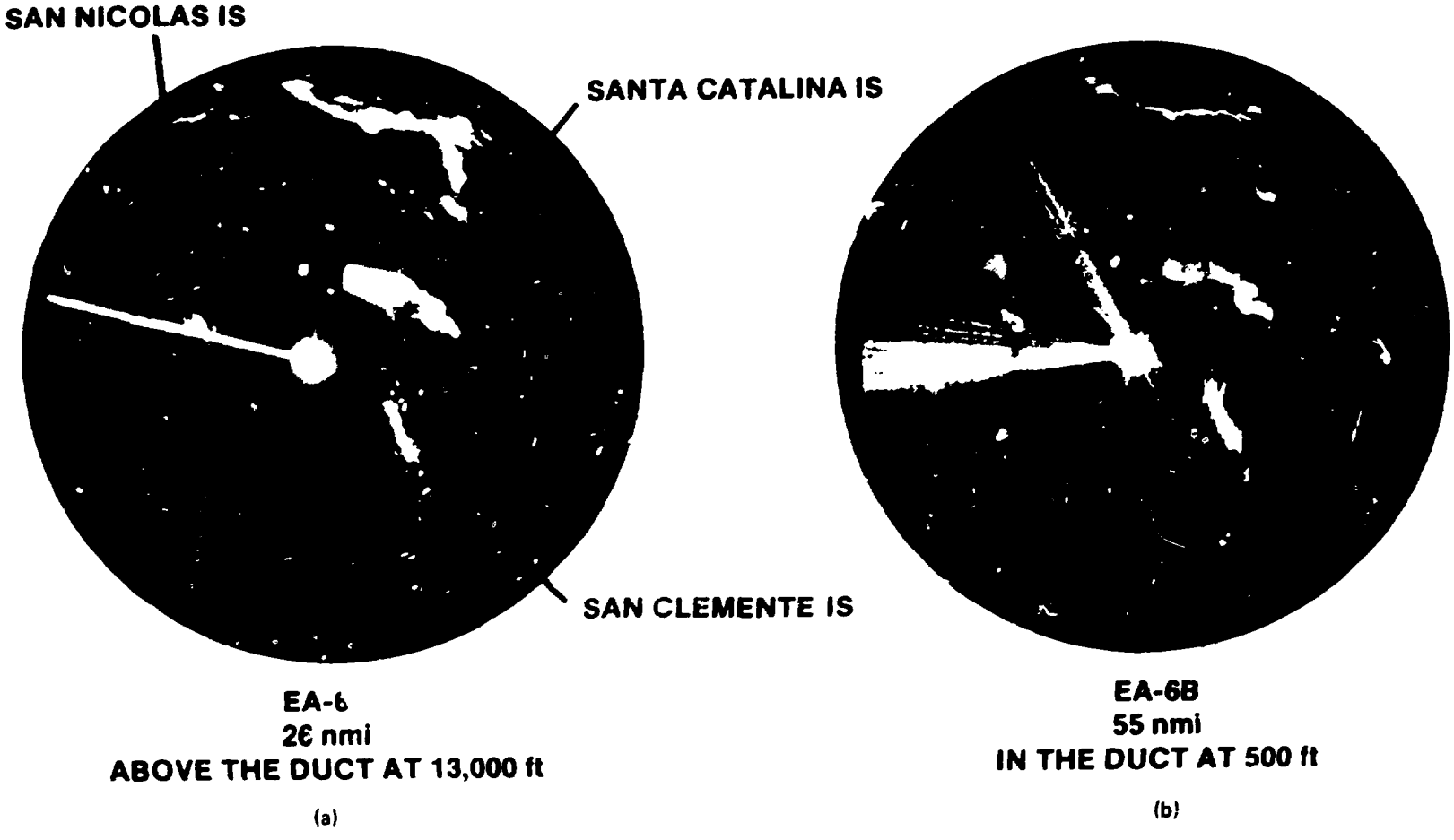

Figure 56. Examples of radar visual display units in the presence of jamming: (a) jamming aircraft above a surface-based duct, and (b) jamming aircraft within a surface-based duct.

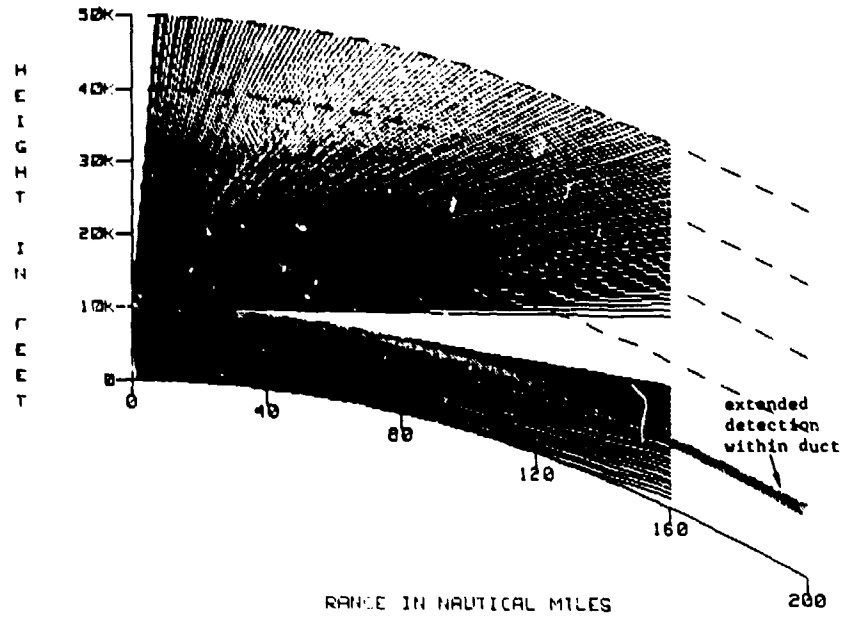

Figure 57. Coverage display for typical AEW radar at 9.5-kft altitude with 200-nmi free-space detection range in the presence of a 9- to 10-kft elevated duct.

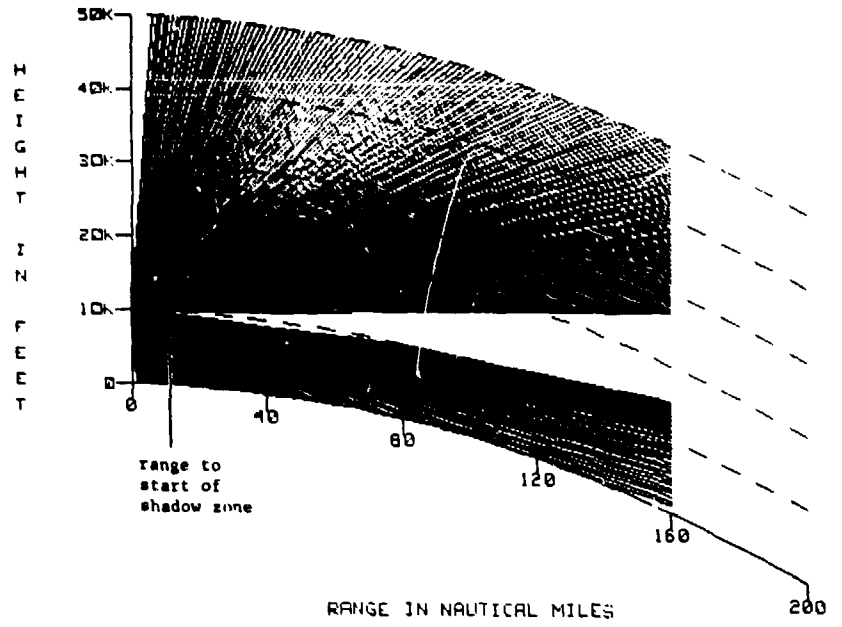

Figure 58. Coverage display for typical AEW radar at 10-kft altitude with 200-nmi free-space detection range in the presence of a 9- to 10-kft elevated duct.

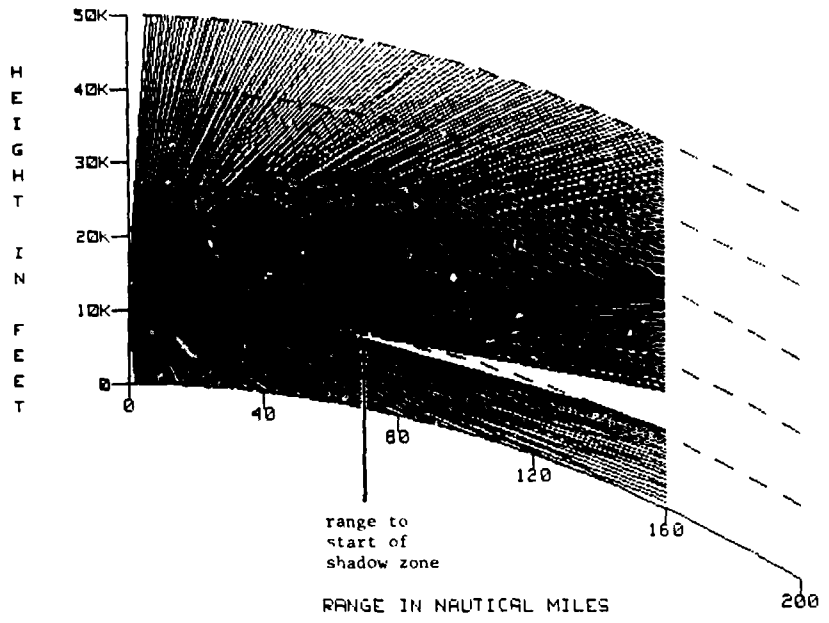

Figure 59. Coverage display for typical AEW radar at 13-kft altitude with 200-nmi free-space detection range in the presence of a 9- to 10-kft elevated duct.

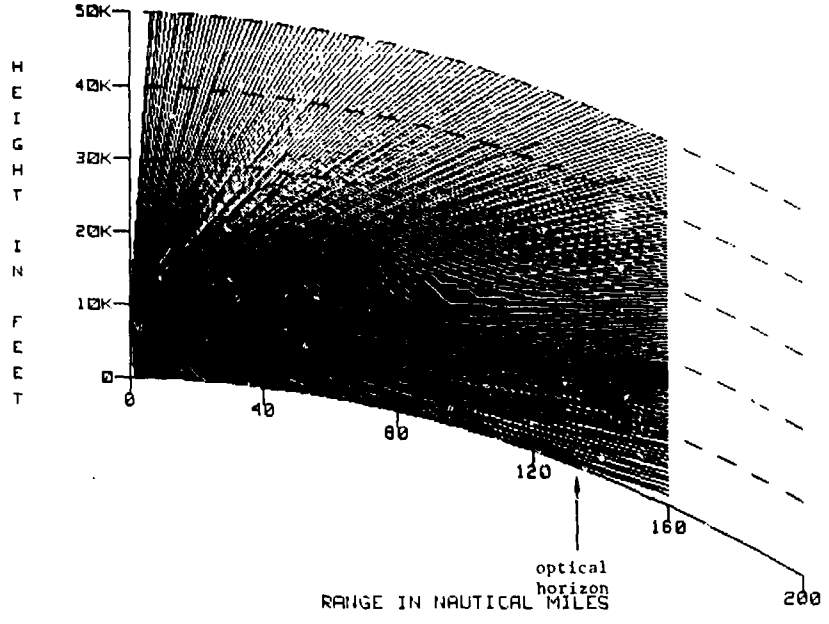

Figure 60. Coverage display for typical AEW radar at 9-kft altitude with 200-nmi free-space detection range in the presence of a 9- to 10-kft elevated duct.

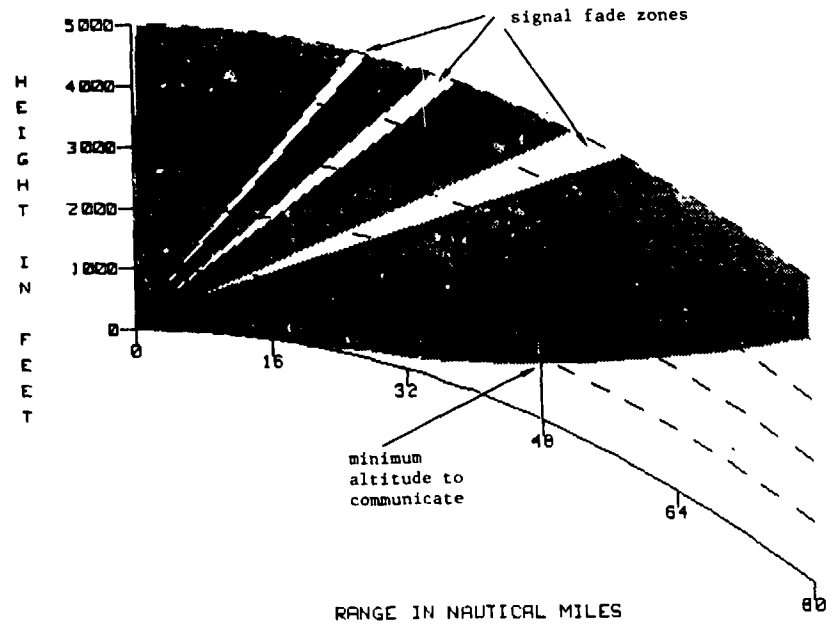

Figure 61. Standard atmosphere coverage display for positioning of ASW aircraft.

A coverage display for surface-to-air UHF communications can show the regions in space where communications are possible, considering the effects of the interference region. This knowledge will enable the aircraft commander to determine his flight profile, thereby minimizing regions of noncommunications.

12.3 USE FOR HARDWARE PERFORMANCE ASSESSMENT

An operator will experience days when detection of targets over the radar horizon is possible and days when extended detection is not possible. In addition, the operator will experience false radar targets or radar "ghosts." Without the knowledge of anomalous propagation conditions, it may be thought that decreased detection ranges are indicative of hardware problems. Without knowledge of the interference patterns, signal fading in UHF line-of-sight communications may also be thought of as indicative of hardware problems. A coverage display for the given day will explain such anomalies and, therefore, preclude unnecessary maintenance calls.

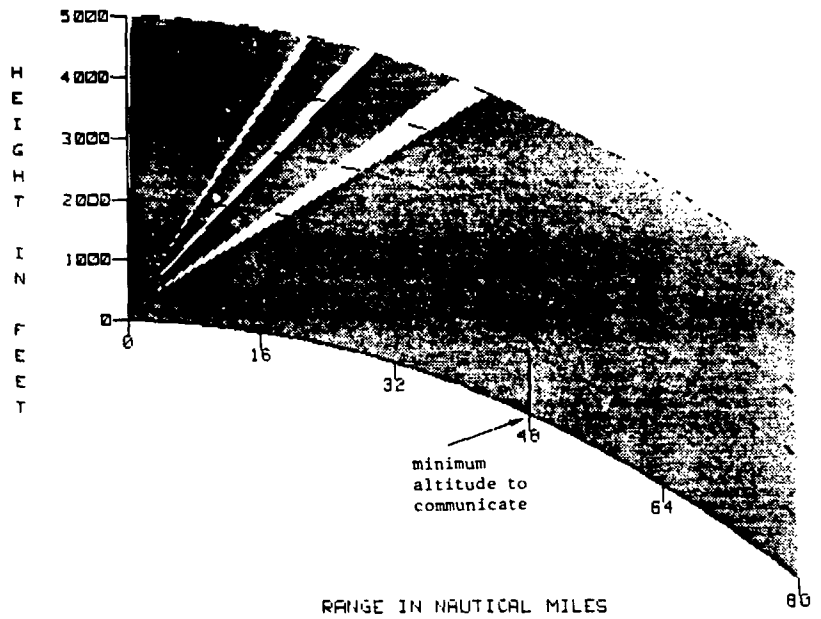

Figure 62. Surface-based duct atmosphere coverage display for positioning of ASW aircraft.

The coverage display may also be used to provide a standard for optimum performance under nonducting conditions. Decreased detection or communications ranges from the standard may, therefore, be a true indication of hardware problems.

12.4 USE WITH FIRE-CONTROL RADARS

The very nature of fire-control radars dictates an antenna which trains both in azimuth and elevation. The coverage for an antenna aimed at the horizon will not be the same as the coverage for an antenna when aimed aloft. The coverage display is designed to show coverage of a radar with a fixed antenna elevation angle.

If the fire-control radar is employed in a search or track mode at a single elevation angle, such as may be the case of a horizon search for low-flying missile targets, the coverage display will produce an accurate representation of the actual radar coverage. It must be understood, however, that once the elevation angle changes, the existing coverage display is no longer valid and coverage must be recomputed based upon the new elevation angle.

Another way to treat the variable antenna elevation angle problem for surface-based fire-control radars is to specify the radar as a "height-finder" radar. In this case, the elevation angle would be fixed at the horizon and the vertical beamwidth of the "height-finder" radar would be the angle covered by the radar's vertical search or track pattern. It must be understood that the coverage indicated at a particular

height/range combination will exist only when the antenna is aimed at the appropriate elevation angle. Or in other words, the coverage displayed is a composite coverage, not an instantaneous coverage. If the fire-control radar is airborne, such as an F-14 stationed in advance of an E-2C, and the radar is being used in a search mode, the antenna would be specified in the normal fashion but the vertical beam width would be the angle covered by the radar's vertical search. Again, the coverage indicated is a composite coverage, not an instantaneous coverage.

In addition to the consideration for antenna elevation angle, the amount of energy directed toward the target must also be taken into account. This is accomplished through the use of a proper free-space range. The best method of determining a free-space detection range is by actual observation. Lacking this a priori knowledge, however, the range may be calculated from certain estimations as discussed within section 9.1. Since fire-control radars do not generally scan the target with a single pulse as the antenna rotates, the fire-control radar must again be treated as a height- finder radar where the number of hits-per-scan may be specified. For complicated search patterns, the number of hits-per-scan must be estimated. This may be accomplished by considering how may pulses are applied to a particular area and the percentage of that area occupied by the target. For radars with variable operating modes, search patterns, and pulse rates, realistic estimations for free-space range calculations may be impossible. Often, a free-space range value may be obtained from the system's operation or maintance manuals.

12.5 USE WITH TARGET DETECTION AND IDENTIFICATION

Identification friend or foe (IFF) assessment between platforms is basically two communications (or ESM intercept) considerations applied simultaneously. In both cases, a determination of the free-space intercept range of both platform's receivers must be made.

To illustrate this concept in a tactical application, the following two questions are asked. First, "How far away may a ship expect to gain radar contact with an aircraft target?" Second, "How close must the ship allow the aircraft to approach before it can be identified?"

These two questions may be resolved by a calculation of the free-space radar, communication, or ESM intercept range as discussed in section 9.0. For the aircraft detection case, equation 17 is solved in the normal manner. To answer the identification question, two considerations are made. For the ship-to-aircraft interrogation, equation 20 is employed using the ship system's transmitted power and frequency and the aircraft system's receiver sensitivity and antenna gain. For the aircraft- to-ship response, equation 20 is employed using the aircraft system's transmitted power and frequency and the ship system's receiver sensitivity and antenna gain.

With these three ranges, a coverage display may be produced with three shading densities such as illustrated in figure 63. Depending upon the sensitivity of the aircraft and ship IFF receivers, the area enclosed by the outer contour may indicate where the aircraft must be in order to have its transponder activated by the ship or where the aircraft must be for detection by the ship. Generally these two ranges will be very nearly the same. The area enclosed by the inner contour indicates where the aircraft must be in order to have the ship receive the aircraft's signal. The area between the contours represents the ranges for which the aircraft is transmitting or is detected but the ship is unable to identify.

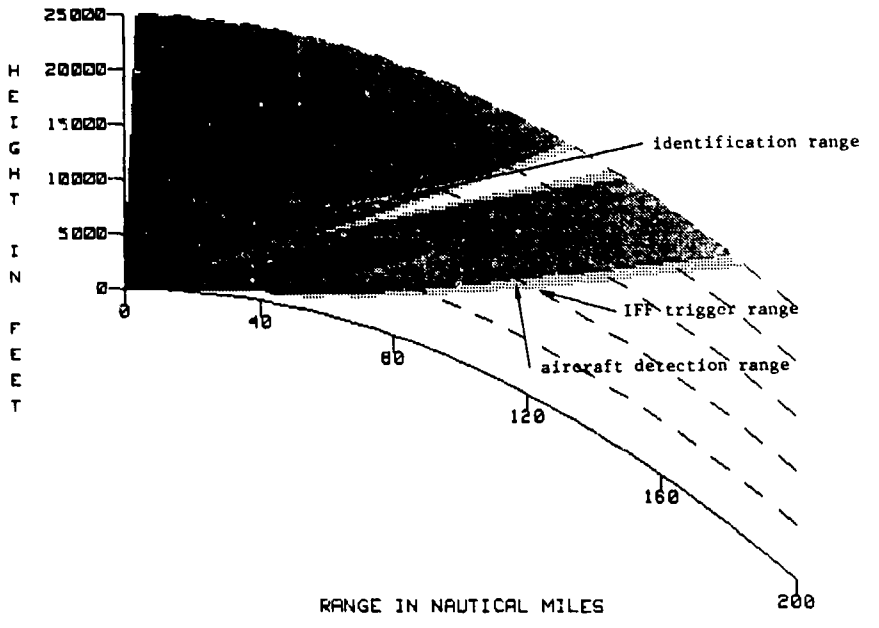

Figure 63. Coverage display illustrating target detection and identification.

12.6 OTHER USES

With careful consideration for the free-space range calculation and understanding the nature of the coverage display, its use may be extended to a number of interesting applications. For example, a coverage display may be generated showing the coverage of a particular surface-based air-search radar against a low flying aircraft. In addition the intercept of the radar by the aircraft's ESM receiver may be superimposed, thus producing a display of ship vulnerability versus target acquisition. Figure 64 illustrates this concept. The area within the inner contour of the figure represents the various height versus range combinations where the ship could expect to gain radar contact of the airborne target. The area within the outer contour represents the height versus range combinations where the ship's radar is vulnerable to ESM intercept. For this example, a standard atmosphere with a 20-meter evaporation duct was selected. Figure 64 shows that a ship should be able to detect a low flyer with an altitude of 600 feet, at a range of 48 nmi. Figure 65 shows the same low flyer should be able to intercept the ship's radar transmission at a range of approximately 200 nmi.

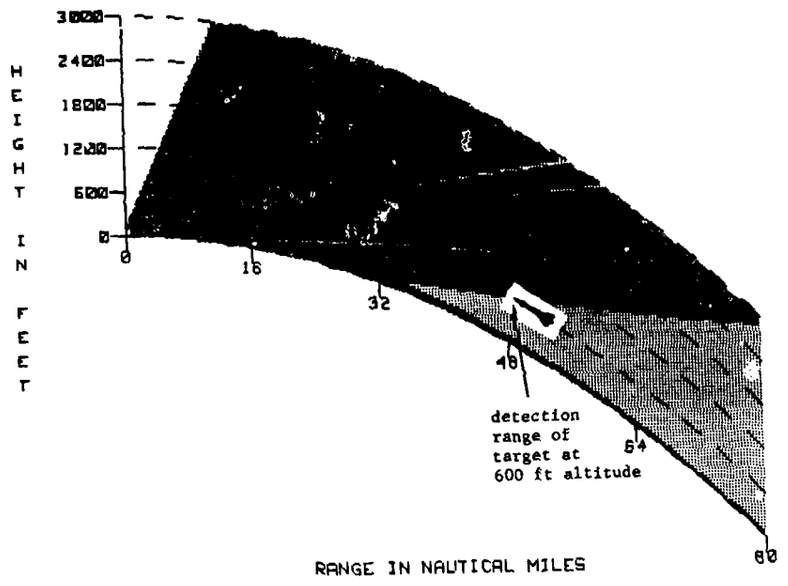

Figure 64. Air coverage against a low flying target by a surface-based air-search radar.

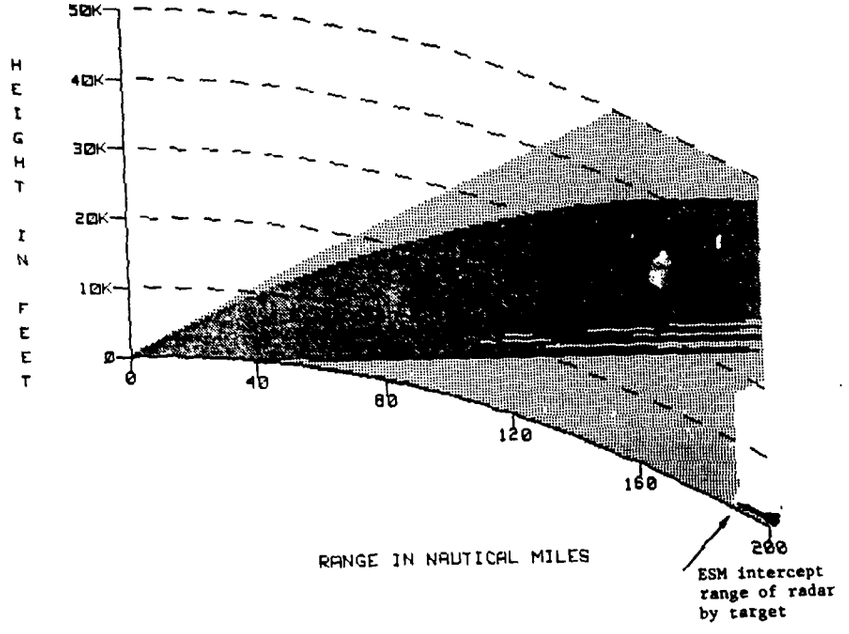

Figure 65. Intercept of a surface-based air-search radar by a low flying antiradiation missile (ARM).

12.7 INAPPROPRIATE USES

12.7.1 Airborne Surface-Search Radars

In the case of airborne (and surface-based) surface-search radars, the transmitted energy is reflected from the earth's surface. While most of this reflected energy will be directed away from the receiver, a portion will be directed back toward the receiver. Radar clutter or backscatter is the term used to describe this undesirable energy. The clutter level may be sufficient to lead to false targets or overpower the return from the desired target, thereby leading to undetected actual targets. Due to the complex nature of the reflecting surface, the TESS/IREPS model does not consider the effect of sea-surface (or land) clutter. Therefore, the assessment provided by the coverage display is designed for use with targets which do not have a reflecting background, or in others words, no radar return from a surface other than the target. For this reason, the coverage display is inappropriate for an airborne surface-search radar. With the proper considerations, the path-loss display discussed in section 13.0 may be used to assess the performance of these radar types.

A second consideration which makes the display inappropriate for an airborne surface-search radar is the very nature of the display design. Recall that the display is designed as a *height* versus range depiction of *airborne* targets by a surface-based radar. Since surface targets are not expected to occur at a height above the surface, a *height* display does not make sense.

12.7.2 Surface-Based Surface-Search Radars

For a surface-based surface-search radar, a major consideration in performance assessment is the target's radar cross section. As explained in section 6.0, the target's radar cross section is a function of the target's shape. Large, flat, smooth surfaces may reflect a large amount of energy, but the scattering will be primarily in one direction. Smaller, more angular surfaces may not reflect as much energy, but the area over which the energy is scattered may be very large indeed. It has been shown that the major energy return from a ship target is not from its smooth, large hull but from its superstructure with its highly angled and complicated structure. In addition, for a very large target, the radar cross section also becomes a function of viewing angle. For these reasons, the radar cross section of a ship must be a composite of many reflectors, or as stated earlier, the ship must be considered a distributed target.

The assessment models employed in generating a coverage display make the assumption that the target is a point source target, independent of viewing angle and composed of only a single reflecting surface. While surface-search radars may be employed for detection of low flying targets such as a missile or aircraft, their major mission is for the detection of ship traffic. The coverage display *is* appropriate for a surface-search radar's coverage against a small point source target such as a missile,

but the coverage display *is not* appropriate for assessing the detection of ships or other large targets and should not be used in this capacity. With the proper considerations, the path-loss display discussed in section 13.0 or the surface-search range tables discussed in section 15.0 may be used to assess the performance of this radar type.

13.0 PATH-LOSS VERSUS RANGE DISPLAY

The path-loss versus range display, as illustrated by figure 66, shows the energy loss along a path parallel to the earth's surface due to spreading, diffraction, scattering, and anomalous propagation. The horizontal dashed line represents an energy level, or threshold, necessary for radar detection, radio communication, ESM intercept, or other electromagnetic system function. The function is possible at all ranges with a path loss above the threshold (lower path loss). The function is not possible or improbable at all ranges with a path loss below the threshold (higher path loss). As with the coverage display, up to four threshold values (one for airborne systems) may be employed upon one path-loss display, with each threshold representing a different receiver sensitivity, transmitter power, probability of detection, target radar cross section, etc.

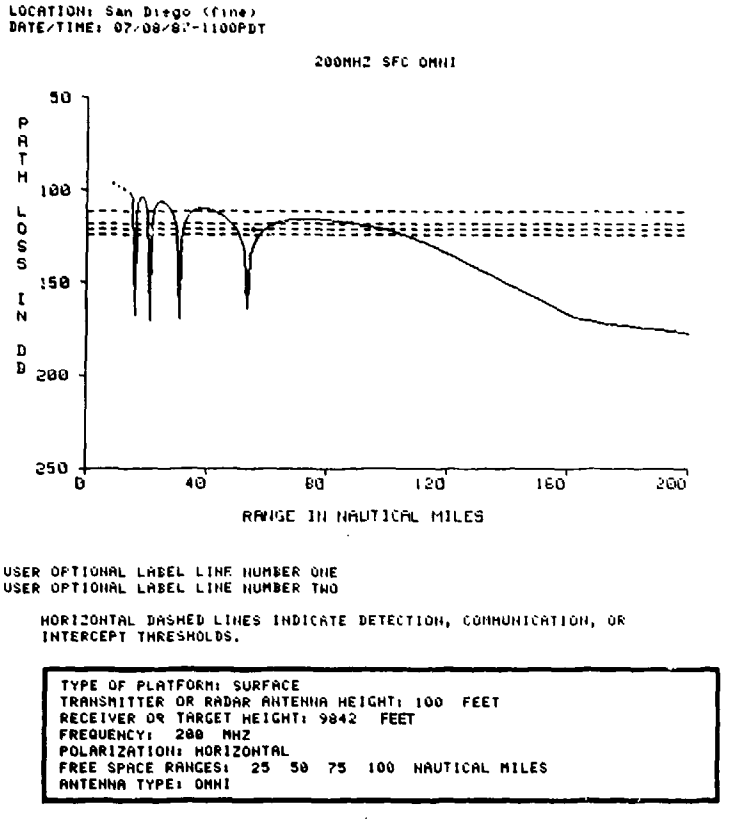

Figure 66. Example of path-loss versus range display.

The same model limitations of atmospheric absorption, system frequency, horizontal homogeneity, etc., as outlined in the coverage display (section 12.0) also apply to the path-loss display.

The use of the path-loss display is appropriate in every situation where a coverage display may be employed. In fact, the path-loss versus range display may be thought of as a horizontal slice of a coverage display. Figure 67 illustrates a path-loss versus range display (for an aircraft target at 20,000 feet) and the corresponding coverage display for a typical surface-based, omnidirectional radiating antenna at a UHF frequency. The free-space range of the coverage display has been converted into a free-space path-loss threshold using the relationships of section 9.0. The points A through E on the coverage display correspond to the points A through E on the path-loss display, illustrating the interference pattern created by the phase difference of direct path and sea-surface reflected waves. The shaded lobes of the coverage display are represented by the portion of the path-loss curve above the path-loss threshold. The unshaded nulls of the coverage display are represented by the portion of the path-loss curve below the path-loss threshold.

Note the aircraft symbols of figure 67 are both at a range of approximately 185 nmi from the transmitter. From the coverage display, the aircraft will be undetected since it is at a range R (approximately 40 nmi) from a lobe (maximum) in the interference pattern. This range corresponds to the signal strength difference ΔS (approximately 22 dB) of the path-loss display, where ΔS is the difference between the minimum signal strength necessary for detection and the actual signal strength at the target.

The simplification of graphics drawing by TESS/IREPS is also seen within figure 67. Note that within the coverage display, the interference pattern detail is smoothed beginning at the fourth lobe. That is, no further lobes or nulls are shown. Within the path-loss display, however, details of two additional lobes and nulls are shown. Beyond the sixth lobe of the path-loss display, only the level of minimum path loss is shown (the dots associated with the letter M). As the range scale of the path loss display changes, the number of lobes plotted will change. The operator must be aware, therefore, that even though the shown path-loss curve is below the minimum path loss, signal fading may still be possible.

In a limited number of cases, the path-loss display may be used to assess systems inappropriate to the coverage display. The path-loss display assumes a point source target. While a large ship target is a distributed target, a careful consideration of its radar cross section will allow for a point source representation. By proper assessment of the target's radar cross section, a specification of both radar and target height, and a recognition of propagation path reciprocity, the path-loss display may be used to assess airborne surface-search radar and surface-based surface-search radar performance against large surface targets.

13.1 USE FOR SURFACE-TO-SURFACE COMMUNICATIONS

The knowledge of the presence or absence of surface-based ducting conditions gives a commander a greater flexibility in deciding the disposition of task force units. For example, if the task force commander wishes to utilize a widely dispersed formation, yet maintain UHF communications among units, he may do so under surface ducting conditions without the necessity of a middleman relay. Presence of surface-based ducting also provides the possibility of UHF backup to over-the-horizon HF communications. This situation is identical to the example associated with figure 88. Note from figure 88, the ASW screening ship is approximately 170 nmi from the nearest ship in the battle group formation. A path-loss versus range display of UHF communications for this example under standard atmospheric conditions is illustrated by figure 68. It may be seen that UHF communications are not possible since the amount of energy needed is 50 dB more than is actually present at the range of 170 nmi.

Under surface-based ducting conditions however, as illustrated by figure 69, surface-to-surface UHF communications would be possible between the screen ASW ship and the battle group. In this case, the amount of energy available is approximately 8 dB above that required.

Since extended ranges for communications also mean extended ranges for ESM intercept, it would be prudent to weigh the benefits of a greatly increased communications range against the much greater increase in the range a potential enemy gains in detection of the radiation. For example, low-power radiation sources, such as flight deck communications (Mickey Mouse) systems, have been intercepted at ranges far greater than the horizon during ducting conditions. Even without the presence of a surface-based duct, the evaporation duct will allow greatly extended intercept ranges, often hundreds of miles. In nature, however, the assumption of horizontal homogeneity discussed in section 10.7 is questionable over these great ranges. The TESS/IREPS operator is cautioned to consider the air mass relationships when confronted with extremely long intercept or detection ranges.

13.2 USE FOR ESM RANGE DETERMINATION

A rough estimate of over-the-horizon ranges to surface ESM contacts can be determined by comparing the range of a surface-based surface-search radar to the range of an ESM intercept. If the ESM contact cannot be seen on the surface-search radar, then it is a fair conclusion that its actual range is between the ranges for surface radar detection and ESM intercept. This range "bracket" could be used for bearing-only missile launches or could be used in conjunction with other information to further localize the contact. Figure 70 illustrates the path-loss display for this situation.

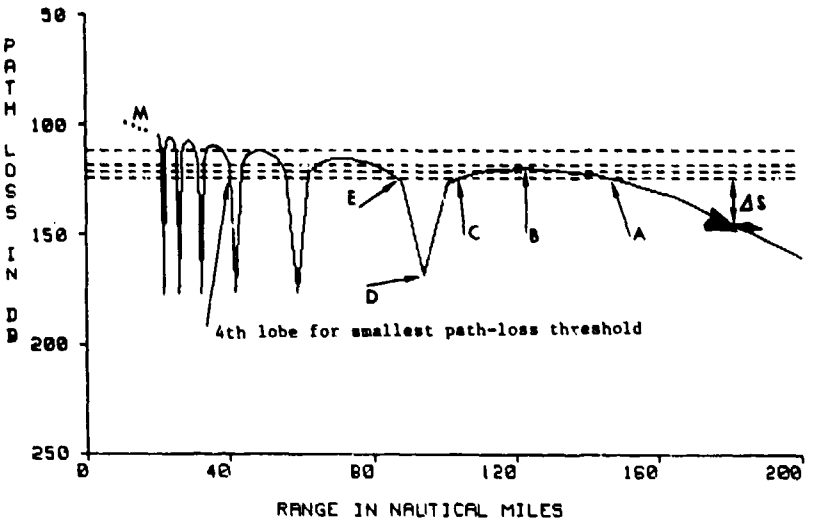

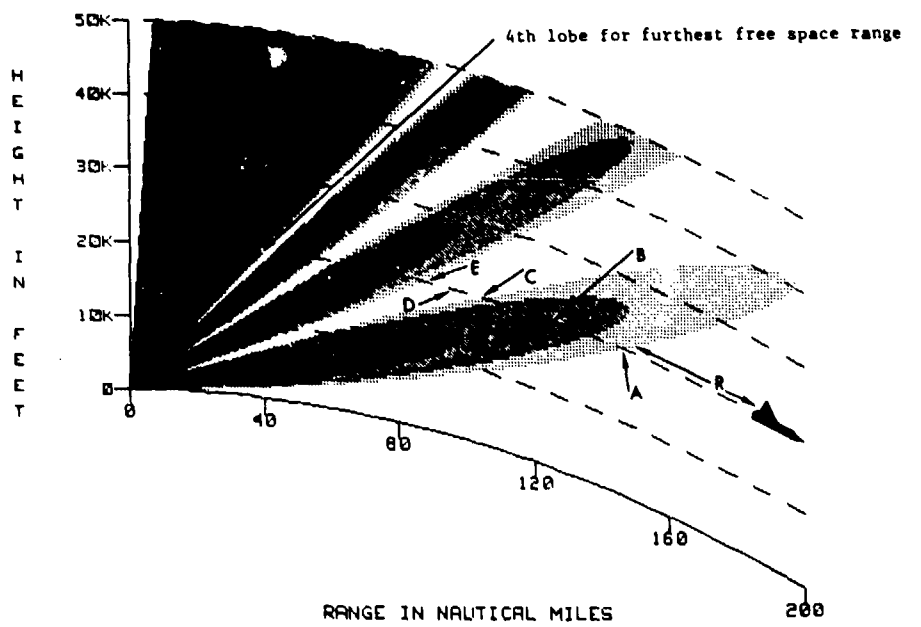

Figure 67. Example coverage display and corresponding path-loss display.

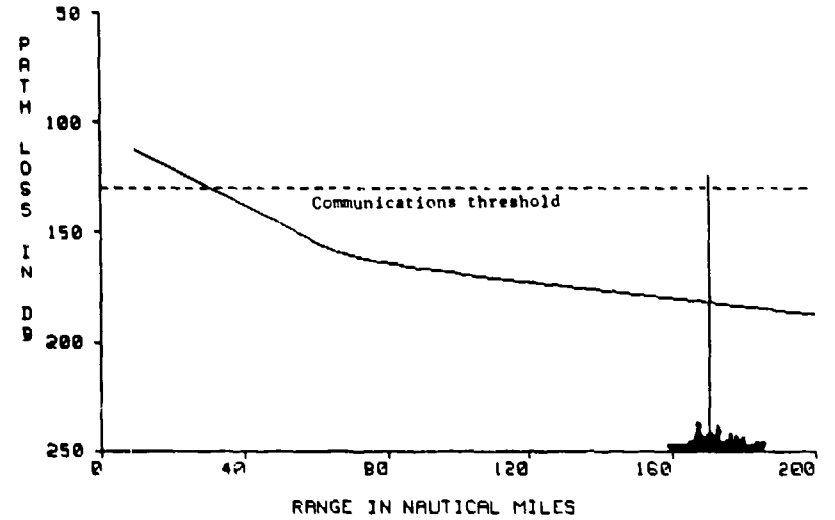

Figure 68. Path-loss versus range display for surface-to-surface UHF communications under standard atmospheric conditions.

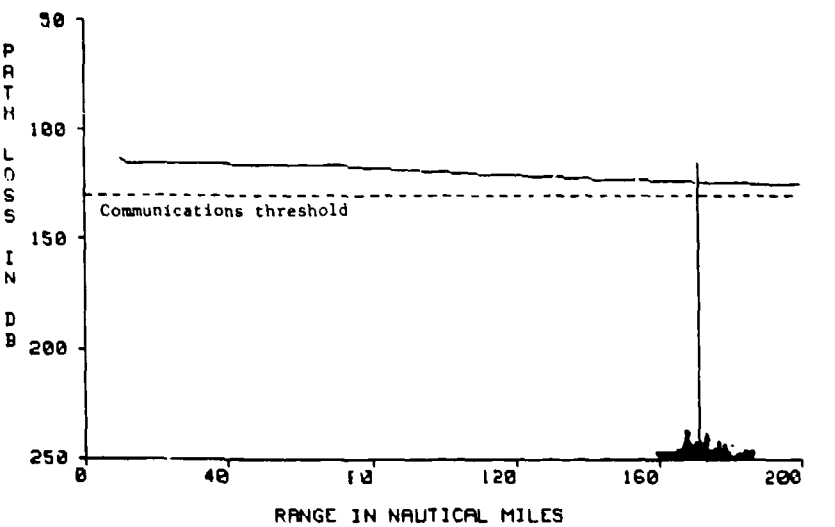

Figure 69. Path-loss versus range display for surface-to-surface UHF communications under surface-based ducting conditions.

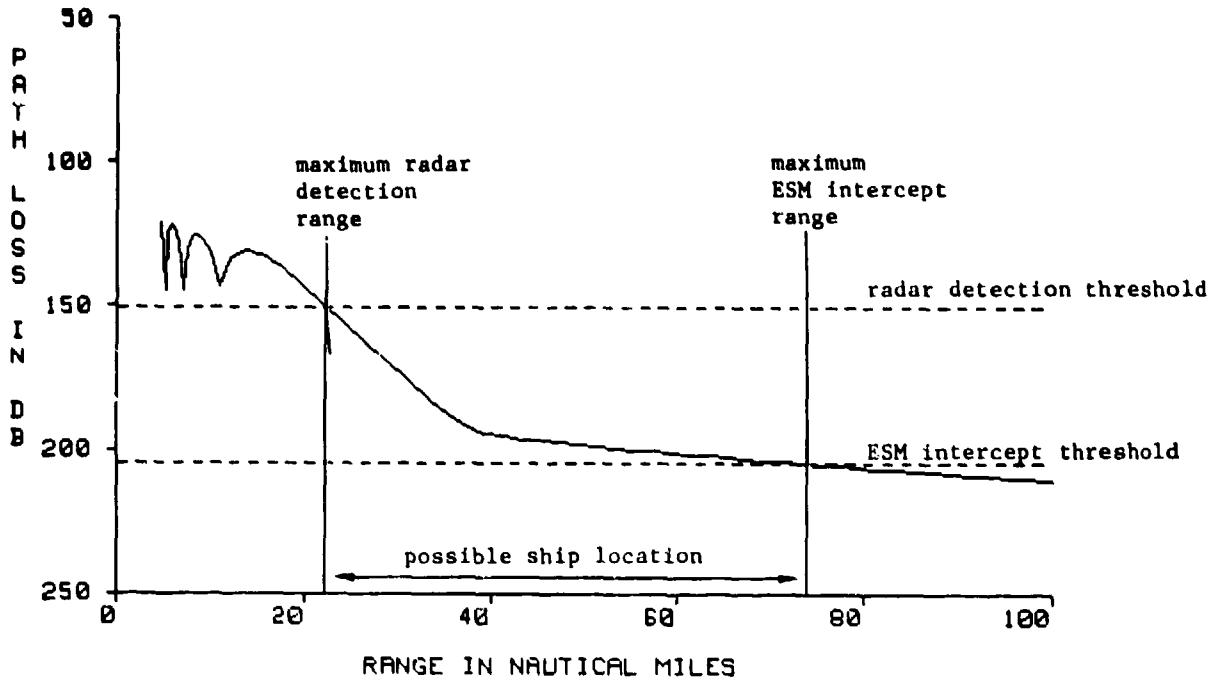

Figure 70. Determination of surface-based contact range using the path-loss versus range display.

13.3 USE FOR ESM VULNERABILITY

As discussed above, an extension of detection or communication range also means an extension of ESM intercept range. The path-loss versus range display may be used to graphically illustrate a transmitter's vulnerability to ESM intercept. Consider the following example. Figure 71 could represent a radiation pattern for a Sin(x)/x antenna of a "pencil beam" directed communications system, a system thought to be highly covert. For this example, the antenna main beam has a width of 3 degrees and a gain of 34 dB. The first side lobe is centered at 15 degrees from the axis of symmetry and is 12 dB down from the main beam. A second side lobe is centered at 30 degrees from the axis of symmetry and is 18 dB down from the main beam. In addition, there is a back lobe 22 dB down from the main beam. Assume the transmitter is radiating a power of 30 watts at a frequency of 200 MHz.

To assess the vulnerability of this system, it may be broken into four separate systems. The first system has a horizontal beamwidth of 3 degrees and an antenna gain of 34 dB; the second, a beamwidth of 30 degrees and a gain of 22 dB; and the third, a beamwidth of 60 degrees and a gain of 16 dB. The fourth system has a horizontal beamwidth of 180 degrees and a gain of 12 dB. Intelligence sources indicate a surface-based ESM receiver capable of a 200-MHz intercept, with a sensitivity of -90 dBm, is operating in the vicinity.

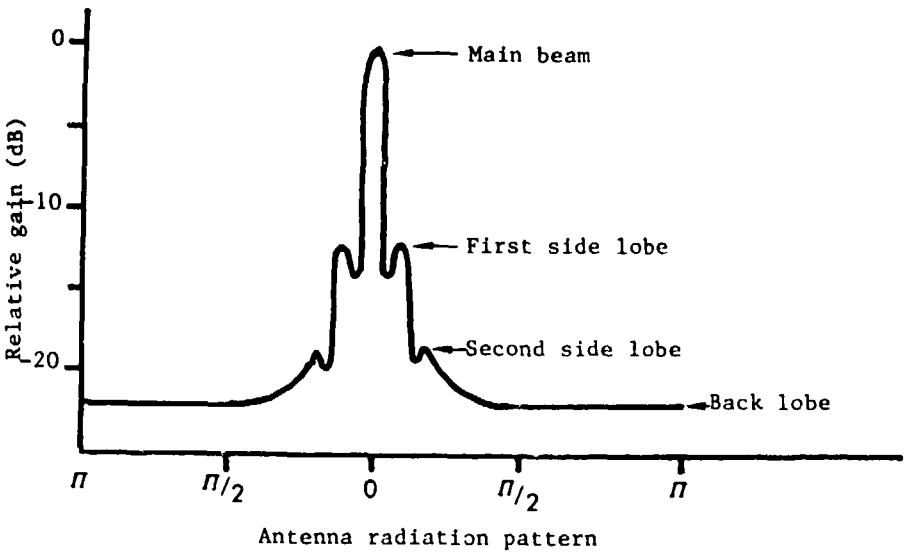

Figure 71. Example antenna radiation pattern for a Sin(x)/x antenna.

By using the ESM intercept range utility program of TESS/IREPS or the relationships of section 9.2, four intercept thresholds are determined and plotted on a path-loss versus range display. Figure 72 illustrates the vulnerability for standard refractive conditions.

From figure 72, it is readily seen that the example ESM receiver, located anywhere within the main beam of the antenna, would be able to intercept the signal at a range of 98 nautical miles. If the receiver were located anywhere within a 30-degree arc of the axis of symmetry, the signal would be intercepted at a range of 62 nautical miles. If the receiver were located anywhere within a 60-degree arc about the axis of symmetry, the signal would be intercepted at a range of 56 nautical miles. If the receiver were within a range of 50 nautical miles of the transmitter, the signal would be intercepted, even if the receiver were directly behind the transmitter. The area of vulnerability on a geographical plot is illustrated in figure 73.

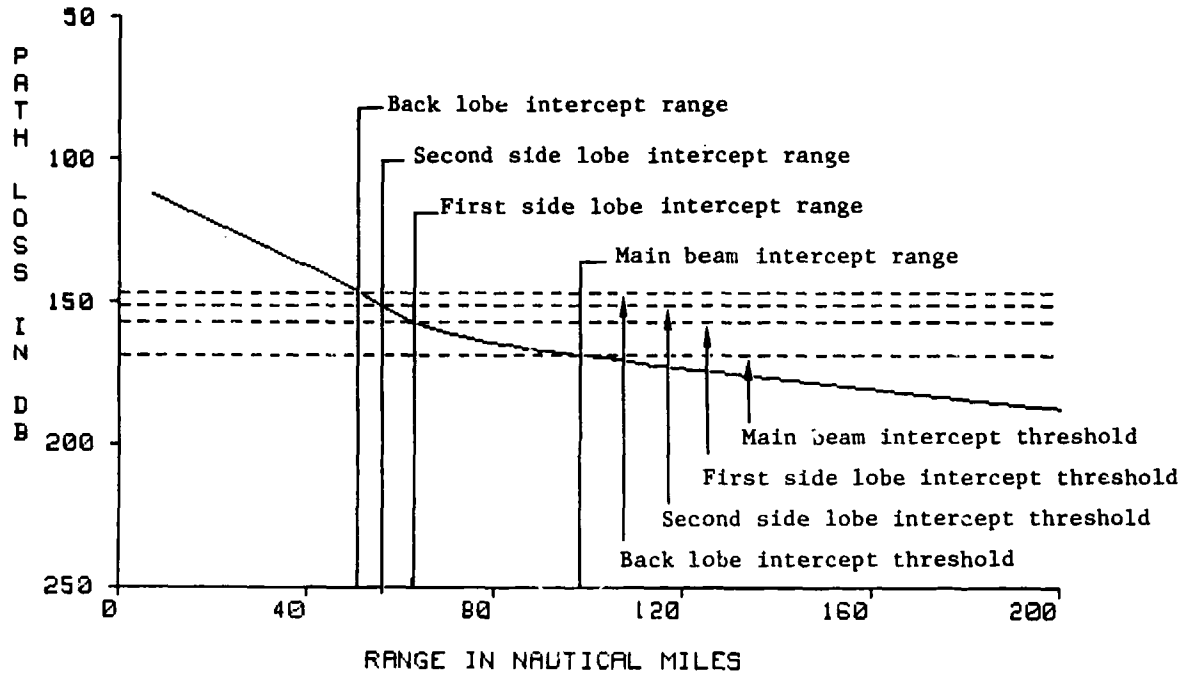

Figure 72. Path-loss versus range display for a 200-MHz transmitter under standard refractive conditions.

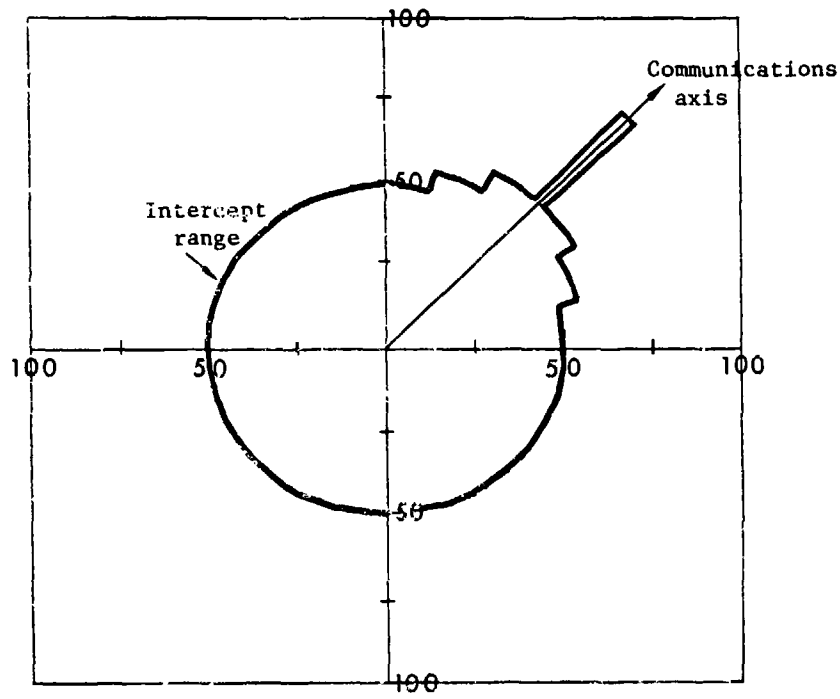

Figure 73. Area of "pencil beam" communications system's vulnerability to ESM intercept.

Figure 74 illustrates the vulnerability to ESM intercept of the communications system under conditions of a 1000-foot surface-based duct. It is easily seen that an intercept can be achieved at ranges in excess of 200 nautical miles, no matter where the ESM receiver is located relative to the transmitter. What, at first glance, appears to be a highly directional, narrow beam, low power, covert communications system is in reality easily intercepted. It must be remembered that as the frequency of the system increases, the evaporation duct will play a larger role in signal propagation. While the percent of occurrence of a 1000-foot surface-based duct may be fairly low, evaporation ducting conditions occur worldwide, most all the time.

For the above example, only intercept in the horizontal plane was considered. The complete vulnerability of the system must also include the vertical beam widths. Under the right refractive conditions and proper geometries, the example communications system could even be intercepted by a satellite-borne ESM receiver.

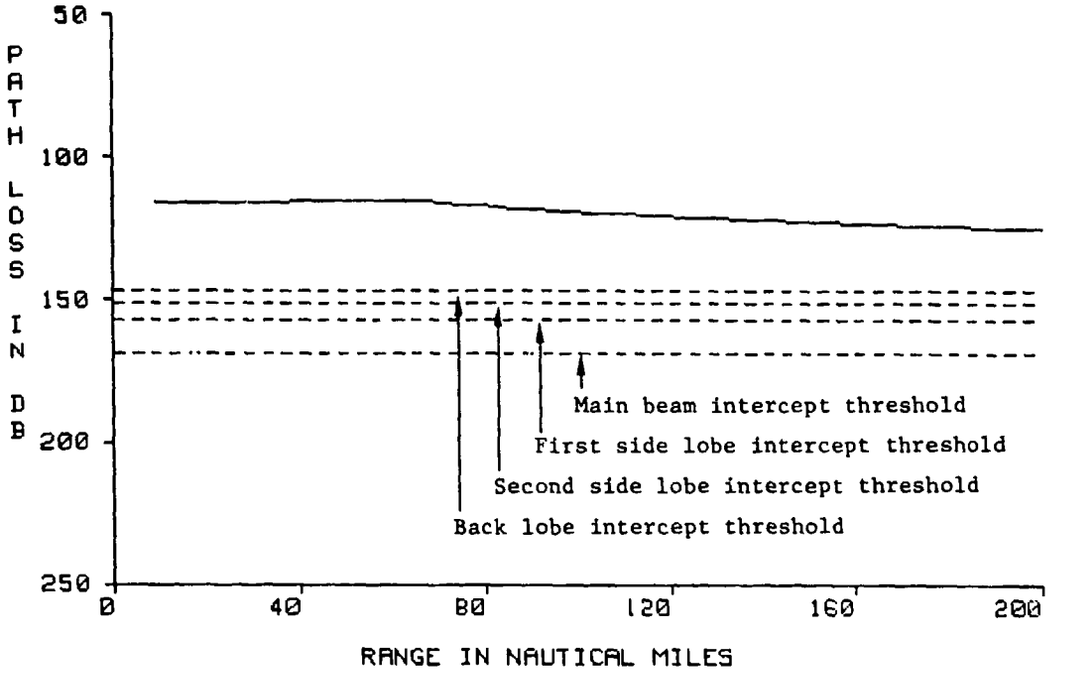

Figure 74. Path-loss versus range display for a 200-MHz transmitter under surface-based ducting conditions.

13.4 USE FOR HARDWARE MAINTENANCE

As with the coverage display, the path-loss display may be used to assess hardware performance by serving as a standard for performance. If, for example, the surface-search radar of figure 70 were to lose contact of an outbound surface target at a range of approximately 22 nmi, it would be a fair conclusion that the radar was functioning normally.

Suppose a ship has entered a gunnery exercise range where the range control station is located on a hill peak overlooking the range, affording the gunfire observer a clear view of the entire range. The ship attempts to contact the range controller via UHF radio as directed by range check-in procedures. The ship is unable to establish communications, however. While the ship is within visual range of the station, a quick inspection of the interference null pattern reveals the ship/station spacing is such that the ship falls within a null, as illustrated in figure 75. In this case, there is most likely nothing wrong with the radio transmitter and an unnecessary maintenance call may be avoided.

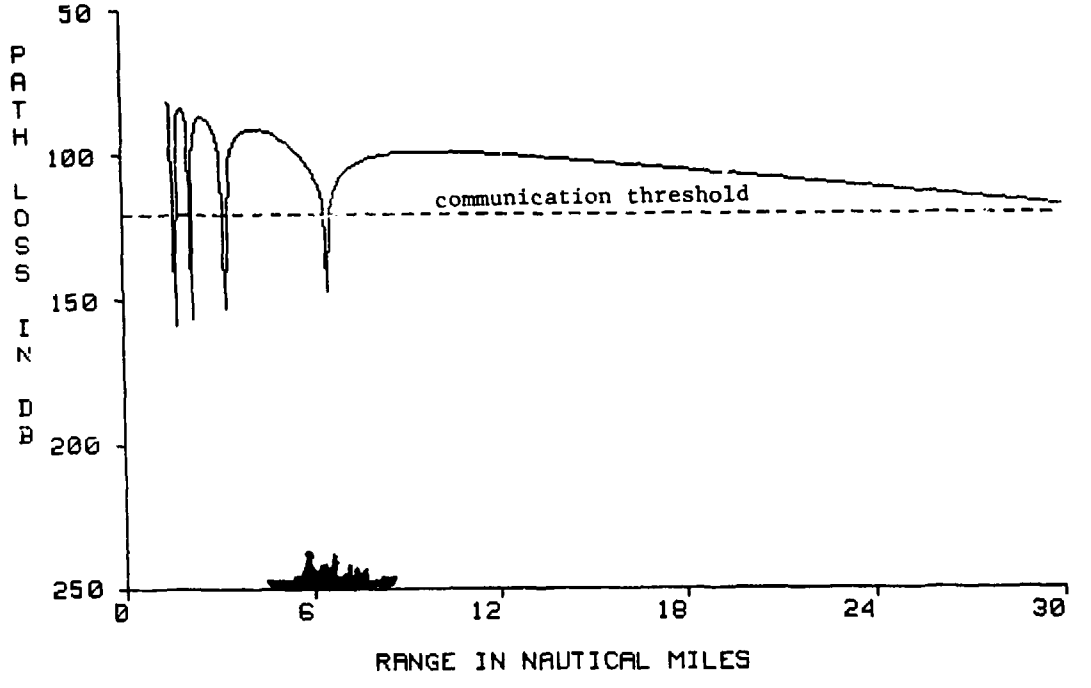

Figure 75. Platform spacing within the optical interference region which would degrade UHF communications.

13.5 USE FOR AIRBORNE SURFACE-SEARCH RADARS

For proper use of the path-loss display for airborne surface-search radars, an appropriate free-space range must be determined. Use of the radar free-space range utility as described in section 9.1 is recommended. The target's radar cross section may be determined from equation 15. The target types used by NOSC in its experimental efforts are listed in table 4. Many publications contain the tonnage for specific ships of interest. Although the tonnage of the CV and the OSA are outside the bounds of valid displacements for equation 15, the path-loss calculations appear to be reasonable with respect to the other combatants.

Table 4. Ship types, estimated tonnage, and radar cross-section height.

Type	Tons	Height (feet)
CV	85360	87
CG	10110	39
DD	5000	42
FF	3400	30
OSA	210	13

Because of reciprocity, an air-to-surface path is the same as a surface-to-air path. Therefore, to insure the propagation algorithms used to consider interference region effects are employed, the airborne radar is treated as if it were a surface-based radar. (As with the coverage display, interference regions effects are not modeled within the path-loss display for airborne system.) The radar antenna height that should be used is the height of the target. For this case, the ship is the target and its radar cross section is distributed over the height interval from the waterline to the mast top. To establish a single target height, it is assumed that the target's entire radar cross section is concentrated at a point approximately one-third the way up the superstructure. The definition of superstructure for this purpose is that portion of the ship above the main deck including all major antennas. Figure 76 illustrates this definition using a *Spruance*-class destroyer. For this example, the target height for the *Spruance*-class destroyer would be approximately 53 feet.

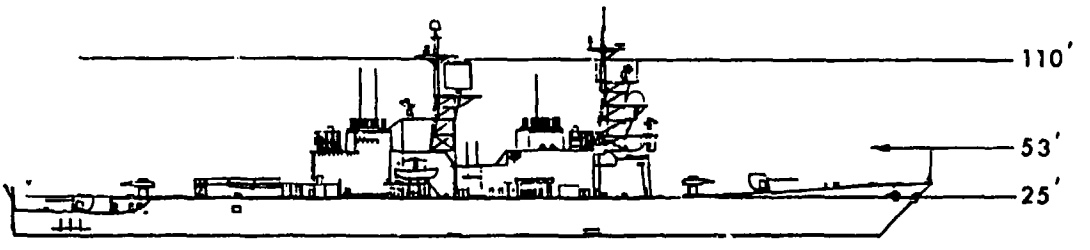

Figure 76. Determination of superstructure height.

For large targets, the caiculated free-space range value may exceed the program limits on entering a free-space range. If this is the case, simply use the corresponding path-loss threshold value.

The final consideration is for a target or receiver height. In this case, the target or receiver height is the expected aircraft altitude. Several path-loss displays may be generated for different aircraft altitudes quite quickly in this manner, providing an appropriate assessment for the airborne surface-search radar. Figure 77 illustrates the path-loss display obtained when using the above described technique. In this example, the airborne surface-search radar is at an altitude of 5000 feet when used for the detection of a *Spruance*-class surface target. As can be seen, the expected detection range is approximately 94 nmi.

Antenna elevation angle should always be set to zero in this application; alternatively, antenna type could be selected as omni.

It should be noted that sea clutter degradation of detection ranges is generally not significant for combatant size targets. However, for small targets such as periscopes, sea clutter, which is not accounted for the the TESS/IREPS models, may be quite significant. For small targets and heavy seas, the path-loss display will be overly optimistic in an actual detection range.

It must also be remembered that the distributed target is being represented as a point source target. This assumption is valid for determining the greatest range of detection but it is increasingly less accurate with decreasing range as the target becomes less of a point source.

13.6 USE FOR SURFACE-BASED SURFACE-SEARCH RADARS

Since both transmitter and target are located at the surface, interference region effects will be properly modeled and, therefore, it is not necessary to reverse the target and transmitter locations as done in the airborne surface-search case. The target's height and radar cross section will still have to be estimated, however, using the same procedure described above.

As with the airborne case, appropriate comments about the mode of radar operation and determination of target characteristics should be included within the display to preclude any misconceptions or to avoid any misunderstandings concerning the validity of the assessment products.

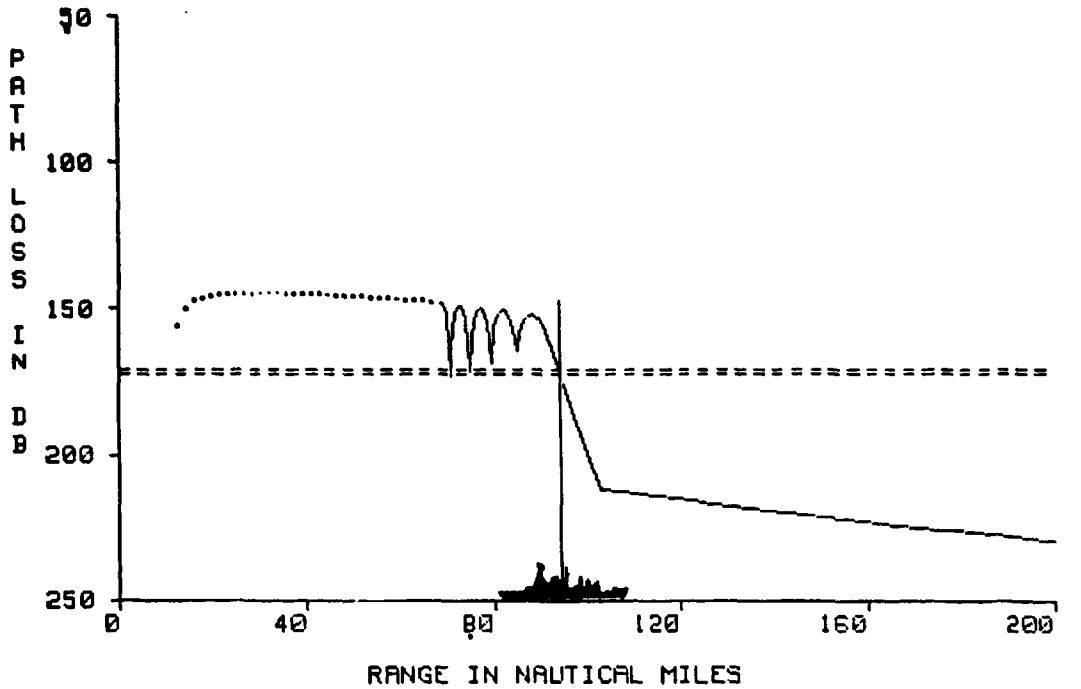

RADAR IN PENCIL-BEAM, LONG-PULSE OPERATION
THRESHOLDS ARE 50% AND 90% POD OF A SPRUANCE CLASS

HORIZONTAL DASHED LINES INDICATE DETECTION, COMMUNICATION, OR INTERCEPT THRESHOLDS.

```
TYPE OF PLATFORM: SURFACE
TRANSMITTER OR RADAR ANTENNA HEIGHT: 53  FEET
RECEIVER OR TARGET HEIGHT: 5000  FEET
FREQUENCY:  9000  MHZ
POLARIZATION: HORIZONTAL
PATH LOSS THRESHOLDS:  171.3  172.1  DB
ANTENNA TYPE: SINX/X
VERTICAL BEAM WIDTH: 3.6 DEGREES
ANTENNA ELEVATION ANGLE: 0 DEGREES
MAXIMUM INSTRUMENTED RANGE IN NM: 203
```

Figure 77. Example of path-loss display for an airborne surface-search radar used for detection of surface-ship target.

14.0 AIRBORNE EARLY WARNING (AEW) AIRCRAFT STATIONING AID

The AEW aircraft stationing aid is designed to show the refractive distortion of normal propagation at a given range for various combinations of radar/transmitter and target/receiver altitudes. Figure 45 is an example of the AEW aircraft stationing aid which shows the distortion at a range of 150 nmi on a height-versus-height plot. The shaded area in the plot corresponds to radar/transmitter and target/receiver altitude combinations for which detection, communication, intercept, or jamming may occur, depending upon the electromagnetic system's characteristics. The fully shaded squares at approximately 2500 to 3500 feet indicate the radar/transmitter and target/receiver altitude combinations which are within a duct, implying multipath with possible signal fading in addition to over-the-horizon propagation at longer ranges. Associated with the trapping layer is a crescent-shaped clear area. This clear area corresponds to altitude combinations which occur within the radar/radio hole. The more heavily shaded area along the lower left of the clear area indicates multipath propagation due to the presence of the trapping layers. The clear area in the extreme lower left of the display represents those altitude combinations which are below the radar/radio horizon. The bar chart to the right of the display indicates the type and vertical extent of anomalies in the refractivity profile: ducting, superrefraction, and subrefraction.

The propagation model used in the generation of this display is a system-independent raytrace model. Figure 78 illustrates a conventional height-versus-range display associated with the technique of ray tracing and the corresponding AEW stationing aid display. Points "A" and "B" demonstrate the relationship between features on both displays. A conventional ray tracing model does not include an indication of signal strength along the ray nor any signal enhancement or degradation due to the waves' phase at ray intersections. Therefore, multipath interference is implied only in a qualitative sense. Multipath propagation due to sea-surface reflection is not considered in this display.

The radar hole (area "C" of figure 78) associated with a duct is the only true "hole" in ray theory. That is, there is no ray, excluding surface-reflected rays, that can be traced into the hole region. In a practical sense, the energy level within the hole area is due to atmospheric scattering and surface reflection (if any) and not by direct path wave propagation into the area.

Superrefractive and subrefractive layers may also produce what appears to be a "hole." Figures 79 and 80 are ray traces with a superrefractive and subrefractive layer respectively between 4500 and 5500 meters. Area "A" of each figure illustrates the "hole" area created by these layers. While the "hole" may look very much like the hole of figure 78, it is not a true hole because a ray can be found that will reach any point within the hole. It may be seen (point "B" of figures 79 and 80) that the

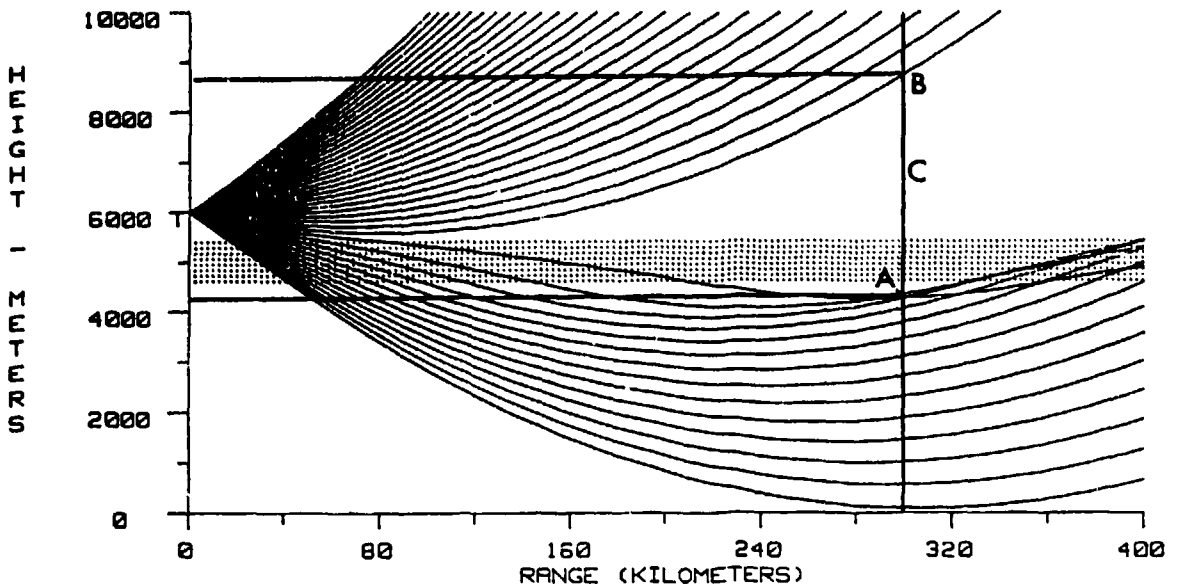

LOCATION: LOCATION LABEL
DATE/TIME: DATE LABEL

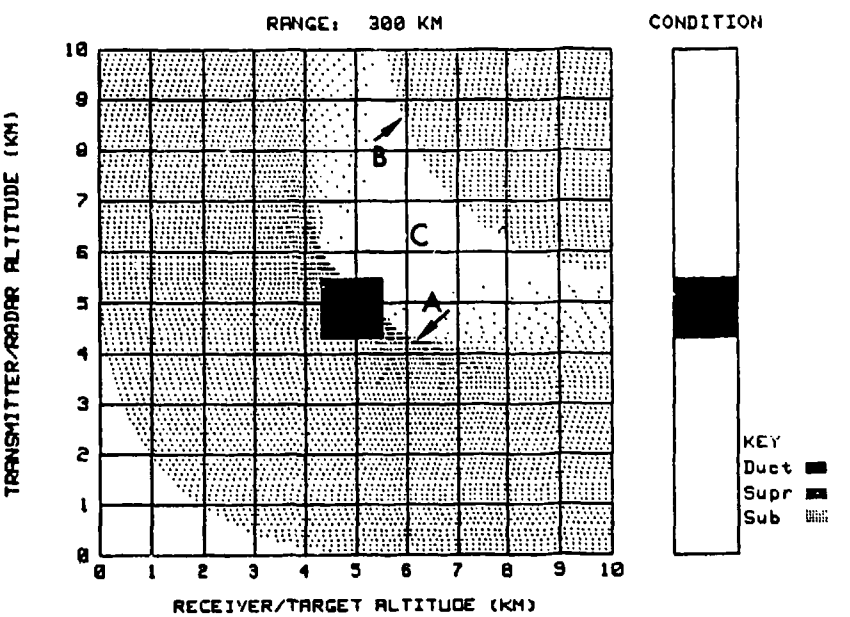

VARIATIONS IN SHADED AREA INDICATE DISTORTIONS IN PROPAGATION AT THIS RANGE

DARKEST SHADING INDICATES RAY CONVERGENCE AND MULTIPATH
LIGHTEST SHADING INDICATES RAY DIVERGENCE

Figure 78. Conventional ray trace and AEW stationing aid for an elevated trapping layer.

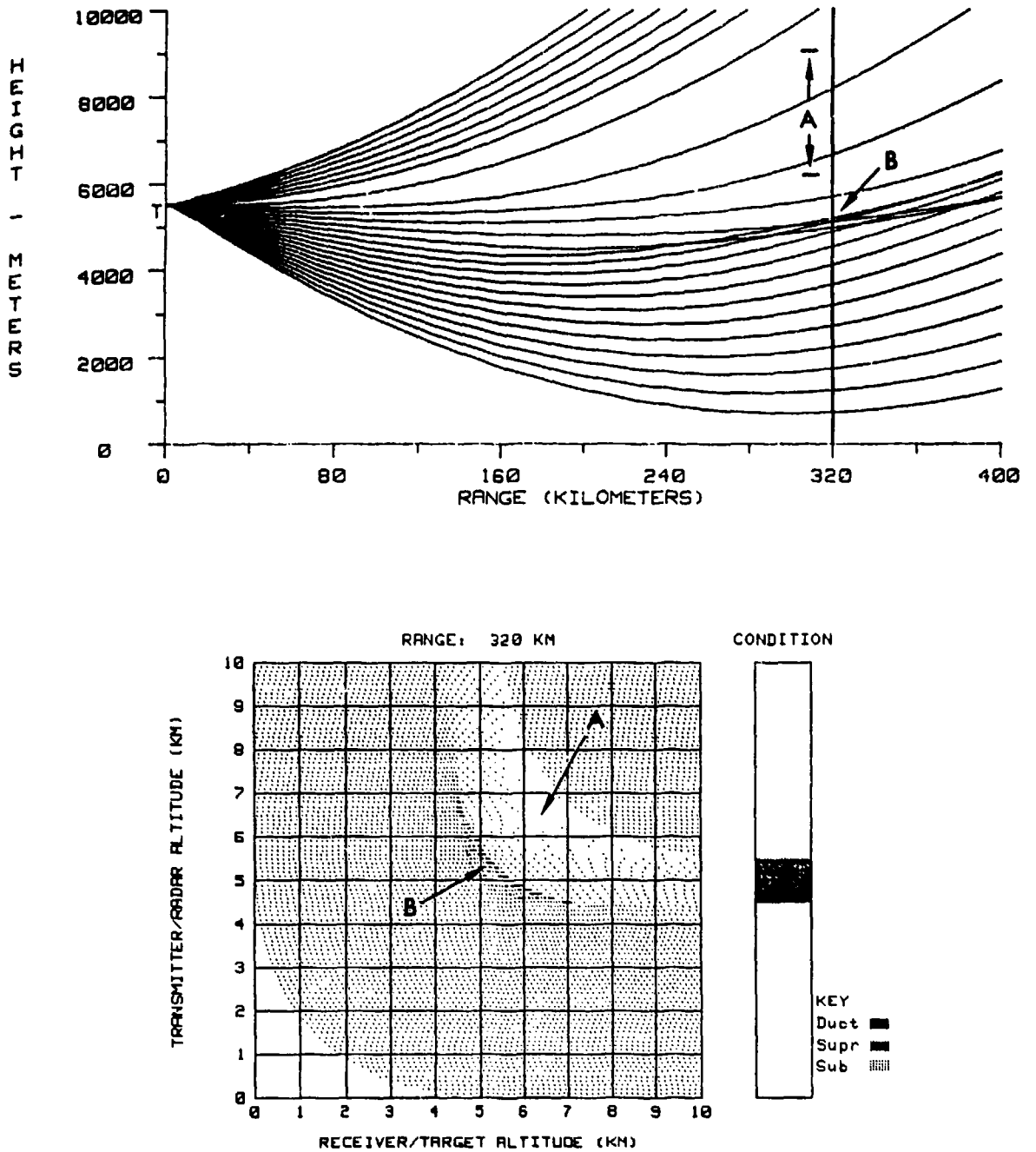

Figure 79. Conventional ray trace and AEW stationing aid for an elevated superrefractive layer.

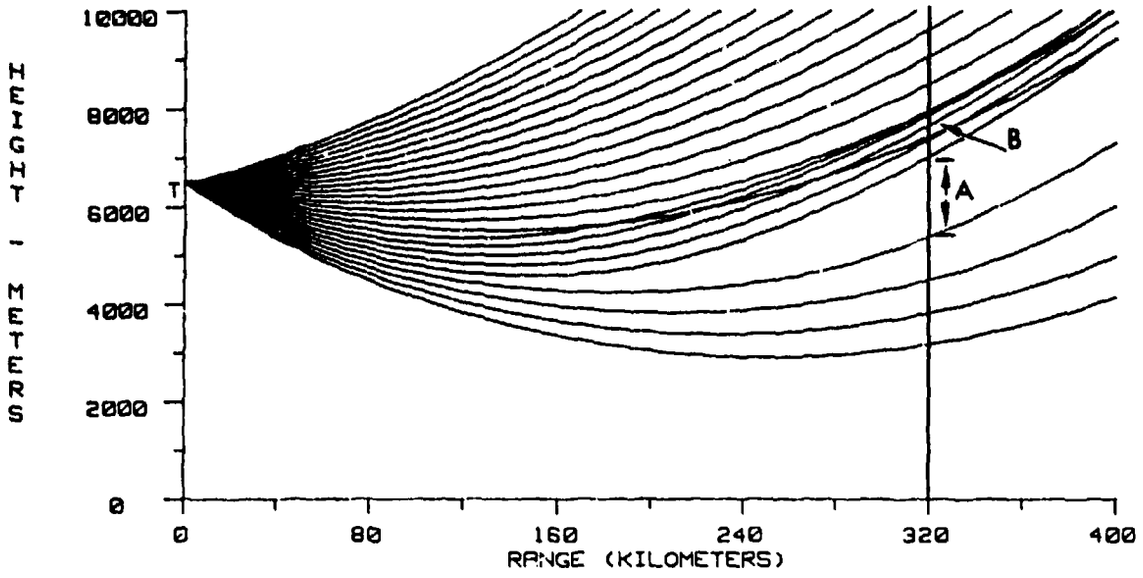

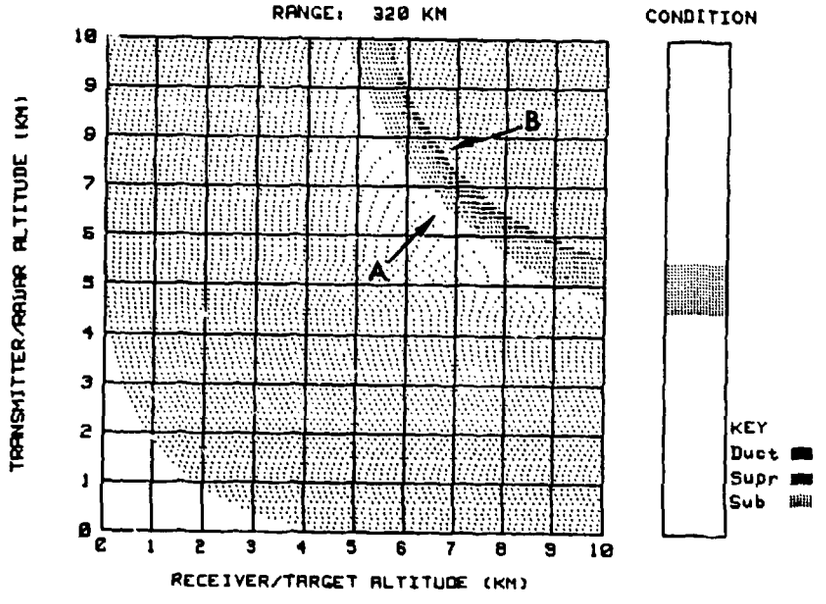

Figure 80. Conventional ray trace and AEW stationing aid for an elevated subrefractive layer.

multipath region will appear below the hole and above the hole for superrefractive and subrefractive layers respectively. In a practical sense, the energy level within the hole area will also have less energy than normal but more energy than accounted for by scattering.

14.1 AIRCRAFT STATIONING AID USES

The primary use of the AEW stationing aid is to assist in the optimum placement of early warning aircraft. For example, if the AEW aircraft were to be placed at an altitude of 22,500 feet, figure 45 indicates that its radar would have coverage from the surface to an altitude of 25,000 feet (at a range of 150 nautical miles). If, however, the aircraft was placed at an altitude of 12,500 feet, it would have good coverage from the surface to 2500 feet, no coverage between 2,500 and 5,000 feet; coverage but with a great deal of signal fading between 5,000 and 10,000 feet; improbable coverage between 10,000 and 12,500 feet; good coverage above 12,500 feet; and again at a range of 150 nautical miles.

The above discussion applies equally to air-to-air or air-to-surface communication or jamming activities. For example, in figure 45, an aircraft at 7,500 feet would be unlikely to communicate via UHF radio with a surface ship 150 nautical miles away because the ship is below the radio horizon of the aircraft. Likewise, a jamming aircraft stationed at 5,000 feet would be unable to effectively jam an aircraft between the altitudes of 5,000 and 12,500 feet.

An aircraft may also use this stationing aid to avoid detection by another aircraft's radar or ESM receiver. If for example, intelligence sources indicate a threat aircraft will be approaching at an altitude of 10,000 feet, an aircraft placed between 2,500 and 5,000 feet or between 12,500 and 15,000 feet will most likely avoid being detected. As illustrated in figure 45, it should be noted again that these altitudes apply for aircraft 150 nautical miles apart. A series of these stationing aids at varying ranges will provide a good representation of three dimensional assessment for an electromagnetic system's performance.

15.0 SURFACE-SEARCH RADAR-RANGE TABLE

The surface-search radar-range table displays a detection range prediction for an operator-specified surface-search radar against a list of pre-defined surface targets. Various editions of TESS/IREPS will have a varying number of target classes available. These classes place a reasonable bound upon surface-based targets likely to be encountered in normal operations. While the radar-range table model integrates over the distributed target and the path-loss model assumes a point source target, the table detection range may be thought of as the range at which the path-loss curve crosses the path-loss threshold, as discussed within section 13.0 and illustrated by point "A" of figure 11.

The physical processes in calculating a detection range are similar to that of the path-loss versus range display except that the targets are now distributed targets rather than point source targets. In section 13.0, a simplification to a distributed target was discussed for the airborne surface-search application. This simplification was to assume all the target's radar cross section was concentrated at one particular height. Within the surface-search radar-range table, however, an actual integration of the target's radar cross section with height is employed.

Since in daily operation it would be time consuming and cumbersome to produce a separate path-loss versus range display for each surface-search radar and target combination, the surface-search radar-range table has been designed to automate the process. The TESS/IREPS operator need only specify the particular surface-search radar of interest. The path-loss/threshold intercept range is calculated for each target, and the results are displayed in a table format. Figure 81 illustrates the format of the surface-search radar-range table.

Note that the table gives a minimum, average, and maximum detection range. These values represent the extreme variations of the radar cross section of the target with viewing aspect (figure 22). While not entirely correct, the minimum, average, or maximum detection range may be thought of as a detection range for a target with a bow\stern, quarter, and beam aspect respectively. The calculation algorithm assumes a fixed number of decibels increase from bow to beam. Since every target is different, however, the TESS/IREPS operator should understand the concept of radar cross section (section 6.1) and evaluate the validity of this assumption.

To insure consistency with reality, the detection range calculated is truncated at the maximum instrumented range of the radar, even if the calculated detection range is sufficiently great to produce multiple-time-around echoes.

LOCATION: HERE
DATE/TIME: NOW

SURFACE SEARCH RADAR: GENERIC SFC-SEARCH

TARGET	DETECTION RANGE IN NM MIN	AVG	MAX
CV	54.1	60.8	73.1
CG	46.6	53.1	64.1
DD	44.2	50.6	61.5
FF	42.0	48.4	59.2
OSA	31.1	37.3	47.7

RADAR ANTENNA HEIGHT: 37 METERS
FREQUENCY: 5000 MHZ
POLARIZATION: HORIZONTAL
FREE SPACE RANGE: 185.32 KILOMETERS
MAXIMUM INSTRUMENTED RANGE IN KM: 185.32

Figure 81. Surface-search radar-range table format.

The calculation of a detection range for a distributed target is computationally intensive. Prior to the availability of high-speed, sophisticated desktop computers, surface-search radar detection ranges were pre-calculated over a range of evaporation duct and surface-based duct environments and stored within the program software in a table lookup format. This pre-calculation effort also limited the number of surface-search radars available to only two: the AN/SPS-10 and the AN/SPS-55. With the availability of higher speed desktop computers, radar detection ranges may now be calculated in real time, and the restriction of two radars and a limited number of environments has been overcome. Some older versions of TESS/IREPS may still be in use, however, and the operator should understand the artificiality of this restriction. If the restriction should pose a problem, a single path-loss versus range display may be generated for each radar/target combination using the technique as discussed in the surface-based surface-search case of section 13.0.

16.0 ELECTRONIC SUPPORT MEASURES (ESM) INTERCEPT-RANGE TABLE

The convenience of multiple path-loss versus range calculations being displayed in a table format, such as in the surface-search radar-range table, has been extended to the calculation of ESM intercept ranges. The ESM intercept-range table product displays the maximum intercept ranges of an operator specified emitter by an operator specified ESM receiver. This maximum intercept range corresponds to the intersection of the path-loss curve and the path-loss threshold as discussed within section 13.0 and illustrated by point "A" of figure 11. The path-loss threshold in this case is determined by equation 21. Figure 82 illustrates a sample format for the ESM intercept-range table. In addition to the emitter's name, its nominal frequency is also given.

For emitter/receiver combinations not shown in the table, the path-loss display may be used as discussed in section 13.3.

ESM RECEIVER: GENERIC RECEIVER

EMITTER CLASS: TESS TEST SPEC

EMITTER	FREQ (MHz)	MAXIMUM INTERCEPT RANGE (nm)	EMITTER	FREQ (MHz)	MAXIMUM INTERCEPT RANGE (nm)
ONE	125	31	NINETEEN	8000	3
TWO	125	55	TWENTY	8000	8
THREE	125	66	TWENTY-ONE	8000	69
FOUR	125	55	TWENTY-TWO	8000	2
FIVE	125	66	TWENTY-THREE	8000	13
SIX	125	76	TWENTY-FOUR	8000	18
SEVEN	125	66	TWENTY-FIVE	8000	10
EIGHT	125	79	TWENTY-SIX	8000	22
NINE	125	96	TWENTY-SEVEN	8000	97
TEN	200	5	TWENTY-EIGHT	15000	5
ELEVEN	200	32	TWENTY-NINE	15000	11
TWELVE	200	47	THIRTY	15000	42
THIRTEEN	200	7	THIRTY-ONE	15000	5
FOURTEEN	200	18	THIRTH-TWO	15000	15
FIFTEEN	200	58	THIRTY-THREE	15000	250+
SIXTEEN	200	11	THIRTY-FOUR	15000	17
SEVENTEEN	200	21	THIRTY-FIVE	15000	23
EIGHTEEN	200	58	THIRTY-SIX	15000	25

Figure 82. ESM intercept-range table format.

Normal intercept ranges can be greatly extended by the evaporation duct, resulting in intercept of signals well beyond the horizon. Even more dramatically, a surface-based duct from an elevated refractive layer can extend intercept ranges far in excess of 200 nautical miles. If a surface-based duct exists, it will be the dominating feature when calculating an ESM intercept range. Within the calculations, the maximum intercept range allowed is 1000 kilometers. The assumption of horizontal homogeneity discussed within section 10.7 is questionable over great ranges and most certainly across air mass boundaries, however. Therefore, very long intercept ranges within a duct will be artificially indicated as 250+, meaning 250 nautical miles or greater for terminals within a surface duct. Any indication of long intercept ranges must be re-evaluated with respect to air mass boundaries. When it is known for certain that horizontally homogeneous conditions extend for many hundreds of nautical miles, the path-loss versus range display may be used to obtain an actual intercept range.

The ESM calculations assume the emitter is radiating at peak power. An attempt to reconcile a predicted ESM intercept-range by cross-correlating several radar contacts may fail by overlooking the obvious—that the emitter is turned off. In addition, the probability of signal intercept also lies within the sensitivity of the receiver. In some cases, a range of 0 will be indicated. This simply means that the emitter is outside of the receiver's band of frequencies.

In addition to the normal limitations of the TESS/IREPS models, i.e., frequencies between 100 and 20,000 MHz, etc., the ESM intercept range table is designed for surface-to-surface intercept or surface-to-air intercept for aircraft altitudes below 10,000 feet. For surface-to-air intercepts at altitudes greater than 10,000 feet, refer to the platform vulnerability display, section 18.0.

The artificiality of pre-calculated intercept ranges, similar to that of early versions of the surface-search radar-range table, also exists in early versions of the ESM intercept-range table. Here, the impetus for pre-calculation was the large number of possible receivers/emitter combinations, not the distributed-target consideration. Again, the operator of an older version must recognize this limitation and, if desired, may produce a single path-loss versus range display on a case-by-case basis.

Under many ducting conditions, a rough estimate of over-the-horizon ranges to surface ESM contacts can be determined by comparing the surface-search radar-range table to the ESM intercept-range table. If the ESM contact cannot be seen on the surface-search radar, then it is a fair conclusion that its actual range is greater than that shown in the surface-search radar-range table, but less than that given in the ESM intercept-range table. This range "bracket" could be used for bearing-only missile launches or could be used with other information to further localize the contact. Conversely, if no ducting conditions exist, then the near-horizon maximum intercept range given by the ESM intercept-range table could establish that the contact is likely to be within the horizon.

17.0 ELECTRONIC COUNTERMEASURES (ECM) EFFECTIVENESS DISPLAY

ECM is the division of electronic warfare which involves actions taken to prevent or hamper an enemy's effective use of the electromagnetic spectrum. ECM may be divided into three categories based upon the actions taken. These are (1) reduction of the target's radar cross section through vehicle construction/materials or the tactical use of radar "holes" in the atmosphere, (2) passive ECM in which the enemy's transmitter power is either reflected, refracted, or absorbed through a non-radiating decoy such as chaff, and (3) active ECM in which the electromagnetic system's receiver is overloaded with noise or the signal is electronically altered to produce a misleading interpretation.

A typical jamming scenario might be the following. An attack aircraft is making a bombing run against a surface ship. The attack aircraft may be coated with an electromagnetic radiation absorbing agent or may have a flight profile such that the aircraft is within a radar hole. This would represent the first category of ECM. A chaff cloud may be dispersed to further hide the attack aircraft. This would represent the second category of ECM. Finally, a supporting jammer aircraft, usually referred to as a standoff jammer, would provide a screen of wide-band electromagnetic noise to overpower any return echo from the attacker. This would represent the third category of ECM. Figure 83 illustrates this scenario.

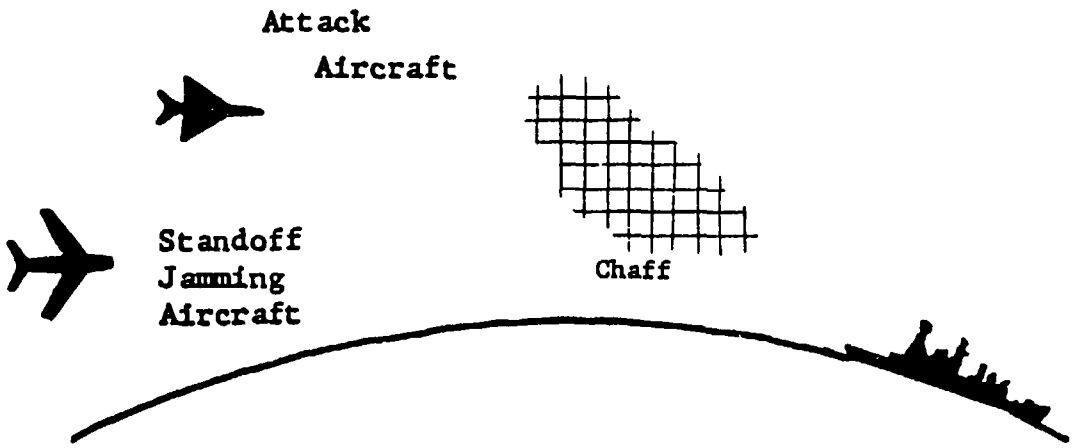

Figure 83. Typical radar jamming scenario.

It may be seen that the standoff jammer will be effective only if its power is able to overload the receiver on board the target ship (the victim). If, for example, the standoff jammer's flight profile is through a radar hole, the jamming will be ineffective. If, on the other hand, the flight profile is within a duct, the jamming will be most effective. The most important consideration is not the power of the jammer, however, but the geometric relationships between the jammer and the victim. Since the jammer and victim are in constant relative motion, the jammer pilot must know at all times where the maximum coupling of energy between himself and the victim will take place.

The ECM effectiveness display is designed to provide a measure of airborne active jammer effectiveness against surface-based radars. The display is a plot of height versus signal strength where the signal strength is the difference between actual signal strength for the current environment and free-space signal strength. The plot of height versus signal strength is presented for several discrete jammer/ victim ranges. Figure 84 illustrates a sample ECM effectiveness display for a narrow-beam jammer within a 1000-foot surface-based duct environment.

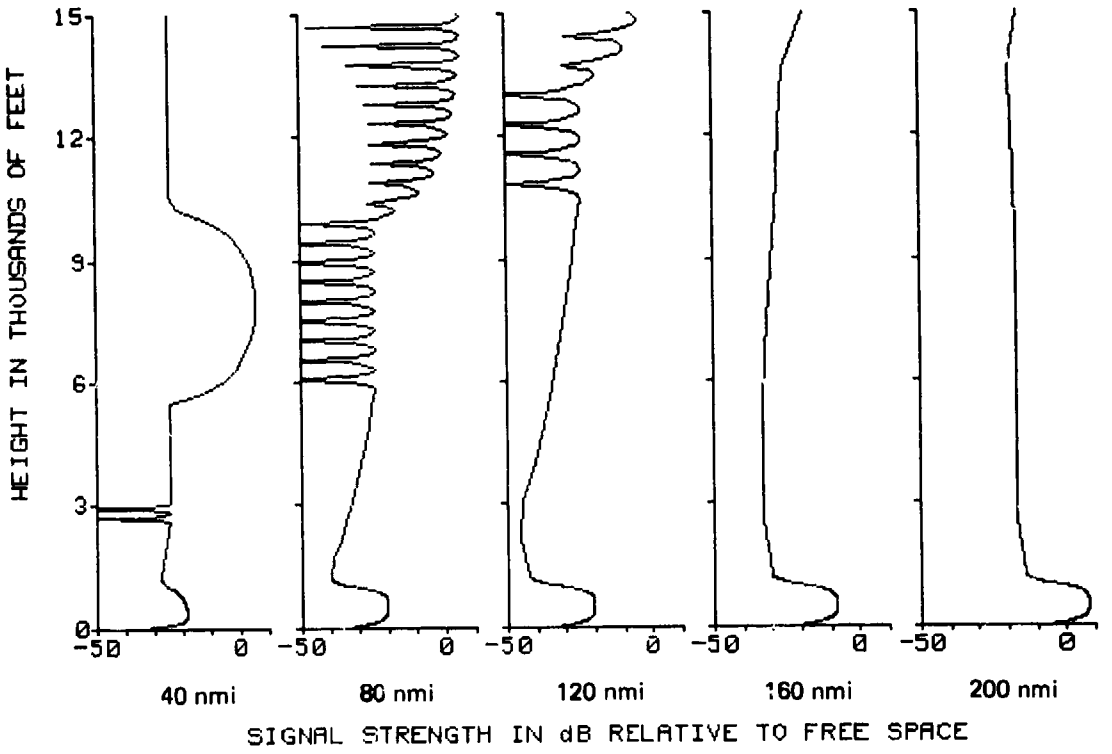

Figure 84. Sample ECM effectiveness display

Mission planners, in addition to ECM aircraft pilots, may use this display to optimize the locations and flight paths of tactical jamming aircraft. For example, the conditions appropriate to figure 84 show a jamming aircraft would have greater effectiveness at an altitude of approximately 500 feet than at 3000 feet, for all ranges. Note, however, at a range of 40 nmi from the target, the effectiveness of the jammer would be improved if its altitude was increased to 8000 feet.

The radiating antenna for many jammer aircraft is positioned such that there is a slight downward looking angle from the horizontal. Because of this downward angle, aircraft flying within a surface-based duct will experience a greater amount of energy being reflected from the surface, and alternatively, a lesser amount of energy traveling within the duct. To take the greatest advantage of the ducting condition and truly achieve the signal enhancement indicated by the ECM display, the aircraft would have to fly at an increased angle of attack.

18.0 PLATFORM VULNERABILITY ASSESSMENT

Often, a table of data with no quick and obvious relationship between the data, makes a cumbersome and sometimes confusing display. Using a bar chart display will allow a user to receive the same information but will, in most cases, bring a quicker realization to the significance of the data. This is the case with the ESM intercept range table display as discussed in section 16.0. For emission control (EMCON) planning, if a commander wanted to assess the vulnerability to intercept for all the emitters on board his platform, a search of tables would have to be made, arranging the ranges in some order based upon the mission. By extending the capability of the ESM intercept range table to include all surface-to-air and air-to-air intercept cases, and by customizing a bar chart display to a particular platform, the vulnerability of that platform's emitters to ESM intercept may easily be seen. This is accomplished by the platform vulnerability assessment display, as illustrated in figure 85.

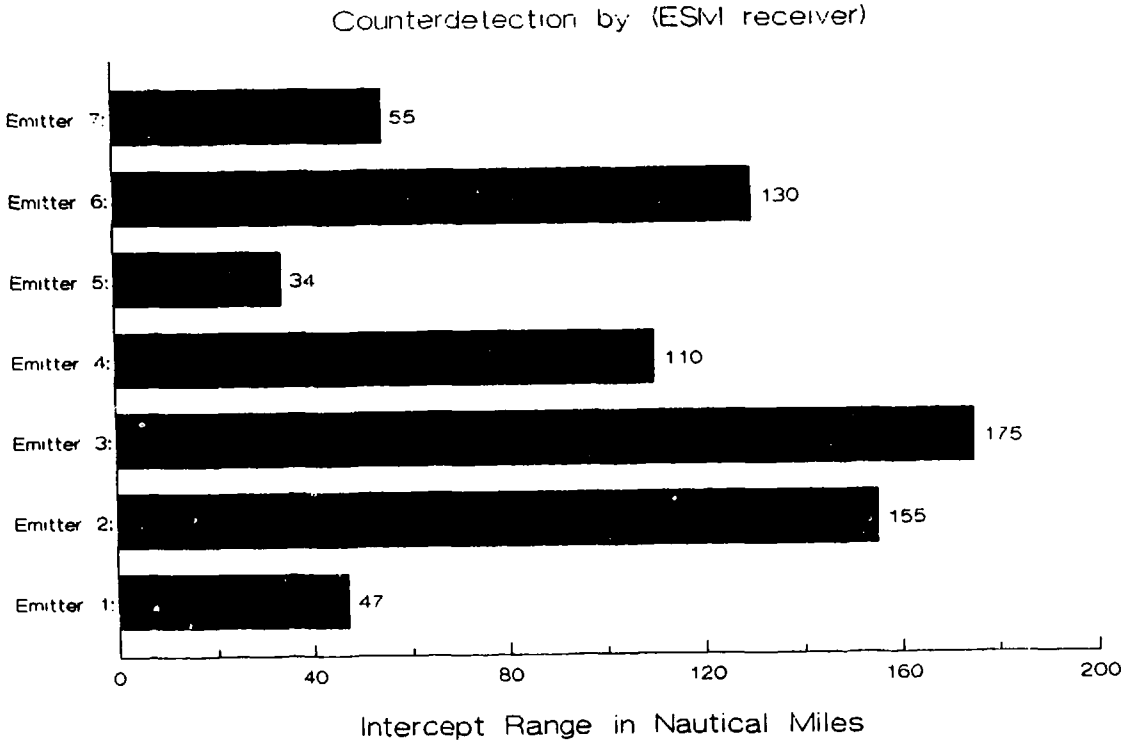

Figure 85. Sample platform vulnerability display.

The model limitations used for this display are the same as the ESM range table display, except the platform vulnerability display will allow for air-to-air intercepts and surface-to-air intercepts for altitudes greater than 10,000 feet.

From this display, it is immediately obvious which emitter on the platform is most vulnerable to intercept. By selectively silencing emitters, the commander can customize an EMCON plan to a particular mission. For example, the mission may be to remain undetected outside of a 100-nautical-mile radius but still retain some radio communications capability. By using the propagation condition summary, section 11.1, it might be determined that an evaporation duct is the only anomalous propagation feature present. Since the trapping of electromagnetic energy within an evaporation duct is highly frequency dependent, a platform vulnerability assessment display could be created for several radio transmitters at varying frequencies. The ideal frequency to maximize communications but still avoid intercept may now be easily determined. As a bonus, it might be seen that a certain air-search radar also has an intercept range of less than 100 nautical miles, thereby allowing for its use within the EMCON guidelines.

A modification to the above example could be the determination of maximum range for air-to-surface communications. Again, a platform vulnerability assessment display could be created for a radio transmitter at varying frequencies. While a coverage display, section 12.0, may show that an aircraft would have to change range or altitude in order to communicate, the platform vulnerability assessment display may indicate that a simple change of frequency will achieve the same result. For an ASW helicopter engaged in an active prosecution, a frequency change could easily be accomplished while a position change might be unacceptable.

19.0 BATTLE GROUP VULNERABILITY DISPLAY

The concept of the platform vulnerability display described in section 18.0 may be extended to include the entire battle group. The longest intercept range from each platform within the group may be used to draw an intercept circle on a geographical plot of the battle group. Figure 86 is an example of such a battle group vulnerability display.

This display is ideal for EMCON planning. Suppose a battle group is to transit a strait such as illustrated in figure 87. By producing a battle group vulnerability display at various times along the track, the EMCON commander could modify the plan to avoid detection by land-based interceptors, yet still allow for necessary communications or radar use.

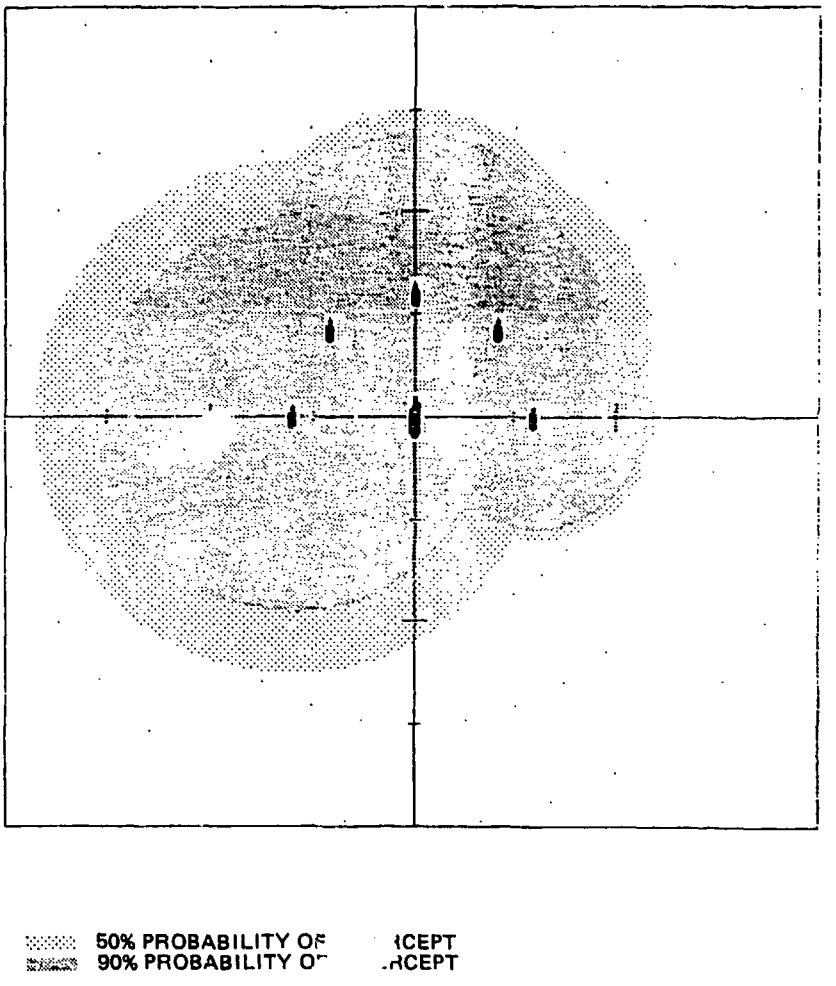

Figure 86. Sample battle group vulnerability display.

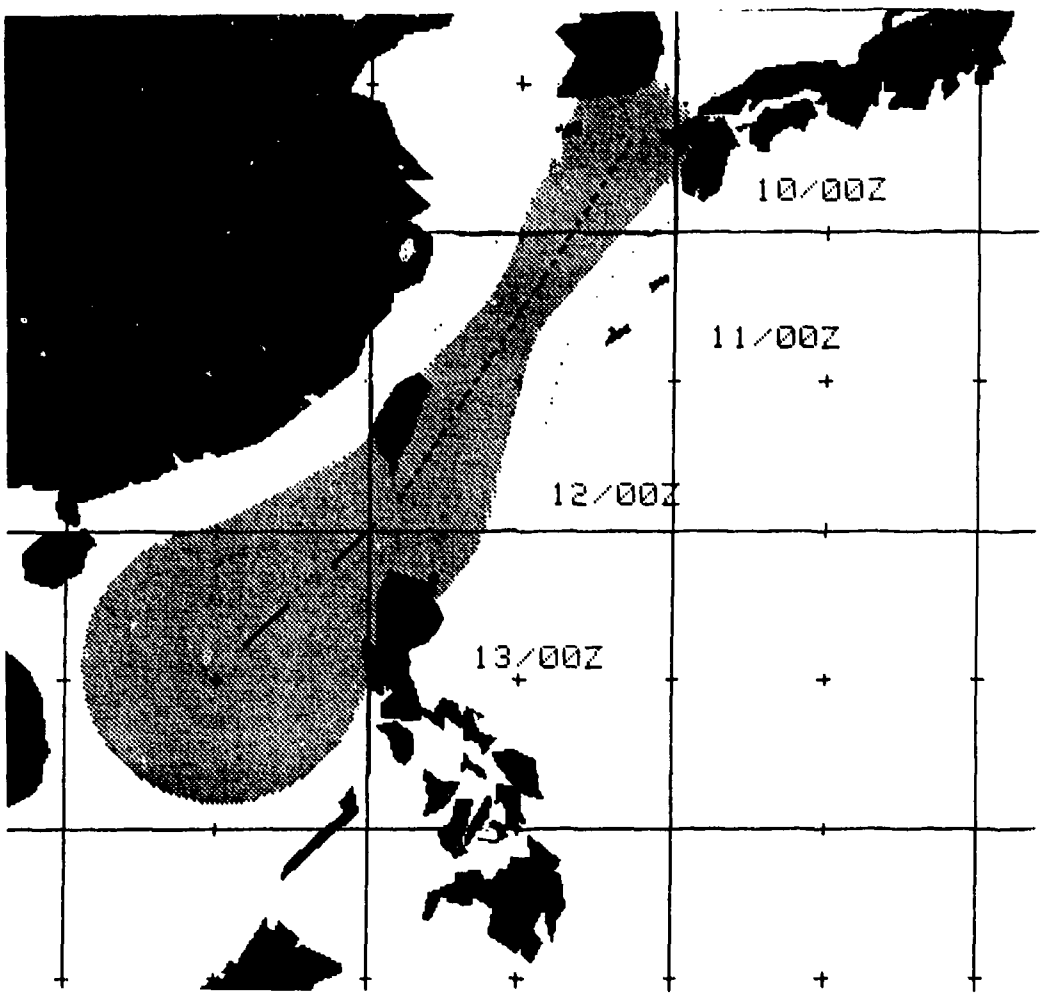

Figure 87. Battle group vulnerability display along a track.

The display is also well suited for battle group formations and screen considerations. For example, an ASW commander may desire the platform with the greatest sonar capability be placed well ahead of the high-value target, along the major threat axis. The battle group vulnerability display, figure 88, may indicate however, that this placement would eliminate UHF radio communications between the platform and the high-value target, thereby necessitating a middleman relay.

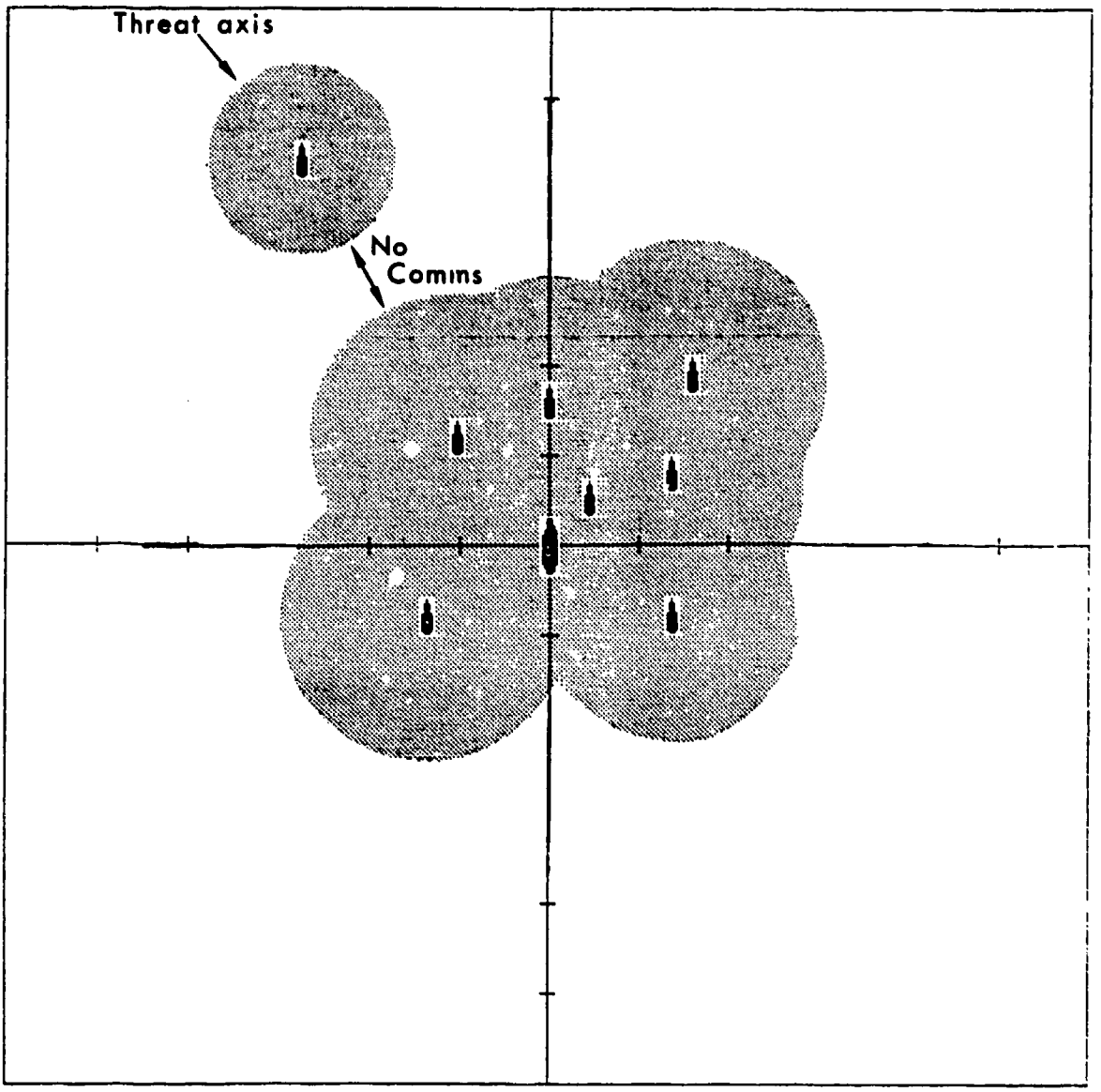

Figure 88. Battle group vulnerability display for screen formation.

20.0 REFERENCES

Barton, D.K. (1965). *Radar System Analysis,* Prentice-Hall, Inc., Englewood Cliffs, New Jersey.

Blake, L.V. (1980). *Radar Range-Performance Analysis*, D.C. Heath and Company, Lexington, MA.

Dotson, M.E. (1987). *An Evaluation of the Impact of Variable Temporal and Spatial Data Resolution Upon IREPS*, Naval Postgraduate School.

Greening, C.P. (1987). *Forward-Looking Infrared (FLIR) Systems for Dick and Jane*, Naval Weapons Center Technical Manual 5528.

Helvey, R.A. (1982). *Guidelines for Correction of Radiosonde-Derived Refractive Profiles and Climatologies*, Pacific Missile Test Center Technical Publication TP000002.

Helvey, R.A., and J.S. Rosenthal (1983). *Guide For Inferring Refractive Conditions From Synoptic Parameters*, Pacific Missile Test Center Technical Publication TP000005.

Huschke, R.E. (1959). *Glossary of Meteorology*, American Meteorological Society, Boston, MA.

Skolnik, M.I. (1980). *Introduction to Radar Systems*, McGraw-Hill Book Co., New York.

21.0 BIBLIOGRAPHY

Dolukhanov, M., (1971). *Propagation of Radio Waves*, Mir Publishers.

Glevy, D. F., (1976). Naval Electronics Laboratory Center, personal communications.

Hall, M. P. M., (1979). *Effects of the Troposphere on Radio Communications*, Alden Press, Oxford, London.

Halliday, D., and R. Resnick, (1970). *Fundamentals of Physics*, John Wiley and Sons, New York.

Hattan, C. P., *Propagation Models for IREPS Revision 2.0*, (1982). Naval Ocean Systems Center Technical Report 771.

Hitney, H. V., et al., "Radio Propagation," *Encyclopedia of Physical Science and Technology*, Vol. II.

Hitney, H. V., et al., (1984). *Electromagnetic Propagation Functions Program Performance Specification (PPS) for the Tactical Environmental Support System (TESS)*, Naval Ocean Systems Center Technical Document 1015.

Hitney, H. V., et al., (1955). "Tropospheric Radio Propagation Assessment," *Proceedings of the IEEE*, Vol. 73, No. 2.

Houghton, D. D., (1985). *Handbook of Applied Meteorology*, John Wiley and Sons, New York.

Meteorological Aspects of Radio-Radar Propagation, (1960). NAVWEPS 50-1P-550, U. S. Navy Weather Research Facility, Norfolk, VA.

The Analysis and Forecasting of Atmospheric Radar Refractivity, (1967). NAVAIR 50-1P-1, Naval Weather Service Command.

Meteorological Refractive Effects Upon Radar Wave Propagation, (1954). NAVAER 50-1P-527.

Lloyd, J. M., (1975). *Thermal Imaging System*, Plenum Press, New York.

Paulus, R. A., (1984). *Practical Application of the IREPS Evaporation Duct Model*, Naval Ocean Systems Center Technical Report 966.

Patterson, W. L., (1986). *Forward-Looking Infrared Performance Function Program Performance Specification (PPS) for the Tactical Environmental Support System (TESS)*, Naval Ocean Systems Center Technical Document 1000.

21.0 BIBLIOGRAPHY (cont'd)

Patterson, W. L., (1987). *Historical Electromagnetic Propagation Condition Database Description*, Naval Ocean Systems Center Technical Document 1149.

Patterson, W. L., et al., (1987). *IREPS 3.0 User's Manual*, Naval Ocean Systems Center Technical Document 1151.

Rosenthal, J. and S. Westerman, (1985). "Inferring Refractivity Conditions from Satellite Imagery," Pacific Missile Test Center Technical Note 96.

Skolnik, M. I., (1970). *Radar Handbook*, McGraw-Hill Book Co., New York.

Van Brunt, L. B., (1978). *Applied ECM*, EW Engineering, Inc., Dunn Laring, VA.